

Final Report  
for  
Fine Attitude Control System  
Phase I

July, 1965

SGC 742R-8

Contract No. NAS5-9056

Volume I of II

Prepared by

Space-General Corporation  
9200 East Flair Drive  
El Monte, California

GPO PRICE \$ \_\_\_\_\_

CFSTI PRICE(S) \$ \_\_\_\_\_

Hard copy (HC) 5.00

Microfiche (MF) 1.00

ff 653 July 65

for

Goddard Space Flight Center  
Greenbelt, Maryland

N66 27324

(ACCESSION NUMBER)

158

(PAGES)

CR-75392

(NASA CR OR TMX OR AD NUMBER)

(THPU)

1

(CODE)

03

(CATEGORY)

FACILITY FORM 802



Final Report  
for  
Fine Attitude Control System  
Phase I

July, 1965

SGC 742R-8


Contract No. NAS5-9056

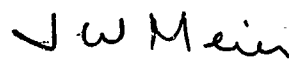
Volume I of II


Prepared by  
Space-General Corporation  
9200 East Flair Drive  
El Monte, California

for  
Goddard Space Flight Center  
Greenbelt, Maryland

Approved by

  
C. A. Jenkins  
FACS Project Engineer

  
J. W. Meier  
FACS Program Manager

  
M. Eimer  
Director of Engineering  
Space Operations

# CONTENTS

	<u>Page</u>
SECTION 1 - INTRODUCTION AND SUMMARY . . . . .	1
SECTION 2 - FACS REQUIREMENTS . . . . .	2
2.1 General . . . . .	2
2.2 Operational Requirements . . . . .	2
2.3 Phase I Requirements . . . . .	3
2.3.1 Basis for IACS Design . . . . .	3
2.3.2 IACS Inertial Reference . . . . .	3
2.3.3 IACS Rate Stabilization . . . . .	4
2.3.4 Torquing Devices . . . . .	4
2.3.5 Despin Control and Initial Capture . . . . .	4
2.3.6 Prelaunch Adjustment . . . . .	5
2.3.7 Maneuver Sequence . . . . .	5
2.3.8 Transfer to SACS Operation . . . . .	5
2.3.9 FACS Packaging Design . . . . .	6
2.3.10 AC Power Supply . . . . .	6
2.3.11 DC Power Supply . . . . .	6
SECTION 3 - FACS DESCRIPTION . . . . .	7
3.1 Configuration and Operation . . . . .	7
3.1.1 FACS Sequence of Operation . . . . .	11
3.1.2 Gyro Caging Interface . . . . .	17
3.1.3 Control Parameters . . . . .	17
3.2 Breadboard FACS . . . . .	21
3.3 Breadboard GSE . . . . .	21
3.4 FACS Subassemblies . . . . .	31
3.4.1 Static Inverter . . . . .	31
3.4.2 DC Power Supply . . . . .	31
3.4.3 Programmer . . . . .	33
3.4.4 IACS Control Electronics . . . . .	33
3.4.5 SACS Control Electronics . . . . .	37
3.4.6 Telemetry Signal Conditioner . . . . .	37
3.4.7 Junction Box . . . . .	37
3.4.8 Roll Stabilized Platform . . . . .	44
3.4.9 Rate Gyros . . . . .	44
3.5 Sensor . . . . .	44
SECTION 4 - FACS PHASE I PROGRAM . . . . .	48
4.1 Work Statement Items . . . . .	48
4.2 Design . . . . .	49

## CONTENTS (Continued)

	<u>Page</u>
4.3 Analysis . . . . .	50
4.3.1 Pneumatics Analysis . . . . .	50
4.3.2 Analog Computer Study . . . . .	50
4.3.3 Roll Slaving Analysis . . . . .	55
4.4 Bench Test . . . . .	55
4.4.1 Subassembly and Module Tests . . . . .	58
4.4.2 System Test and Calibration . . . . .	58
4.4.3 VIT Test . . . . .	59
4.5 Three-Axis Simulator Test . . . . .	60
4.5.1 Test Description . . . . .	60
4.5.2 Maneuver Evaluation . . . . .	67
4.5.3 Acquisition Evaluation . . . . .	77
4.5.4 Limit Cycle Evaluation . . . . .	89
4.5.5 Configuration Comparison . . . . .	98
4.5.6 Final Configuration Summary . . . . .	99
4.5.7 Correlation With Analog Computer Studies . . . . .	100
4.5.8 Delayed Feedback - Preliminary Investigation . . . . .	123
 SECTION 5 - SYSTEM CHANGES (PHASE II) . . . . .	 127
5.1 Optional Features - Selection of Alternate . . . . .	127
5.2 Design Changes . . . . .	127
 SECTION 6 - CONCLUSIONS AND RECOMMENDATIONS . . . . .	 130
 APPENDIX I - FUNCTIONAL DESCRIPTIONS AND SCHEMATICS	
APPENDIX II - BREADBOARD FACS PARTS LIST	
APPENDIX III - PNEUMATIC ANALYSIS OF AEROBEE ACS FORCE CONTROL SYSTEM	
APPENDIX IV - BREADBOARD FACS SUBASSEMBLY AND MODULE TEST DATA	
APPENDIX V - FACS SYSTEM TEST AND CALIBRATION DATA	
APPENDIX VI - BREADBOARD FACS TELEMETRY SIGNAL-CONDITIONER CALIBRATION	
APPENDIX VII - OPERATIONAL PROCEDURES AND PARAMETER CHANGES	
APPENDIX VIII - FACS TECHNICAL NOTE RE-EVALUATION OF RAMP MANEUVER CHARACTERISTICS	
APPENDIX IX - EXPLANATION OF THE DEFERMENT OF ROLL SLAVING UNTIL COMPLETION OF ATTITUDE CAPTURE	
APPENDIX X - CORRECTION OF THE EFFECT OF INNER GIMBAL ANGLE ON TORQUING RATE	

# ILLUSTRATIONS

<u>Figure</u>		<u>Page</u>
1	Fine Attitude Control System, Simplified Block Diagram . . . . .	8
2	FACS Pitch and Yaw, Block Diagram . . . . .	9
3	FACS Roll and Slave Roll, Block Diagram . . . . .	10
4	FACS Pitch and Yaw, Control Block Diagram . . . . .	18
5	FACS Roll and Slave Roll, Control Block Diagram . . . . .	19
6	FACS Body Axis Definition . . . . .	20
7	Breadboard FACS, View No. 1 . . . . .	24
8	Breadboard FACS, View No. 2 . . . . .	25
9	Breadboard FACS, View No. 3 . . . . .	26
10	Breadboard FACS, View No. 4 . . . . .	27
11	Breadboard GSE, Front View . . . . .	28
12	Breadboard GSE, Panel . . . . .	29
13	Breadboard GSE, Inside View . . . . .	30
14	Breadboard Static Inverter Subassembly . . . . .	32
15	Breadboard DC Power Supply Subassembly . . . . .	34
16	Breadboard Programmer Subassembly, Front View . . . . .	35
17	Breadboard Programmer Subassembly, Rear View . . . . .	36
18	Breadboard IACS Control Electronics Subassembly, Front View . . . . .	38
19	Breadboard IACS Control Electronics Subassembly, Rear View . . . . .	39
20	Breadboard SACS Control Electronics Subassembly, Front View . . . . .	40
21	Breadboard SACS Control Electronics Subassembly, Rear View . . . . .	41
22	Breadboard Telemetry Conditioning Subassembly, Front View . . . . .	42
23	Breadboard Telemetry Conditioning Subassembly, Rear View . . . . .	43
24	Roll Stabilized Platform Subassembly . . . . .	45
25	Rate Gyro Subassembly . . . . .	46
26	IACS Position Signal Limiter Change, Servo Block Diagram . . . . .	52
27	IACS Position Signal Limiter Change, Analog Computer Circuit . . . . .	53

# ILLUSTRATIONS (Continued)

<u>Figure</u>		<u>Page</u>
28	Maneuver Torquing Change, Servo Block Diagram . . . . .	56
29	Maneuver Torquing Change, Servo Block Diagram . . . . .	57
30	GSFC Three-Axis Simulator Facility . . . . .	61
31	Position Channel "Soft Limiting" Characteristic . . . . .	68
32	FACS Maneuver Characteristics for Acceleration = $1.4 \text{ deg/sec}^2$ (Three-Axis Simulator Run 47). . . . .	70
33	FACS Maneuver Characteristics for Acceleration = $1.4 \text{ deg/sec}^2$ (Three-Axis Simulator Run 47 Continued). . . . .	71
34	FACS Maneuver Characteristics for Acceleration = $1.9 \text{ deg/sec}^2$ (Three-Axis Simulator Run 48) . . . . .	72
35	FACS Maneuver Characteristics for Acceleration = $3.0 \text{ deg/sec}^2$ (Three-Axis Simulator Run 49) . . . . .	73
36	FACS Maneuver Characteristics for Acceleration = $3.6 \text{ deg/sec}^2$ (Three-Axis Simulator Run 51) . . . . .	74
37	FACS Maneuver Characteristics for Acceleration = $3.6 \text{ deg/sec}^2$ (Three-Axis Simulator Run 51 Continued). . . . .	75
38	Comparison - Rate Gyro Performance at $0.2 \text{ deg/sec}$ . . . . .	79
39	Comparison - Rate Gyro Performance at $0.1 \text{ deg/sec}$ . . . . .	80
40	FACS Acquisition Characteristics for $\alpha_c = 1.9 \text{ deg/sec}^2$ (Three-Axis Simulator Run 40) . . . . .	85
41	FACS Acquisition Characteristics for $\alpha_c = 3.0 \text{ deg/sec}^2$ (Three-Axis Simulator Run 49) . . . . .	86
42	FACS Acquisition Characteristics for $\alpha_c = 3.6 \text{ deg/sec}^2$ (Three-Axis Simulator Run 50) . . . . .	87
43	FACS Acquisition Characteristics for Reduced $\alpha_F$ (Three-Axis Simulator Run 52) . . . . .	88
44	SACS Limit Cycle - Correlation of Sensor to Autocollimator . .	92
45	SACS Limit Cycle Characteristics for Switching Threshold $\pm 22.5 \text{ Arc Seconds}$ . . . . .	94
46	SACS Limit Cycle Characteristics for Switching Threshold $\pm 10 \text{ Arc Seconds}$ . . . . .	95
47	SACS Limit Cycle Characteristics for Switching Threshold $\pm 5 \text{ Arc Seconds}$ . . . . .	96

# ILLUSTRATIONS (Continued)

<u>Figure</u>		<u>Page</u>
48	75° Maneuver at $\alpha_c = 1.4 \text{ deg/sec}^2$ (Analog Run 21M) . . . . .	101
49	75° Maneuver at $\alpha_c = 3.6 \text{ deg/sec}^2$ (Analog Run 24M) . . . . .	102
50	20° Maneuver at $\alpha_c = 1.4 \text{ deg/sec}^2$ (Analog Run 10M) . . . . .	103
51	20° Maneuver at $\alpha_c = 3.6 \text{ deg/sec}^2$ (Analog Run 7M). . . . .	104
52	IACS Switching Logic Derived from Position-Limiter Calibration ( $K_1''/K_1 = 1.55 \text{ sec}$ ) . . . . .	108
53	Comparison Between Analog and 3-Axis Simulation Switch Points (75° Maneuver) . . . . .	110
54	Acquisition and Limit Cycle for $\psi_{EO} = 0$ (Analog Run 21A-1) . . . . .	116
55	Acquisition and Limit Cycle for $\psi_{EO} = + 3^\circ$ (Analog Run 21A-2) . . . . .	117
56	Acquisition and Limit Cycle for $\psi_{EO} = - 3^\circ$ (Analog Run 21A-3) . . . . .	118
57	Acquisition and Limit Cycle for $\psi_{EO} = 0$ (Analog Run 24A-1) . . . . .	119
58	Acquisition and Limit Cycle for $\alpha_F = 0.06 \text{ deg/sec}^2$ (Analog Run 11A-1) . . . . .	120
59	Acquisition and Limit Cycle for $\epsilon_{TF} = 10 \text{ arc sec}$ (Analog Run 25A-1) . . . . .	121
60	Delayed Feedback in SACS, Block Diagram . . . . .	124
61	Acquisition and Limit Cycle with Delayed Feedback (Three-Axis Simulator Run 56) . . . . .	126

# TABLES

<u>Table</u>		<u>Page</u>
1	Phase and Polarity Definition - IACS . . . . .	22
2	Phase and Polarity Definition - SACS . . . . .	23
3	DFG Settings for Position Signal Limiter Simulation . . . . .	54
4	Breadboard Face Programmer Sequence for 3-Axis Simulator Test . . . . .	62
5	Telemetry Measurements for Three-Axis Simulator Test of FACS . . . . .	64
6	Maneuver Parameters from Three-Axis Simulator Tests . . . . .	76
7	Effect of Mixing Ratio on Acquisition . . . . .	82
8	Effect of Acceleration on Acquisition from Three-Axis Simulator Tests . . . . .	84
9	SACS Limit Cycle Characteristics (Without Delayed-Feedback) from Three-Axis Simulator Tests . . . . .	97
10	Index of Selected Runs . . . . .	105
11	Analog Simulation Maneuver Parameters for 75 Degrees Yaw Maneuver . . . . .	106
12	Comparison of Analog and 3-Axis Simulator Maneuver Results for 75 Degree Maneuver . . . . .	111
13	Maximum Lag Angle Comparison for 20 Degree Maneuver . . . . .	111
14	Effect of Acceleration on Acquisition, Configuration I . . . . .	113
15	Analog Simulation Effect of Mixing Ratio on Acquisition . . . . .	114
16	Analog Simulation SACS Limit Cycle Characteristics . . . . .	122



## Section 1

### INTRODUCTION AND SUMMARY

Space-General Corporation (SGC) under Contract NAS5-9056 from the National Aeronautics and Space Administration, Goddard Space Flight Center (NASA-GSFC), has completed Phase I of a program for development of a Fine Attitude Control System (FACS).

The FACS will point the experiment package of an Aerobee 150 series rocket at the sun or at a series of stellar targets. Utilizing a combination of gyro-inertial and optical sensors, rapid acquisition and precision pointing are achieved.

The Phase I program involved design, fabrication, and test of a breadboard model of the FACS and of associated ground support equipment. The work was based upon an earlier feasibility demonstration program carried out by SGC under Contract NAS5-2666. The breadboard FACS was constructed by integration of individual breadboard subassemblies into a structure suitable for mounting on a flight simulator. Subassemblies were individually tested prior to incorporation into the system. The final demonstration of acceptability was carried out at the 3-axis gas bearing simulator facility located at GSFC.

The breadboard FACS successfully met all requirements. Phase II of the program, to be initiated shortly, will culminate in flight test of the FACS.

This document constitutes final fulfillment of all requirements under Phase I.

A close working relationship between GSFC and SGC has persisted throughout this work and the feasibility work under NAS 5-2666. The feasibility-demonstration program has been reported in Reference 4. The feasibility model included the uni-directional switchover implementation proposed by GSFC and described in Reference 5.

During this FACS Phase I program, GSFC has provided important contributions in the following areas:

- a. The fine sun sensor for the FACS is a Goddard designed and developed unit. GSFC conceived the basic idea of a sun sensor whose output characteristics would closely match those of the long-planned stellar sensor, thus permitting the FACS to be used interchangeably as a solar pointing or a stellar pointing system.

GSFC specified and evaluated the Ball Brothers Fine Eyes and Burr-Brown amplifiers, which are components of the sun sensor unit, designed the electronic circuitry to shape the output signal properly, packaged the sun sensor components into a breadboard sub-assembly and made an exhaustive evaluation of the packaged sun sensor. The results of this design and development effort were reported in Reference 6.

- b. GSFC initiated and tested a modification of the SGC Variable Time Torquing (VIT) Scheme that utilizes fewer components. This modification, known as the "current-only mode" was later tested by SGC. Good test results were obtained by both SGC and GSFC. This mode has been selected for incorporation in Phase II, resulting in a simplification of the VIT circuitry.
- c. GSFC proposed, implemented and investigated a lag feedback scheme for the FACS which has resulted in a marked improvement in the fine limit cycle performance. This same technique was also applied by GSFC to the IACS with a corresponding improvement in coarse limit cycle performance. GSFC has optimized the lag feedback circuitry for both coarse and fine modes, and has transmitted the results to SGC for incorporation in Phase II.
- d. GSFC also proposed and established the values for the soft-limiting technique in the coarse pitch and yaw channels. This permitted a reduction in rate gain with a consequent reduction in the valve "hammering" that occurred at high acceleration.
- e. GSFC conceived, designed and developed a sophisticated 3-axis air bearing facility capable of demonstrating the fine pointing performance of the FACS. This facility has an operating and measurement resolution of about  $\pm 1$  arc-second.

## Section 2

### FACS REQUIREMENTS

#### 2.1 GENERAL

The Fine Attitude Control System (FACS) has been designed to be suitable as either a solar pointing or a stellar pointing FACS for the Aerobee 150 series rockets. Initially, the system will be used as a solar pointing FACS. However, the same system, with minor modifications and adjustments (including substitution of a fine stellar sensor for the fine solar sensor), will be suitable as a stellar pointing FACS.

The FACS consists of two basic subsystems: an Inertially - Referenced Attitude Control System (IACS) that places the rocket longitudinal axis approximately on target and provides roll control for the entire coasting portion of flight, and a Solar (or Stellar)-Referenced Attitude Control System (SACS). The SACS senses the pointing errors in pitch and yaw after the IACS has stabilized the rocket approximately on target, and takes corrective action to remove these errors. In addition, the SACS initially corrects the accumulated pitch and yaw errors in the IACS and continually maintains this correction during the viewing time on the target.

The system design permits use of just the IACS portion of the system in the normal IACS mode. Five roll-pitch or roll-yaw maneuver capability is required, each maneuver ranging from  $10^{\circ}$  to  $75^{\circ}$  per axis.

#### 2.2 OPERATIONAL REQUIREMENTS

The Aerobee rocket flies as a spinning, aerodynamically-stabilized vehicle through the powered portion of flight. After burnout of the Aerobee 150 rocket, the IACS maneuvers and stabilizes the rocket in three axes so that the vehicle longitudinal axis is pointed at the desired target within  $2^{\circ}$  in each axis. At this time the vehicle is oscillating in each axis in a limit cycle that is approximately  $\pm 0.25^{\circ}$  in amplitude. The SACS thereafter takes over

control in pitch and yaw to accomplish two functions. First is the correction of the pitch and yaw reference errors in the IACS. The second is the control of the rocket in pitch and yaw in such a way that the rocket is stabilized within  $\pm 28$  arc sec of the reference established by the solar (or stellar) sensor; i.e., each axis is stabilized within  $\pm 20$  arc sec ( $28 \text{ arc sec}/\sqrt{2}$ ). Fine jets are used in the SACS to accomplish this fine stabilization. It is desired that fine stabilization occur within 10 sec after the IACS has stabilized the rocket approximately on target. The IACS continues to maintain roll control and stabilization during the entire coasting flight. The IACS roll limit cycle amplitudes and frequencies are acceptable if they do not affect the fine stabilization performance requirements in pitch and yaw.

During the viewing time on target, the SACS continually nulls out the reference errors in the IACS by caging the pitch and yaw gyros to the reference established by the fine sensor. In the stellar pointing FACS, control is switched back to the IACS at a pre-programmed time. The rocket is maneuvered to new coordinates near another stellar target, at which time the previously described sequence is repeated.

## 2.3 PHASE 1 REQUIREMENTS

The objective of the Phase I program was to provide an FACS design meeting the above basic requirements. Additional specific features of system design were specified as follows.

### 2.3.1 BASIS FOR IACS DESIGN

The IACS portion of the FACS shall be based in general on the configuration developed under contract NAS 5-299 together with certain modifications incorporated in IACS Serial No. 17.

### 2.3.2 IACS INERTIAL REFERENCE

The inertial reference in the IACS shall consist of a roll stabilized platform containing two 2-degree-of-freedom gyros. The gyros are to be mounted such that their spin axes are nominally horizontal and orthogonal to

one another, with the outer gimbal of each gyro serving as an inertial roll reference. The roll synchro output of one gyro shall serve as the error detector in a servo drive that stabilizes the platform in roll for Aerobee 150 spin rates up to 3.0 rps. A platform synchro, similar to the gyro synchro, shall serve as the roll error detector for the IACS after despin. It is also permissible to mix the platform synchro output with the roll gyro output to form the roll error signal. The inner gimbal of one gyro shall serve as the inertial reference in pitch while that of the other gyro provides the yaw reference for the positional orientation of the rocket after despin.

#### 2.3.3 IACS RATE STABILIZATION

The positional control loop in each axis shall utilize fixed rate feedback from a rate gyro for stabilization purposes. A single value of rate gain feedback per axis shall be used for all maneuvers. The value of rate feedback shall be such as to provide critical or over-damped orientation for roll step maneuvers up to  $180^{\circ}$  after despin and for ramp maneuvers up to  $75^{\circ}$  in each axis through the remainder of coasting flight. After roll despin and capture, a one-time change in rate gain feedback in roll only is desired to optimize ramp maneuvers up to  $75^{\circ}$ . A design goal should be the use of a single fixed level of rate feedback in each of the pitch and yaw axes, if at all compatible with reasonable IACS limit cycle operation as well as FACS operation.

#### 2.3.4 TORQUING DEVICES

The torquing devices in each axis shall be on-off jets operating from the residual helium in the rocket tanks after powered flight and despin. The selected single value of rate feedback in each axis for critical or over-damped orientation shall take into account the expected variation in jet thrust during coasting flight as the tank pressure drops, as well as the variation in vehicle inertia from one payload to another.

#### 2.3.5 DESPIN CONTROL AND INITIAL CAPTURE

Despin control shall use rate information from the roll rate gyro to bring the rocket spin rate to near zero after powered flight. At this point,

roll capture shall be performed by means of the positional control system followed by vehicle pitch and yaw stabilization to the initial gyro settings.

#### 2.3.6 PRELAUNCH ADJUSTMENT

The initial inertial reference settings of the position gyros in pitch, yaw, and roll shall be performed on the ground prior to launch by appropriate precision torquing and monitoring of the spin axis of each gyro. These offset angles shall be limited to  $20^{\circ}$  maximum in each axis, and shall be accurate to within  $\pm 1/4^{\circ}$  of the desired values. The breadboard system design and associated ground equipment shall contain provision for offset caging of the gyros via three-wire gyro synchros in addition to offset caging via two-wire gyro synchros.

#### 2.3.7 MANEUVER SEQUENCE

After stabilization to initial coordinates, subsequent maneuvers are to be performed as follows. The roll gyro is to be torqued to the predetermined angle with the vehicle following in roll during this time. Pitch and yaw gyro torquing and pitch and yaw maneuver are to be disarmed until both the roll torquing is complete and the vehicle has stabilized in roll within some small angle. At this point, pitch gyro torquing and pitch maneuver are to be activated. At the completion of the pitch maneuver, yaw gyro torquing and yaw maneuver are to be activated, enabling the IACS to complete the vehicle maneuver. The torquing angles shall be accurate to within 1% of the desired values or within  $1/4^{\circ}$ , whichever is greater, for all inverter frequency and voltage variations and for a range of temperature from  $32^{\circ}\text{F}$  to  $140^{\circ}\text{F}$ .

#### 2.3.8 TRANSFER TO SACS OPERATION

When the IACS has stabilized the vehicle approximately on target, with an oscillation of  $\pm 0.3^{\circ}$  or less for about one second, the pitch and yaw gyros are to be caged to the fine solar (or stellar) sensor. The output error voltage of each gyro will very quickly rise to a level determined by the fine sensor error voltage. The remainder of the IACS remains in operation so that

the IACS jets torque the rocket to a new position that will minimize these gyro error voltages. When each gyro error voltage again decreases to a level corresponding to  $\pm 0.3^\circ$  or less, for about 1 second, that axis can independently switch over completely to fine jet stabilization, using the appropriate axis error information of the fine sensor. The caging of the pitch and yaw gyros to the fine sensor is to remain locked-in during the entire viewing time on target. If, for any reason, the attitude error of the vehicle in any axis increases to a point where the caged gyro output voltage exceeds that corresponding to  $\pm 0.3^\circ$ , vehicle stabilization in the axis shall revert to the coarse jets of the IACS. Re-transfer to the fine jets shall take place as described previously. In the case of the stellar pointing FACS, the subsequent pre-programmed maneuver will remove the lock-in of the gyro caging and cause appropriate torquing of the gyro axes and vehicle stabilization to the new target via the IACS. Transfer to the SACS will occur as previously described.

A design goal should be the use of a single level detector in each of the pitch and yaw axes to serve as both the SACS-enable level detector ( $0.3^\circ$  nominal) and as a detector indicating completion of IACS-controlled maneuvers.

#### 2.3.9 FACS PACKAGING DESIGN

The design shall be based on a modular concept of distinct, readily interchangeable components and subassemblies.

#### 2.3.10 AC POWER SUPPLY

A single, sine-wave inverter shall supply the two-phase, 26-volt, 400-cycle requirements for the FACS. The inverter shall have a frequency regulation of  $\pm 0.2\%$  and a voltage regulation of  $\pm 2\%$  for input voltages from 24 to 34 VDC, output load variations from 25% load to full load, and temperature variations from  $32^\circ\text{F}$  to  $140^\circ\text{F}$ .

#### 2.3.11 DC POWER SUPPLY

A single regulated DC power supply, fed solely from the inverter, shall supply all the regulated DC voltages required in the FACS.

## Section 3

### FACS DESCRIPTION

#### 3.1 CONFIGURATION AND OPERATION

A simplified block diagram of the FACS is shown in Figure 1. It shows the designation of IACS and SACS used herein to identify the two basic FACS subsystems.

The IACS is a self-contained control system, capable of use by itself or in conjunction with the SACS subsystem. The major assemblies of the IACS are: roll-stabilized platform incorporating two free gyros, rate gyro package, static inverter, DC power supply, programmer, IACS control unit, and reaction jet pneumatic circuits.

The SACS provides the auxiliary control channels needed for pitch and yaw fine-pointing control using line-of-sight error signals from a stellar (or solar) sensor. The SACS consists of sensor, derived-rate networks, logic circuitry for changeover from IACS to SACS operation, reaction jet control electronics, and low-thrust jet pneumatic circuits. All power requirements are provided by the IACS. The IACS programmer provides an initiation signal for SACS operation when a target-seeking maneuver is completed.

More detailed block diagrams are shown in Figure 2 (pitch and yaw) and in Figure 3 (roll and slaved roll). The following description covers all of the logic and timing functions shown in these diagrams. Several optional provisions are included. These optional features were incorporated in the breadboard FACS for subsequent evaluation. A selection of the preferred configuration was then made during tests on the 3-axis simulator. Appendix VII describes the method of implementation for each of the optional features. This appendix also covers operating procedures for the breadboard FACS and its associated GSE.



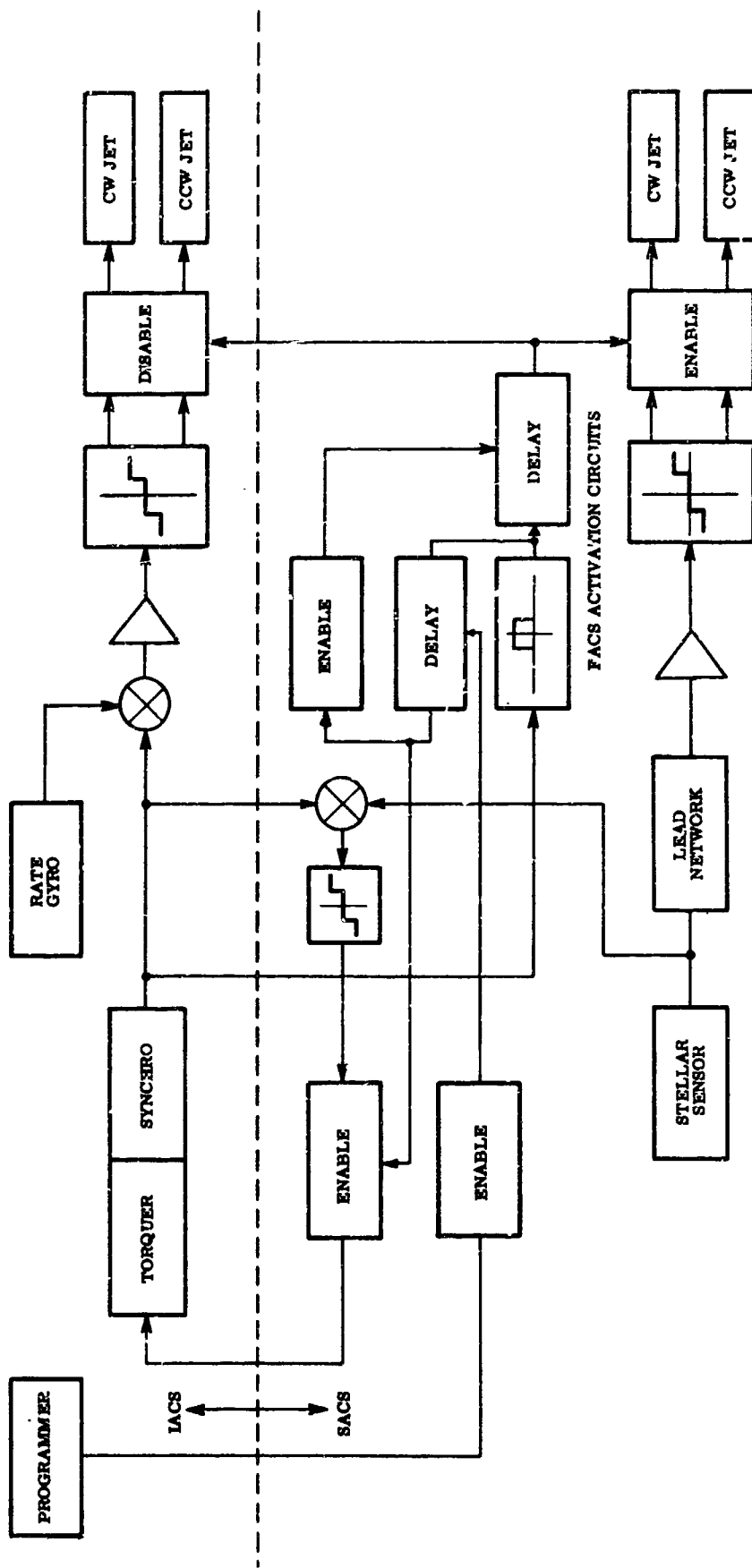
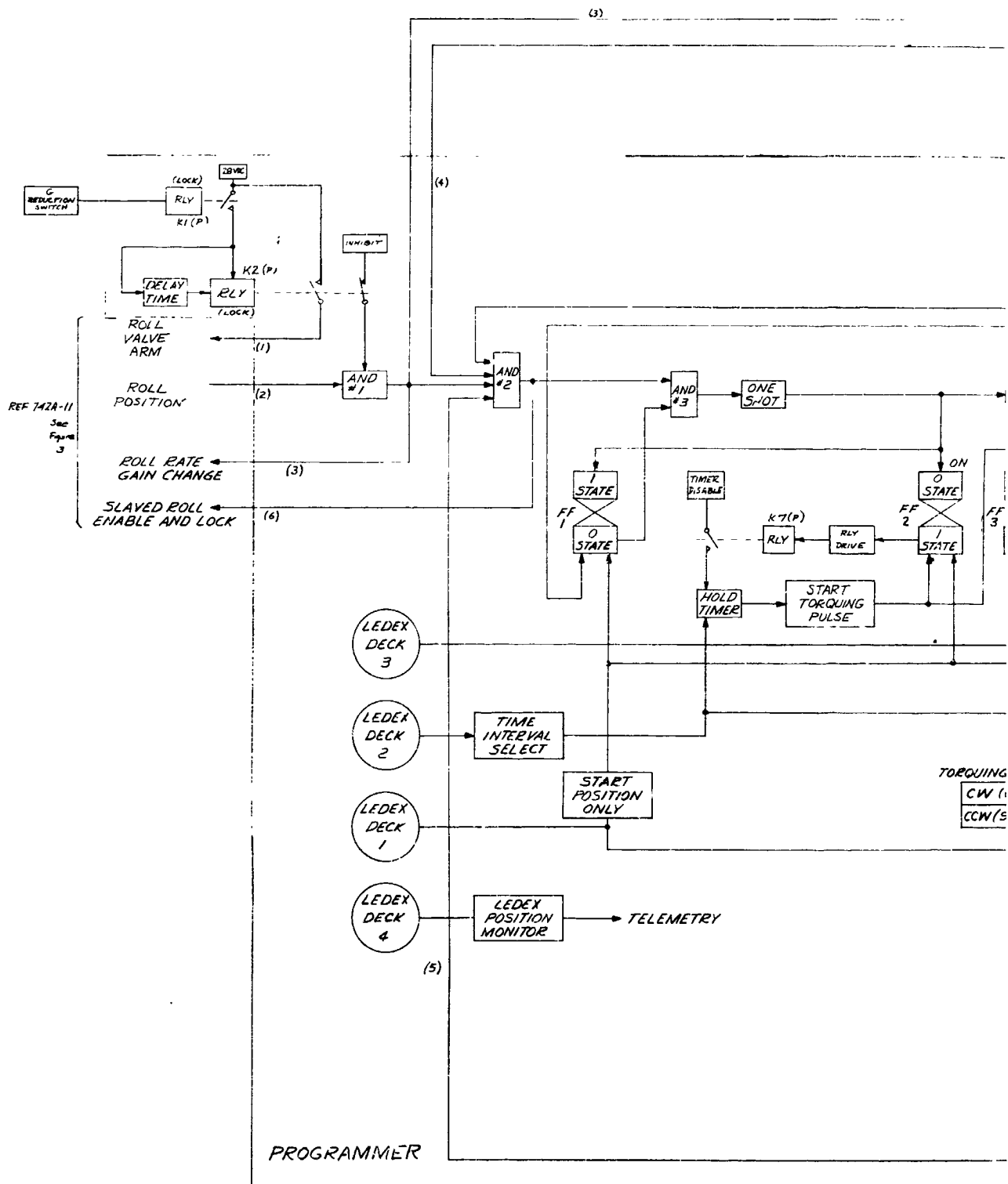


Figure 1. Fine Attitude Control System, Simplified Block Diagram



9-1.

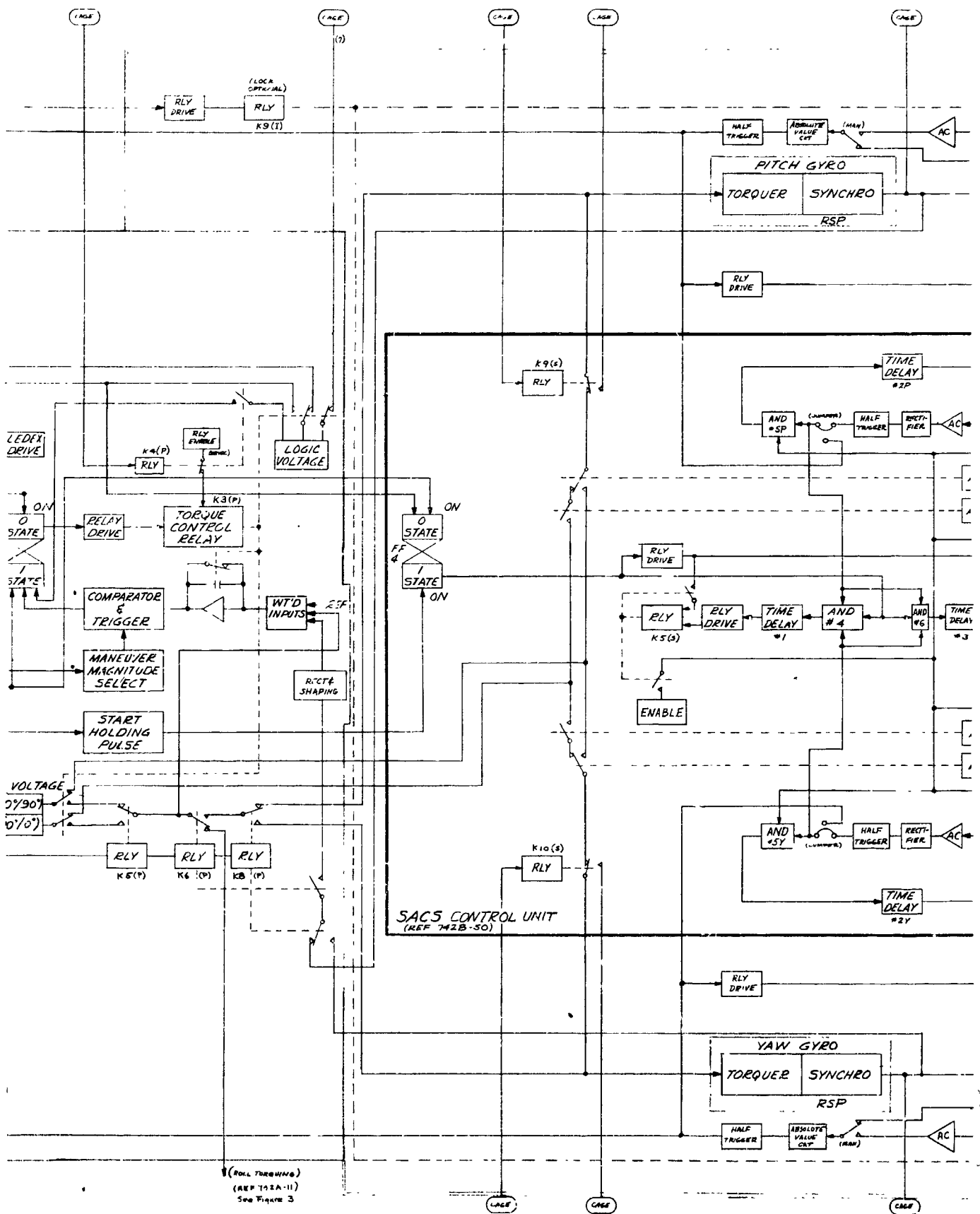
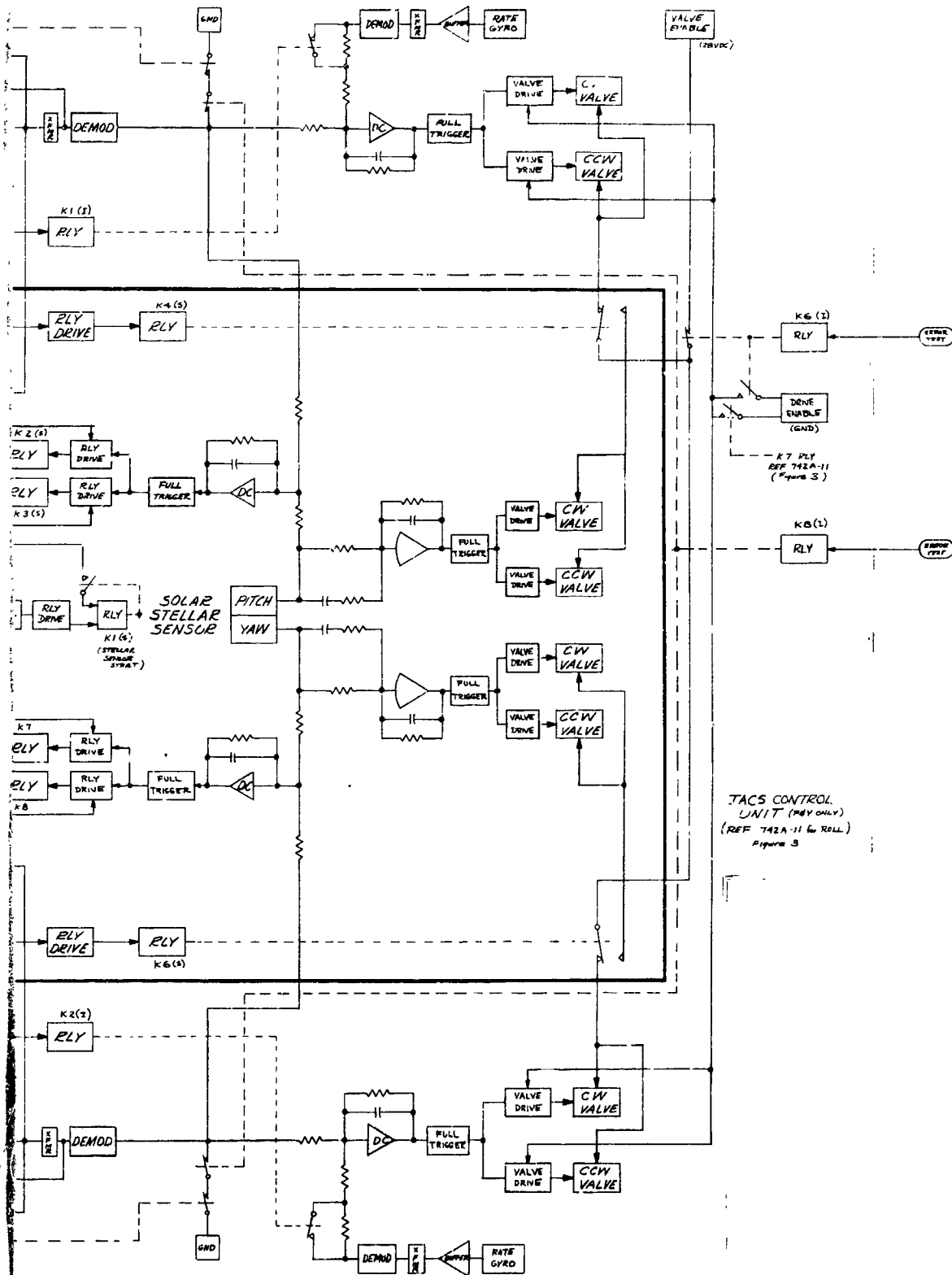


Figure 2. FACS Pitch and Yaw, Block Diagram

NOTE: PARENTHETICAL LETTERS  
FOLLOWING RELAY DESIGNATIONS  
INDICATE SUBASSEMBLIES:  
(I) FOR JACS CONTROL UNIT  
(S) FOR SACS CONTROL UNIT  
(P) FOR PROGRAMMER



JACS CONTROL  
UNIT (MAY ONLY)  
(REF 742A-11 6 ROLL)  
Figure 3

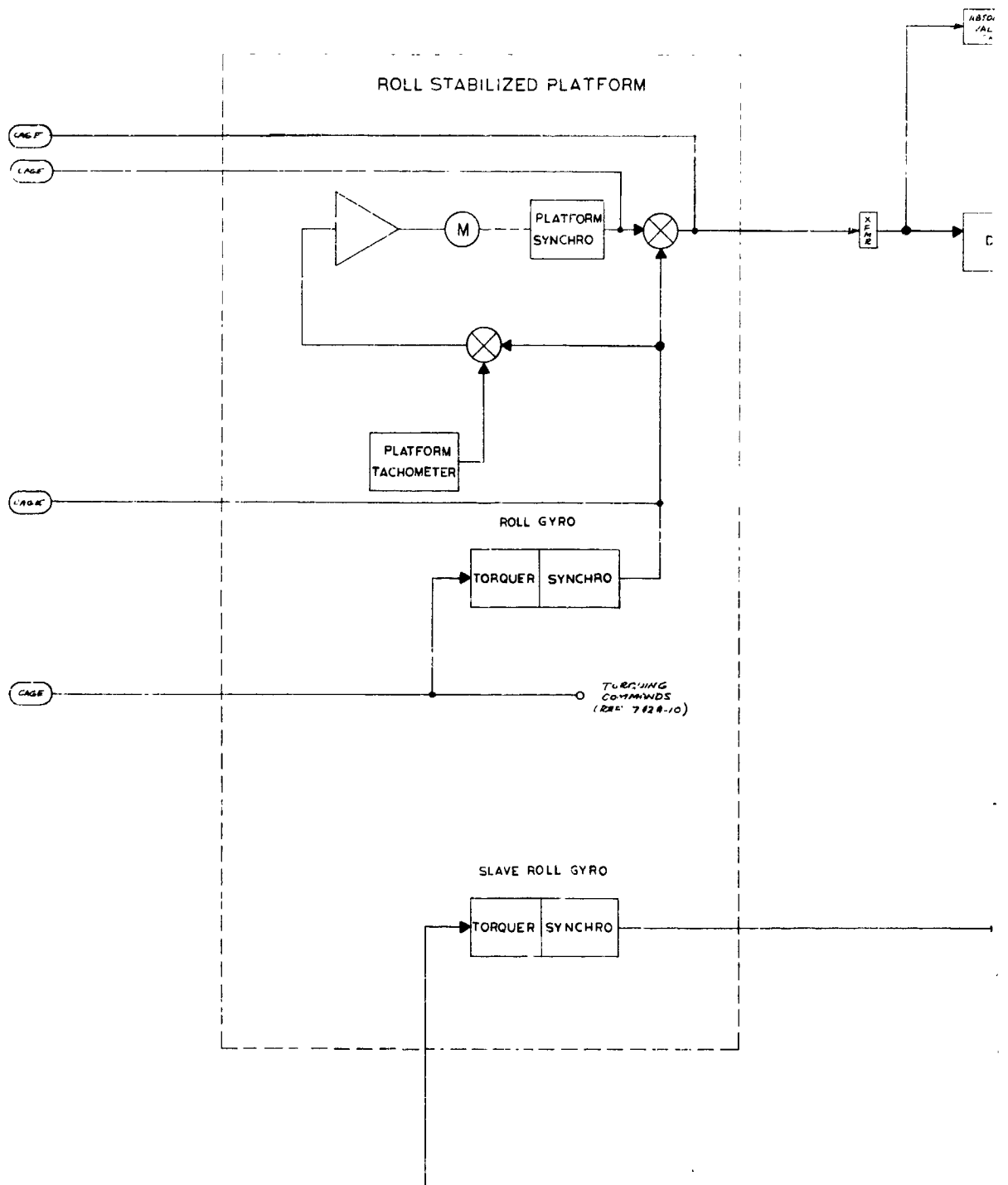
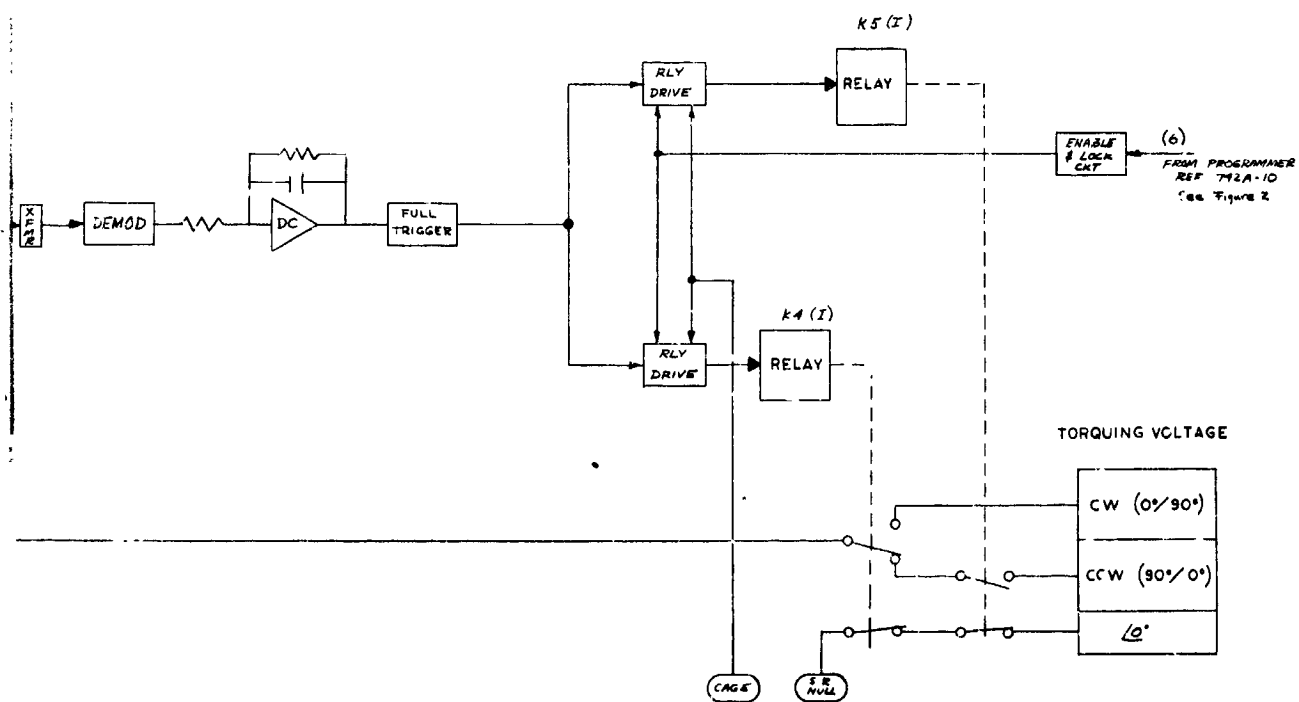
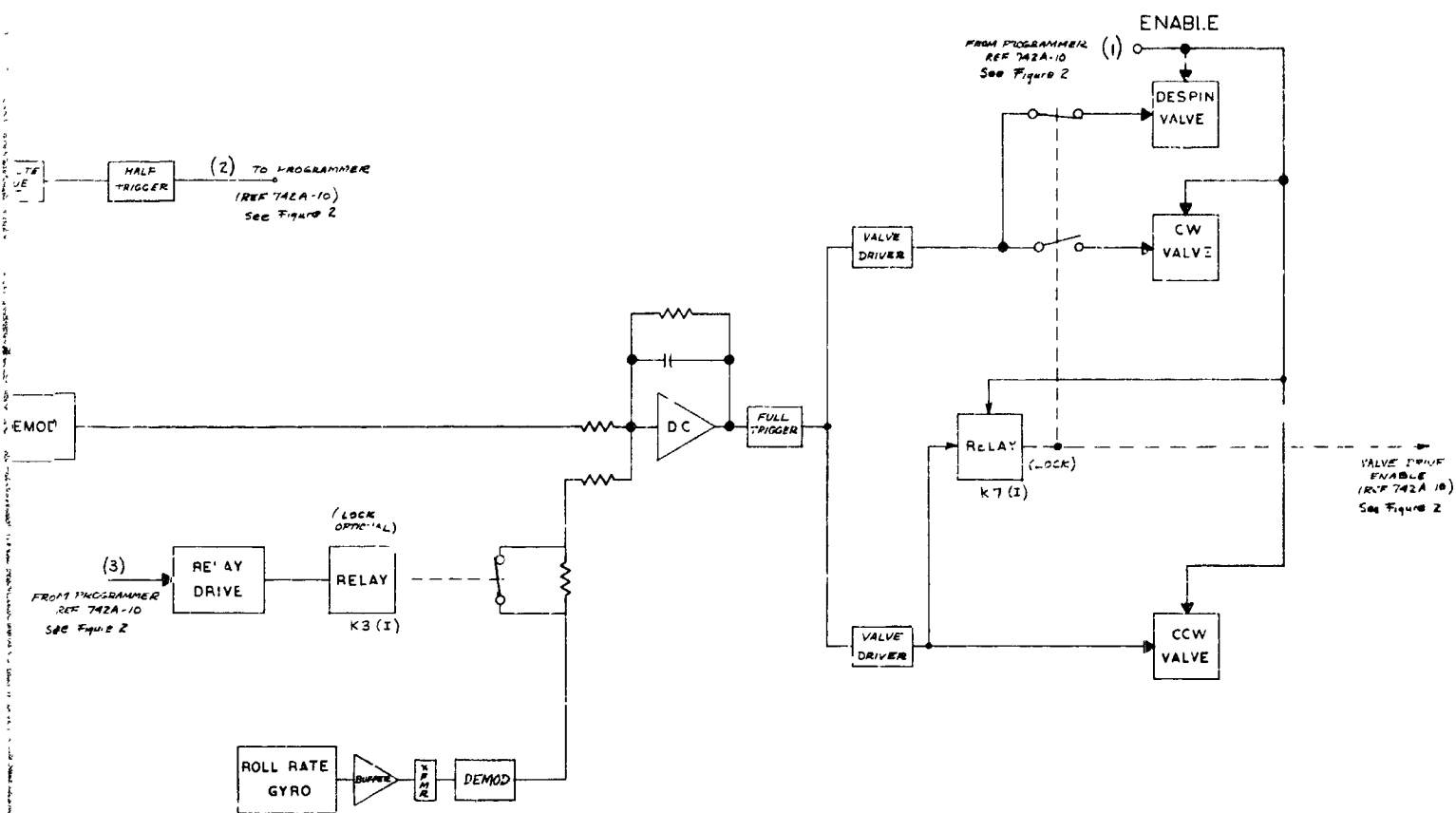


Figure 3. FACS Roll and S:



ave Roll, Block Diagram

### 3.1.1 FACS SEQUENCE OF OPERATION

#### 3.1.1.1 BEFORE LIFTOFF

External power is applied to the system 20 min prior to launch. The offset conditions required to compensate for gyro drift, tower tilt, and launch delays are determined and appropriate offset commands are applied to the gyros.

#### 3.1.1.2 POWERED FLIGHT

During powered flight the gyros maintain their offset-caged position except for small drift. The predictable portion of this drift is taken into consideration at the time of introducing offset commands. At burnout the gyros provide the inertial reference upon which the programmed maneuvers are based.

#### 3.1.1.3 SUSTAINER BURNOUT

At sustainer burnout, the thrust decay activates the propellant shutoff valves. Actuation of the "g" reduction switch initiates action of a unijunction timer by energizing self-locking relay K1(P)\*. The time-delay delays the despin operation until the vehicle altitude is sufficient to minimize roll aerodynamic moments.

#### 3.1.1.4 DESPIN AND ROLL CAPTURE

Upon completion of the delay-time interval, the timer circuit energizes self-locking relay K2(P) which arms the despin and roll-control valve circuit (1)\*\* , and also provides the first of two "AND" No. 1 signals needed for progression of the programmer sequence.

At this time the roll control channel is receiving position-plus-rate information from the roll stabilized platform and the roll rate gyro.

---

\* (P) designates programmer relay, (I) designates IACS control unit relay, and (S) designates SACS control unit relay.

\*\* Parenthetical numbers refer to points designated in Figures 2 and 3.

The presence of a vehicle CCW spin rate turns on the despin valve. The despin valve remains on until the roll position-plus-rate signal is reduced to within the switching thresholds. The roll control channel continues to produce appropriate valve switching action until the vehicle is oriented to the roll gyro null and body roll rate is low. The first turn-on of the roll CCW valve energizes self-locking relay K7(I), thus disabling the despin valve and permitting the roll CW valve to respond to switching commands. Energization of relay K7(I) also enables the IACS pitch and yaw valve drivers. Since the output signals of the pitch and yaw position gyros are grounded, the valve driver circuits operate off the rate gyro signals and thereby provide rate stabilization during the remaining period of roll capture.

At completion of roll capture, when the absolute value of the roll position error is reduced to within a fixed threshold level, the second necessary "AND" signal (2) is provided to the sequence logic at "AND" No. 1. Suitable filter action in the absolute value circuit prevents premature continuation of the sequence should the condition of zero position error plus high rate occur.

Presence of the necessary inputs at "AND" No. 1 results in programmer output (3) energizing relay K9(I) which isolates the pitch and yaw position error signals from ground and results in position-plus-rate control of the IACS valve trigger circuits. Relay K9(I) can be wired to provide a self-locking contact. In this configuration, position-plus-rate control is maintained without subsequent interruption. Programmer output (3) also energizes relay K3(I) which reduces roll rate gain after initial capture. Relay K3(I) can be wired to provide a self-locking contact. When used, the low value of roll rate gain is maintained without subsequent interruption.

#### 3.1.1.5 PITCH AND YAW CAPTURE

Completion of despin and roll capture permits removal of any pitch or yaw errors. The presence of error signals produces appropriate control valve action to orient the vehicle to the pitch and yaw gyro nulls and thus reduce error signals to a low value.

The absolute value detector circuits in the pitch and yaw channels provide inputs (4) and (5) to the programmer, and also energize relays K1(I) and



K2(1) used for rate-gain change. The rate-gain is automatically selected, depending upon whether position error is greater or less than the threshold of the half-trigger following the absolute value circuit. Relays K1(I) and K2(I) are energized when the position error is less than the trigger level.

#### 3.1.1.6 SLAVE OUTER GIMBAL OF YAW GYRO

Pitch and yaw position signals (4) and (5) together with roll-position signal (2) indicates completion of 3-axis capture. These inputs are applied to "AND" No. 2. The fourth condition necessary at "AND" No. 2 is always present when gyro torquing is not in process (i.e. relay K3(P) is de-energized). The presence of all four inputs at "AND" No. 2 produces a programmer output at (6) which triggers an SCR and enables the slaved-roll torquing relay drivers. These drivers control actuation of relays K4(I) and K5(I) to apply torquing voltages as necessary to hold the slaved-roll gimbal near null. This function is uninterrupted for the remainder of flight.

#### 3.1.1.7 BEGIN PROGRAMMED MANEUVERS AND HOLDS

The program sequence is now ready to begin the programmed maneuvers and holds. When the output from "AND" No. 2 is present, and flip-flop No. 1 is in the "zero" state, "AND" No. 3 provides a trigger for the one-shot multivibrator. Flip-flop No. 1 is held in the "zero" state in the ledex start position. Subsequent ledex action removes this "hold-zero" condition, and thereafter flip-flop No. 1 can be put in the "zero" state only at initiation of gyro torquing. Flip-flops Nos. 2 and 3 are each held in the "one" state in the ledex start position.

Action of the one-shot multivibrator provides a pulse which:

- a. Puts flip-flop No. 1 in "one" state. (With flip-flop No. 1 in the "one" state, changes in output of "AND" No. 2 are prevented from initiating repeat one-shot action.)
- b. Places flip-flop No. 2 in the "zero" state thereby initiating the hold timer (i.e., relay K7(P) is de-energized, thereby removing the shunt around the timing capacitor, and the integrator is permitted to operate).
- c. Steps the ledex one position.

#### 3.1.1.8

##### FIRST HOLD

Each ledex position establishes a hold time and maneuver command.

The function of each ledex deck is as follows:

- a. Ledex deck No. 1 controls the actuation of relays to make the appropriate selections on the sign and axis of maneuver. The maneuver itself does not occur until after the hold-time interval is over. Relay K5(P) determines the direction of maneuver, and relays K6(P) and K8(P) establish the axis of maneuver.
- b. Ledex deck No. 2 provides the resistance value required by the timer-integrator to produce the desired hold time and provides a signal to flip-flop No. 4 in the SACS when SACS operation is desired.
- c. Ledex deck No. 3 provides a patched-in comparison voltage to the comparator and trigger, thereby fixing the magnitude of the maneuver (i.e., angle through which the gyro is torqued).
- d. Ledex deck No. 4 provides a digitized output which permits identification of the ledex position at any time.

When the hold-time interval is complete, the output of the uni-junction timer puts flip-flop No. 2 in the "one" state thereby resetting the timer (i.e., energizing relay K7(P), and puts flip-flop No. 3 and flip-flop No. 4 in the "zero" state.

#### 3.1.1.9

##### INITIATE FIRST MANEUVER

Placing flip-flop No. 3 in the "zero" state actuates the torque-control relay driver. When the torque-control relay K3(P) is energized:

- a. Torquer voltage circuits are completed and torquing action is started. Since ledex deck No. 1 has established maneuver parameters, precession of only one of the gyro gimbals occurs. If the maneuver is in either the pitch or yaw axes, relays K6(P) and K8(P) apply an input to the torquing-control integrator to compensate for variations in gyro inner gimbal lag angle. (A discussion of lag angle compensation is included in Appendix X.)
- b. The shunt around the operational amplifier is removed, thereby permitting integration of the torquer voltage and current.

- c. Logic voltage is applied to place flip-flop No. 1 and flip-flop No. 4 in the "zero" state; concurrently the fourth input is removed from "AND" No. 2. (A one-shot trigger cannot occur with this input removed.)

#### 3.1.1.10 COMPLETE GYRO TORQUING

Gyro torquing continues until the desired torquing angle has been obtained. At this time, the comparator and trigger provide an output which returns flip-flop No. 3 to the "one" state. When flip-flop No. 3 goes to the "one" state, the torque control relay K3(P) is de-energized and:

- a. Torquer circuits are opened.
- b. The integrator capacitor is discharged.
- c. The flip-flop No. 1 and flip-flop No. 4 "zero" state signals are removed (the flip-flops remain in the "zero" state).
- d. The fourth signal (indicating not torquing) is reapplied to "AND" No. 2.

#### 3.1.1.11 COMPLETE FIRST MANEUVER

When all necessary inputs are present at "AND" No. 2 and "AND" No. 3 (i.e., all axis errors low, not torquing, and flip-flop No. 1 in "zero" state), the one-shot is again triggered and the ledex is stepped. This next ledex position can produce either a hold or a maneuver, as desired. The SACS portion of the FACS would be operative only during hold periods.

#### 3.1.1.12 ENABLE SACS

When flip-flop No. 4 is in the "zero" state, the SACS is disabled. When the IACS hold timer is started, a pulse is transmitted to flip-flop No. 4 in the SACS, placing it in the "one" state. The flip-flop state change provides an input to "AND" No. 4. This represents one of three conditions necessary at "AND" No. 4 to permit the SACS acquisition sequence to proceed.

### 3.1.1.13 SACS ACQUISITION

When both the pitch and yaw gyro errors are below a desired threshold value ( $0.4^{\circ}$ ) the output of half-trigger circuits provide the remaining two conditions at "AND" No. 4. With all three inputs present, time delay No. 1 is permitted to operate. When this condition persists for the time-delay interval, relay K5(S) is energized thereby enabling the relay drivers in the pitch and yaw gyro torquing circuits and enabling the IACS-to-SACS valve switchover circuits. Once K5(S) has energized, it is held energized through another relay driver which is operable so long as flip-flop No. 4 remains in the "one" state.

A similar sequence applies to "AND" No. 6, time delay No. 3, and relay K1(S). This relay provides a start signal for the stellar sensor.

With the gyro torquing circuits enabled, the presence of a fine sensor pointing error produces gyro torquing toward the desired target. Gyro torquing is controlled by relays K2(S), K3(S), K7(S) and K8(S). In general, initial gyro torquing occurs so rapidly that the half-trigger inputs at "AND" No. 5P and "AND" No. 5Y disappear and consequently valve switchover does not immediately occur. The IACS jets then accelerate the vehicle toward the target.

As the line-of-sight pointing errors become small, the gyro error signals also are reduced. When either the pitch or yaw gyro error signal is below the desired threshold level, the corresponding half trigger produces an input to "AND" No. 5. This input permits operation of time delay No. 2. When the gyro error remains below the threshold level for the time delay No. 2 interval, the IACS jets in that axis are disabled, and the SACS jets are enabled. This action is produced by relays K4(S) (pitch) and K6(S) (yaw).

The SACS jets are controlled by circuits operating off the fine sensor output signals. These circuits consist of operational amplifiers with low-lag characteristics, triggers, and valve drivers.

### 3.1.1.14 RETURN TO IACS CONTROL

When gyro torquing is again initiated by the programmer, flip-flop No. 4 is restored to the "zero" state. This removes the "AND" No. 4 input

and disables the K5(S) and K1(S) relay driver. De-energization of K5(S) disables the valve switchover circuits and control reverts to the coarse jets. The torquing relay drivers are disabled.

### 3.1.2 GYRO CAGING INTERFACE

Operation of the GSE caging circuits energizes relays which perform the following functions:

- K9(S) Connects the GSE torquing relays to the pitch gyro torquer (and isolates the SACS torquing circuits).
- K10(S) Provides the same function as above for the yaw gyro torquer.
- K4(P) Disables torque control relay K3(P) and sets flip-flop No. 3 in the "one" state thereby preventing application of torquing voltages through the programmer. Programmer output (7) must be present at the GSE before torquing voltages are applied from the GSE. This insures that relay K3(P) has been de-energized.
- K6(I) Disables all pitch and yaw valves; enables the IACS valve drivers. The valve drivers are used to provide a GSE monitor of the driver circuits.
- K8(I) Isolates the pitch and yaw position gyro demod outputs from ground so that position signals are transmitted to the valve-drive triggers.

Operation of the GSE caging circuit also enables the slaved roll torquing relay drivers, thereby caging the slaved roll gimbal.

### 3.1.3 CONTROL PARAMETERS

For convenience, block diagrams have been prepared to show parameter values in the FACS control circuit. These diagrams include all gain terms, filter characteristics, and trigger levels. Figure 4 shows pitch and yaw channels for both the IACS and SACS. Figure 5 shows the roll and slave roll channels.

Figure 6 shows the convention employed for roll, pitch, and yaw, body axis definition, and direction of rotation.









The polarity of DC signals and phase of AC signals in the FACS is related to angular rotation about the body axes in Tables 1 and 2. Table 1 shows the IACS sign and polarity designations and Table 2 shows the SACS designations.

### 3.2 BREADBOARD FACS

Photographs of the breadboard FACS structure, with all of the subassemblies mounted thereon, are shown in Figures 7, 8, 9, and 10. Each photo shows a different quadrant of the cruciform-shaped structure. There are two compartments in each quadrant for a total of eight subassembly compartments.

All of the breadboard subassemblies, except for the "J" box, are easily removable from the main FACS mounting structure. The "J" box, and associated system pig-tail harnessing, was assembled on the structure. The programmer, IACS control electronics, SACS control electronics, and telemetry signal conditioner are all plug-in units to the main structure. The photograph in Figure 8 shows the structure harness/subassembly plug-in connector technique used for these four units. The vacant compartment (spare) shown in the photo was later used to mount the GSFC delayed-feedback circuitry for the SACS.

### 3.3 BREADBOARD GSE

The FACS breadboard ground support equipment is shown in Figures 11, 12, and 13. This equipment was used for system checkout during the bench tests at SSC and the 3-axis simulator tests at GSFC. The GSE console provides all necessary switching control and gyro caging (or offset caging) circuitry required for full remote control of the FACS during test. The GSE is connected to the FACS, except during 3-axis tests, via an umbilical cable. When more complete information about the system is required during static tests, a test cable is provided for further interconnection between the system and GSE.

Table 1

## PHASE AND RELAY ACTIVITY DEFINITION - IACS

Axis	Cause					Effect				
	Programmer Maneuver Command To Torquer	Voltage Applied To Torquer Control Winding	Vehicle Motion	Vehicle Rate	Demod Output Polarity	Phase of Resulting Error	Console Indicator	Jet Actuated	Vehicle Response To Jet	
Roll	CW	<u><math>\angle +90^\circ</math></u>	CCW	CCW	+	$0^\circ$	CW	CW	CW	
	CCW	<u><math>\angle 0^\circ</math></u>	CW	CW	-	$180^\circ$	CCW	CCW	CCW	
Pitch	CW	<u><math>\angle +90^\circ</math></u>	CCW	CCW	+	$0^\circ$	CW	CW	CW	
	CCW	<u><math>\angle 0^\circ</math></u>	CW	CW	-	$180^\circ$	CCW	CCW	CCW	
Yaw	CW	<u><math>\angle +90^\circ</math></u>	CCW	CCW	+	$0^\circ$	CW	CW	CW	
	CCW	<u><math>\angle 0^\circ</math></u>	CW	CW	-	$180^\circ$	CCW	CCW	CCW	

Axis	Phase of Error	Demod Output Polarity	Relay Actuated	Voltage Applied To Torquer Control Winding
S. Roll	$0^\circ$	+	K12	$\angle 0^\circ$
	$180^\circ$	-	K11	$\angle +90^\circ$

Table 2

## PHASE AND POLARITY DEFINITION - SACS

Axis	Cause		Effect					
	S. Sensor Output Polarity	Vehicle Position	Gyro Torqued	Demod Output Polarity	LT Valve Actuated	HT Valve Actuated	Console Valve Indicator	Vehicle Response To Jet
Pitch (Look in Jet 2)	+	CW	CCW	-	CCW	CCW	CCW	CCW
	-	CCW	CW	+	CW	CW	CW	CW
Yaw (Look in Jet 3)	+	CW	CCW	-	CCW	CCW	CCW	CCW
	-	CCW	CW	+	CW	CW	CW	CW



742/009

Figure 7. Breadboard FACS, View No. 1



742/007

Figure 8. Breadboard FACS, View No. 2

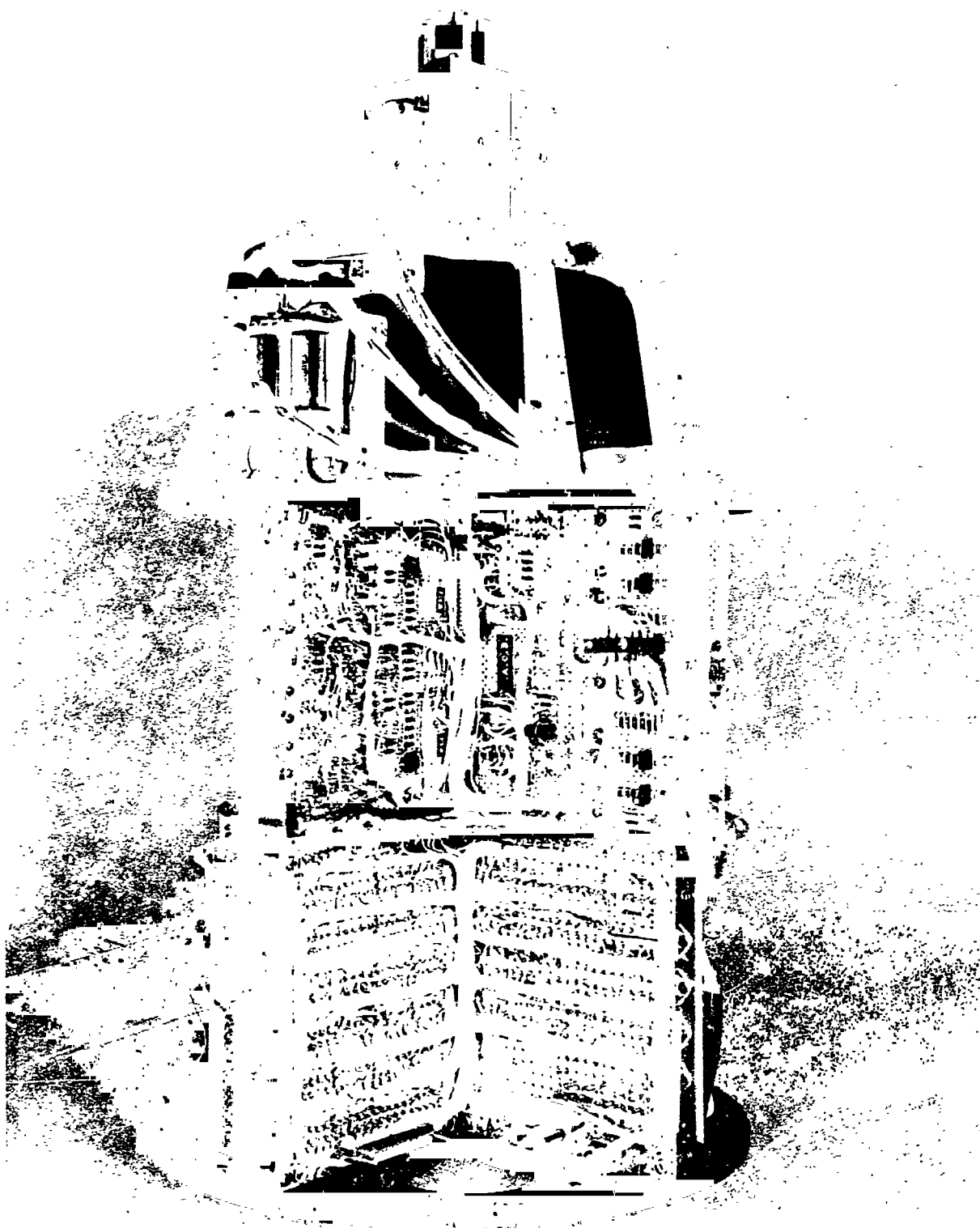
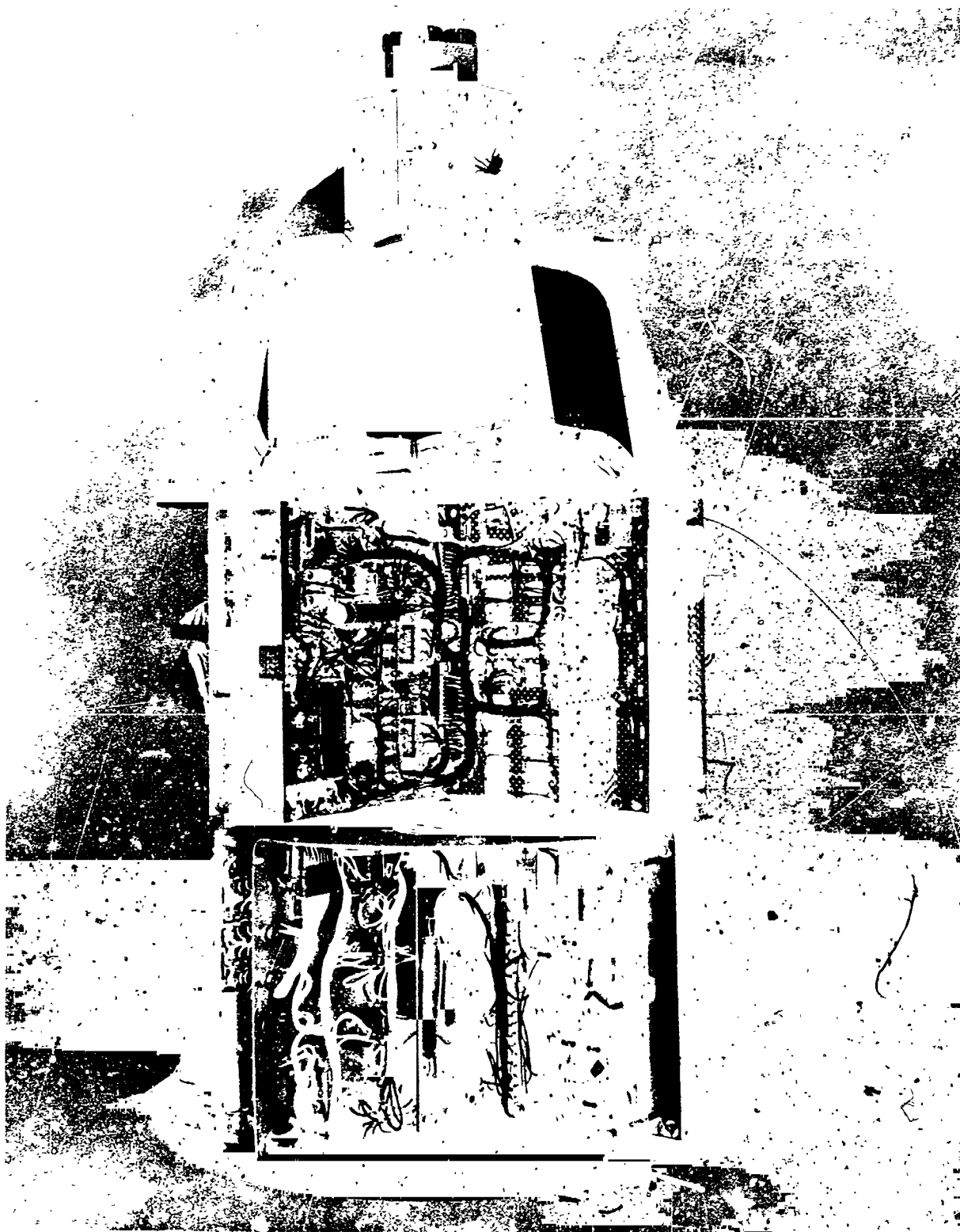
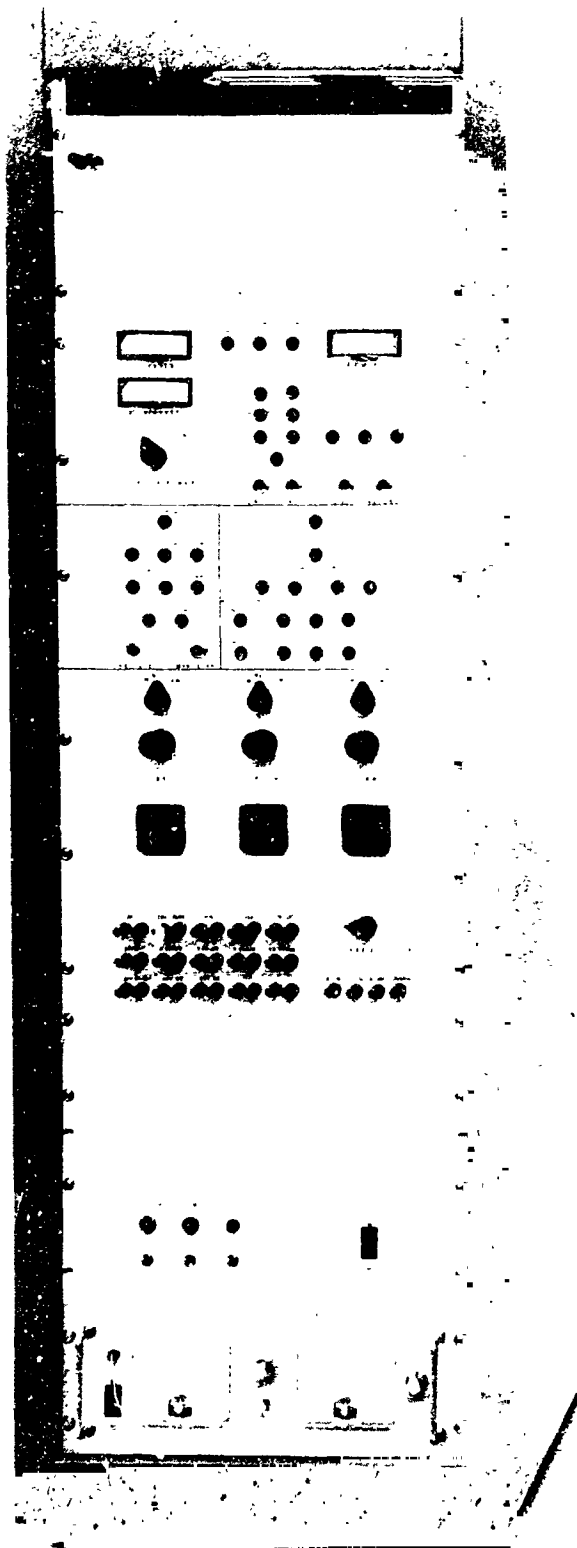


Figure 9. Breadboard FACS, View No. 3



7-2/68

Figure 10. Breadboard FACS, View No. 4



42, 14

Figure 11. Breadboard GSE, Front View



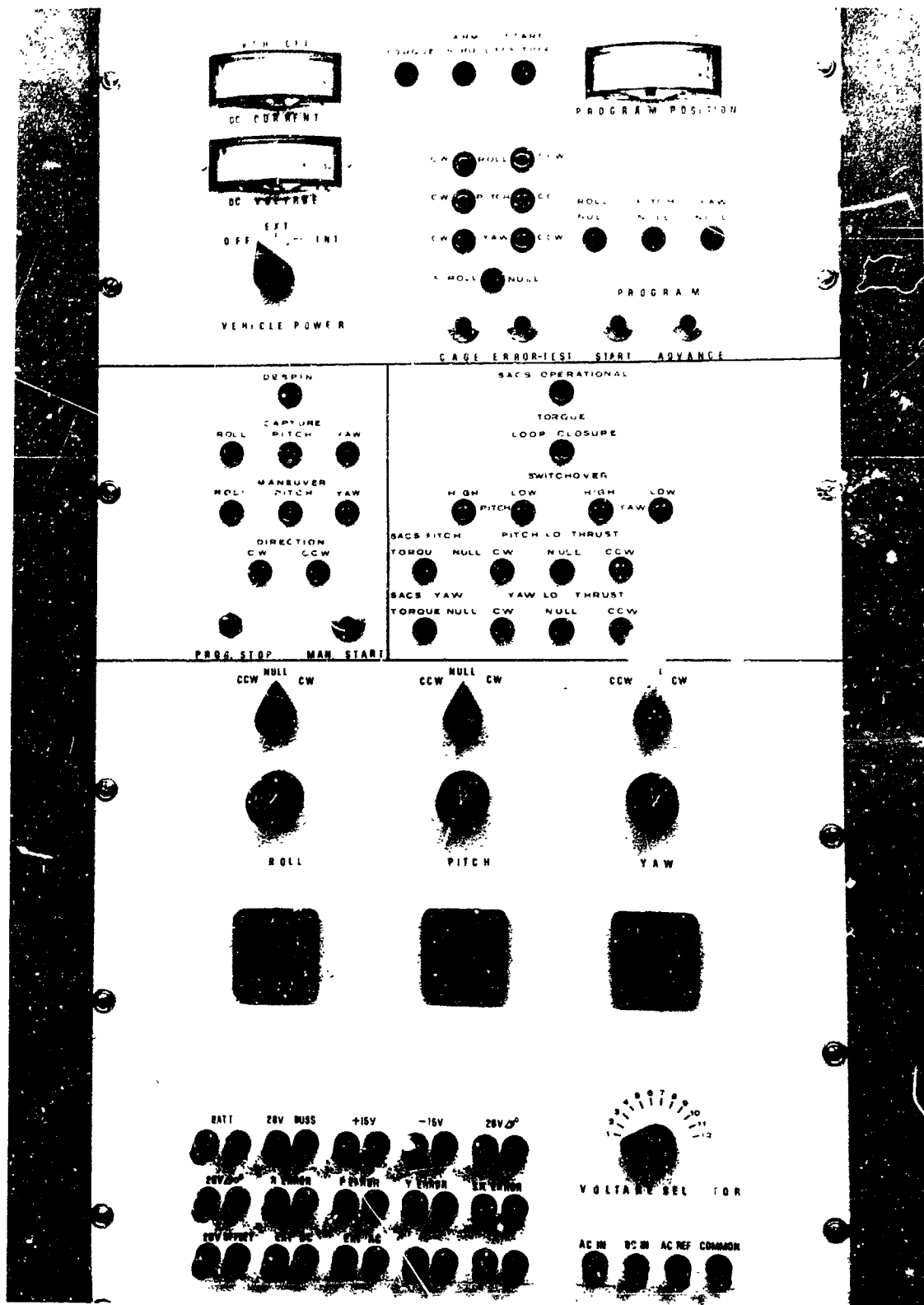
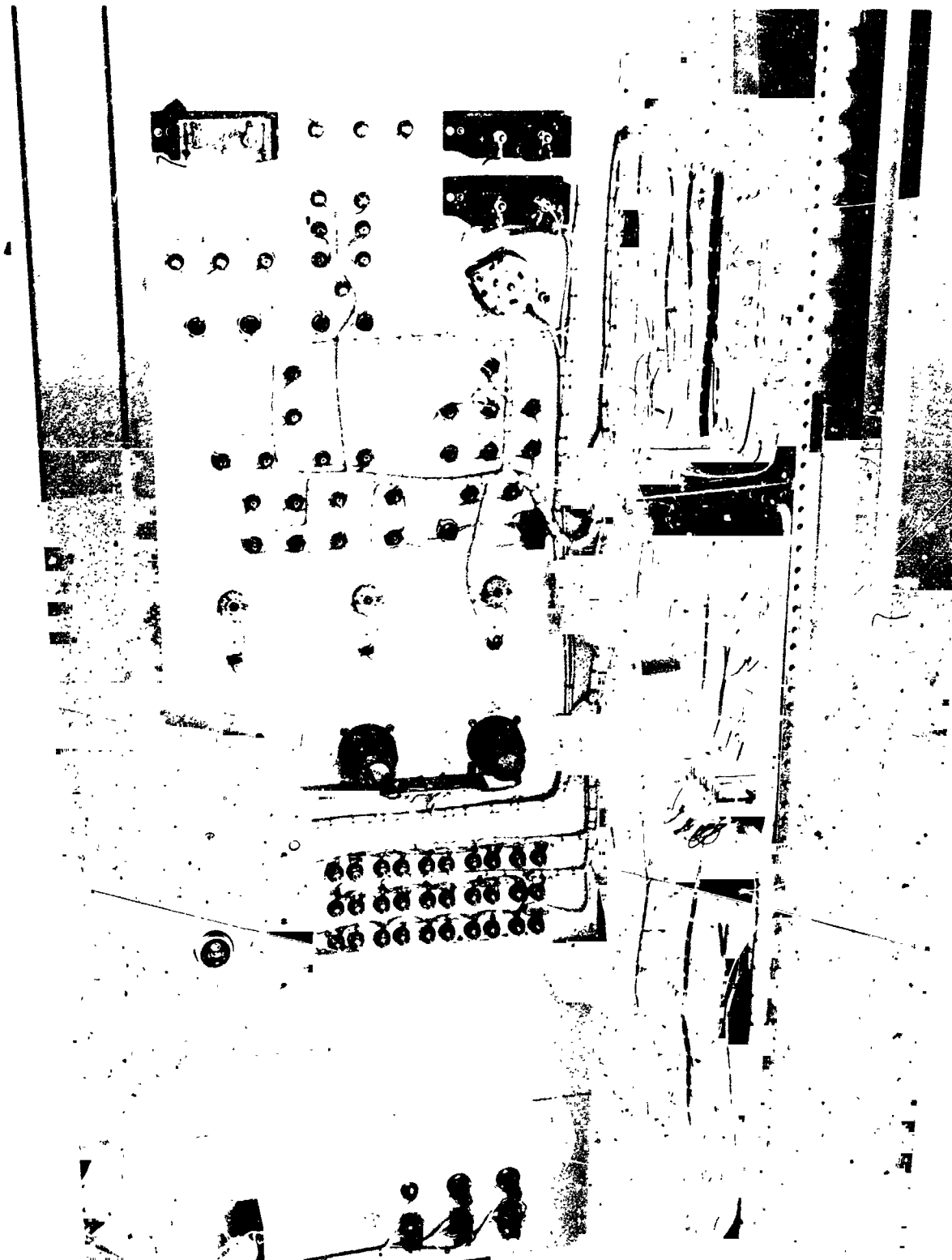


Figure 12. Breadboard GSF, Panel



742/005

Figure 13. Breadboard GSE, Inside View

### 3.4 FACS SUBASSEMBLIES

The breadboard FACS is divided into ten major subassemblies as follows:

Static Inverter	Telemetry Signal Conditioner
DC Power Supply	"J" Box
Programmer	Roll Stabilizer Platform
IACS Control Electronics	Rate Gyros
SACS Control Electronics	Fine Sensor (Stellar or Solar)

Complete subassembly detailed functional descriptions, schematic diagrams, and component layout drawings are presented in Appendix I. A complete parts list of all the FACS subassemblies is presented in Appendix II. Test data from the bench tests for the subassemblies (and the modules contained within them) are presented in Appendix IV.

#### 3.4.1 STATIC INVERTER

The static inverter is a sine-wave, 2-phase, DC-to-AC inverter. All of the 400-cycle AC power for the FACS and supporting GSE is supplied by this subassembly. A photograph of the breadboard static inverter is shown in Figure 14. This photo was taken prior to bench testing and therefore doesn't show the heat sink transfer block into which the output power transistors were later mounted. During the static inverter bench tests, all of the specified requirements for the AC power supply described in Section 2 of this report were achieved.

#### 3.4.2 DC POWER SUPPLY

The FACS logic and control circuits require a  $\pm 15$ -VDC power supply. The requirements for the DC power supply, Section 2 of this report, were modified prior to construction of the breadboard. The original GSFC requirement was that the static inverter be the source of input power for both the positive and negative DC regulators of the DC power supply. Approval to

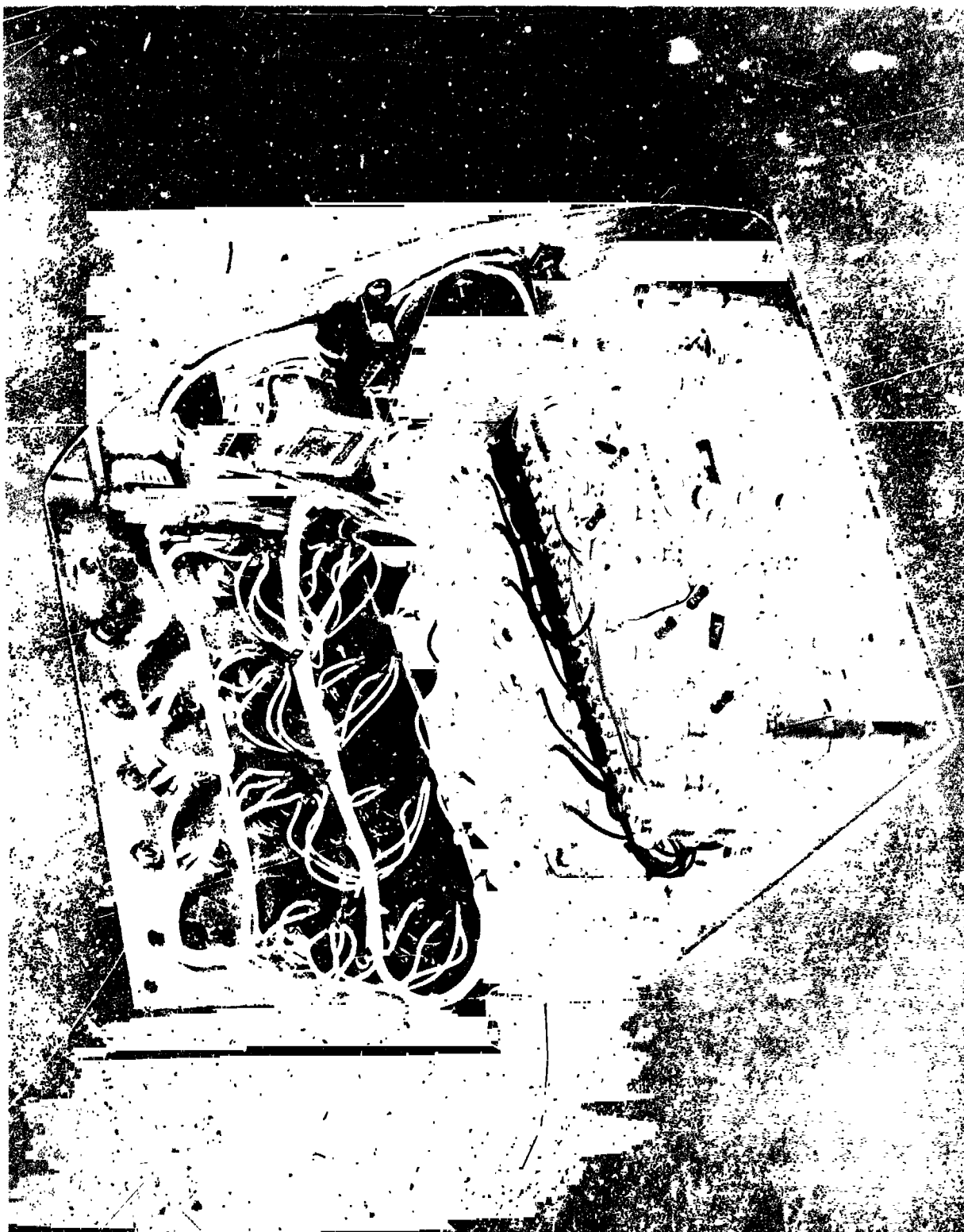


Figure 14. Breadboard Static Inverter Subassembly

742/001

supply only the -15-VDC regulator by the static inverter, and to use the unregulated + 28 VDC of the FACS for the + 15-VDC regulator, was later acquired from GSFC. A photograph of the breadboard DC power supply is shown in Figure 15.

### 3.4.3 PROGRAMMER

The programmer subassembly includes the necessary logic/timing circuitry for coast-time delay, maneuver-command storage, gyro torquing, target viewing time, and sequence control.

The programmer contains all of the system logic and sequencing required for use of just the IACS portion of the FACS in the IACS mode. Additionally, appropriate logic signals are provided at the interface with the SACS control electronics to enable the SACS circuits at the start of target-holding, and to disable the SACS circuits upon start of IACS maneuvers.

A patchboard panel is incorporated in the programmer to provide maximum flexibility with minimum time required for programming. The patchboard panel consists of a printed circuit matrix where the vertical and horizontal strips are on opposite sides of the board. Small screws connect a horizontal and a vertical crossing point to effect a program function.

Program functions that are patched include the axis and direction for each maneuver, and the sequence of hold times on each target. Duration of each "hold" is determined by resistors mounted on a terminal strip next to the patch-board panel. Maneuvers and holds can be patch-programmed in any sequence desired by the experimenter. The magnitude of each maneuver is selected by setting precision potentiometers for a suitable reference voltage to be applied to the comparator circuit in the variable-time-torquing section of the programmer. Photographs of the breadboard programmer are shown in Figures 16 and 17.

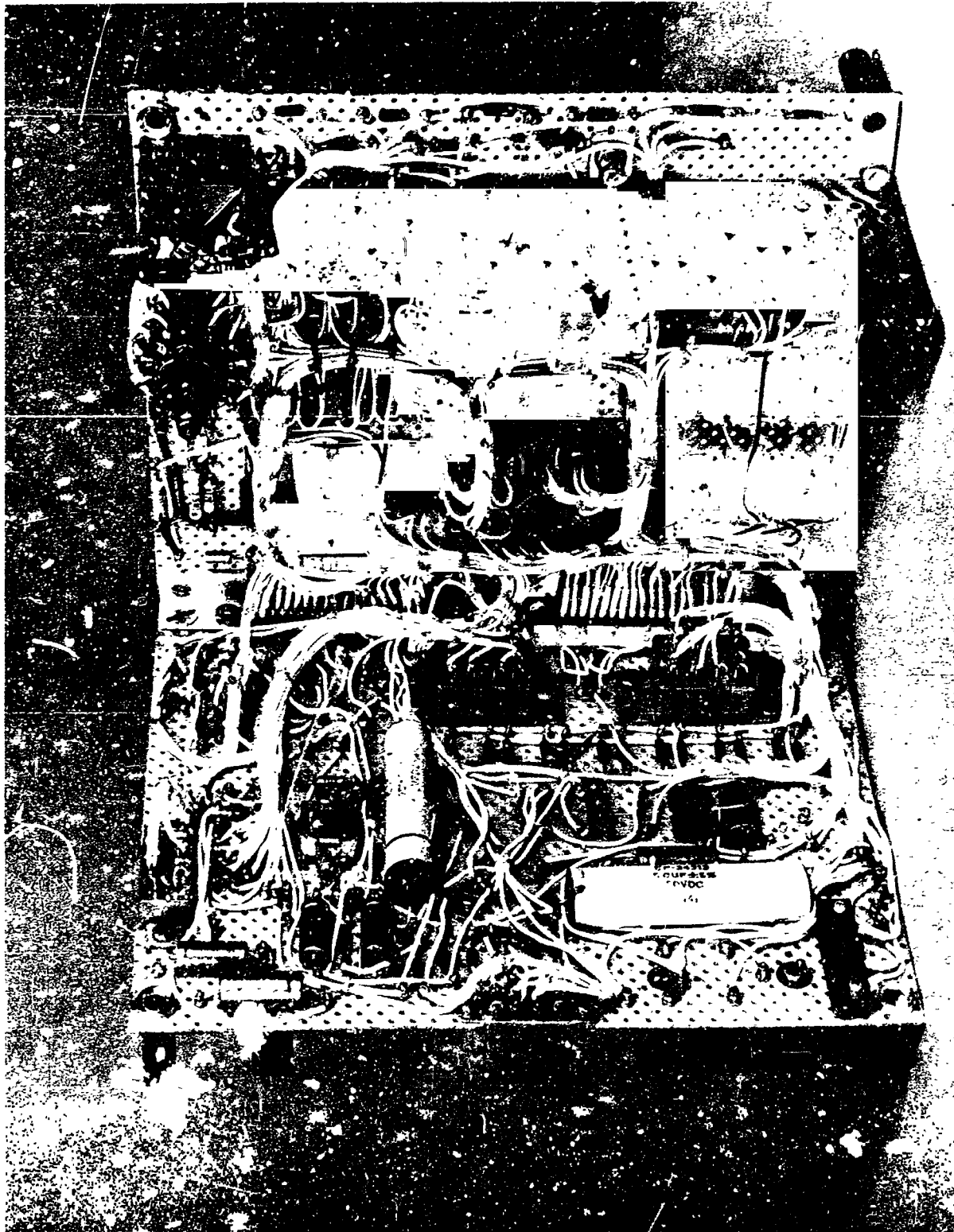
### 3.4.4 IACS CONTROL ELECTRONICS

The IACS control electronics subassembly contains the required control circuitry for the roll, pitch and yaw high thrust valves as well as the slaving of the yaw gyro outer gimbal. Also included in the IACS control electronics are the absolute value level detector circuits which monitor the position



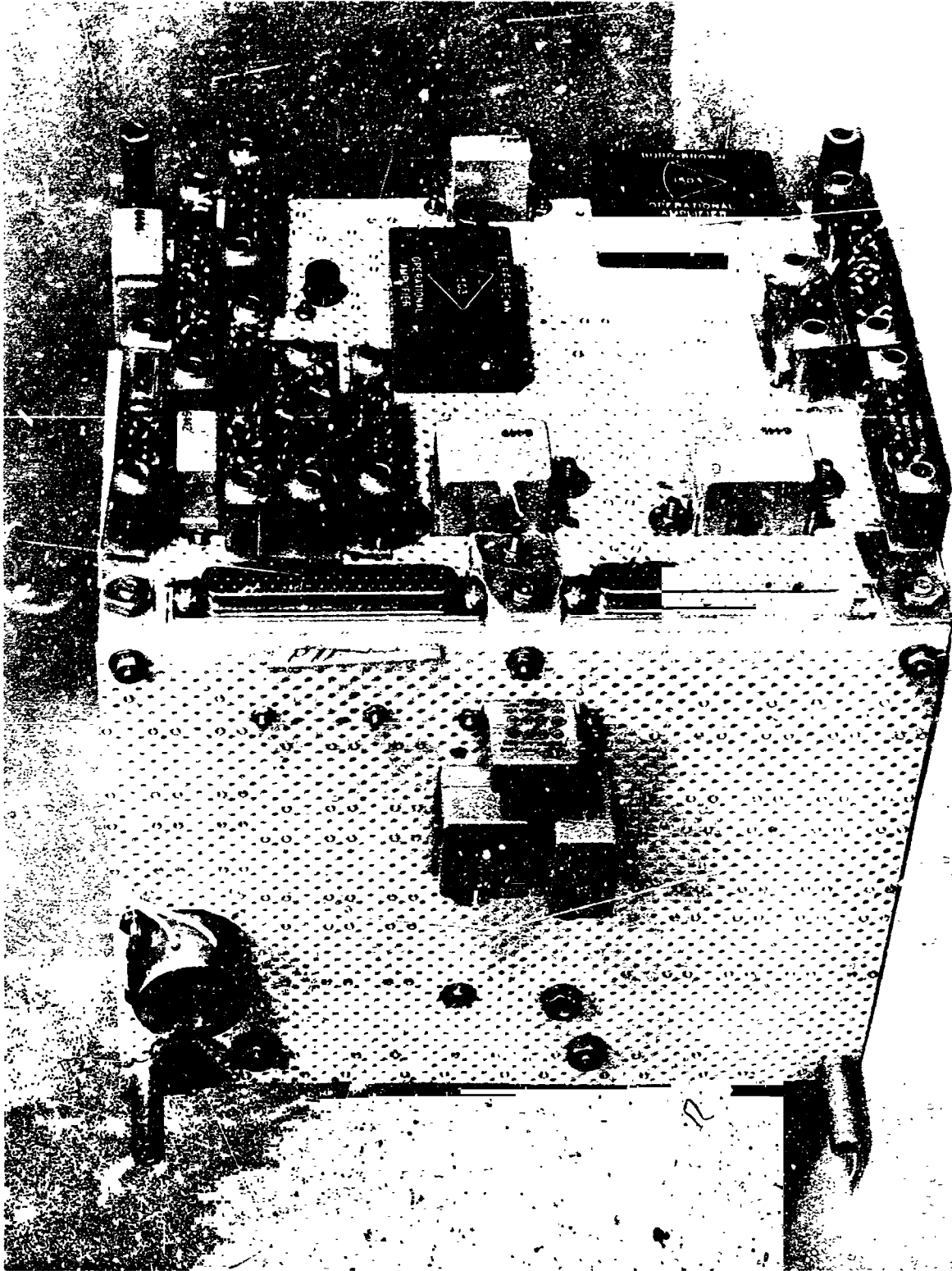
Figure 15. Breadboard DC Power Supply Subassembly

742/019



742/012

Figure 16. Breadboard Programmer Subassembly, Front View



742/002

Figure 17. Breadboard Programmer Subassembly, Rear View



gyro error signals in roll, pitch and yaw, and provide an output which indicates vehicle "capture" in each respective axis. These "capture" outputs are used to control bi-level rate gain in the coarse control circuitry and also are used by the programmer for program logic sequencing. Photographs of the IACS control electronics subassembly are shown in Figures 18 and 19.

#### 3.4.5 SACS CONTROL ELECTRONICS

The SACS control electronics subassembly contains all the logic/timing and control circuitry necessary for the adaptation of an IACS to a full FACS configuration. Provision is made for all logic and sensing circuitry needed for target acquisition and subsequent transfer of control from the IACS to the SACS.

The SACS control circuits amplify and shape the fine sensor output to provide position-plus-rate signals to the switching circuits that drive the fine control valves. Provision is also made for gyro torquing control to produce the desired correspondence between gyro and fine sensor reference. Photographs of the SACS control electronics subassembly are shown in Figures 20 and 21.

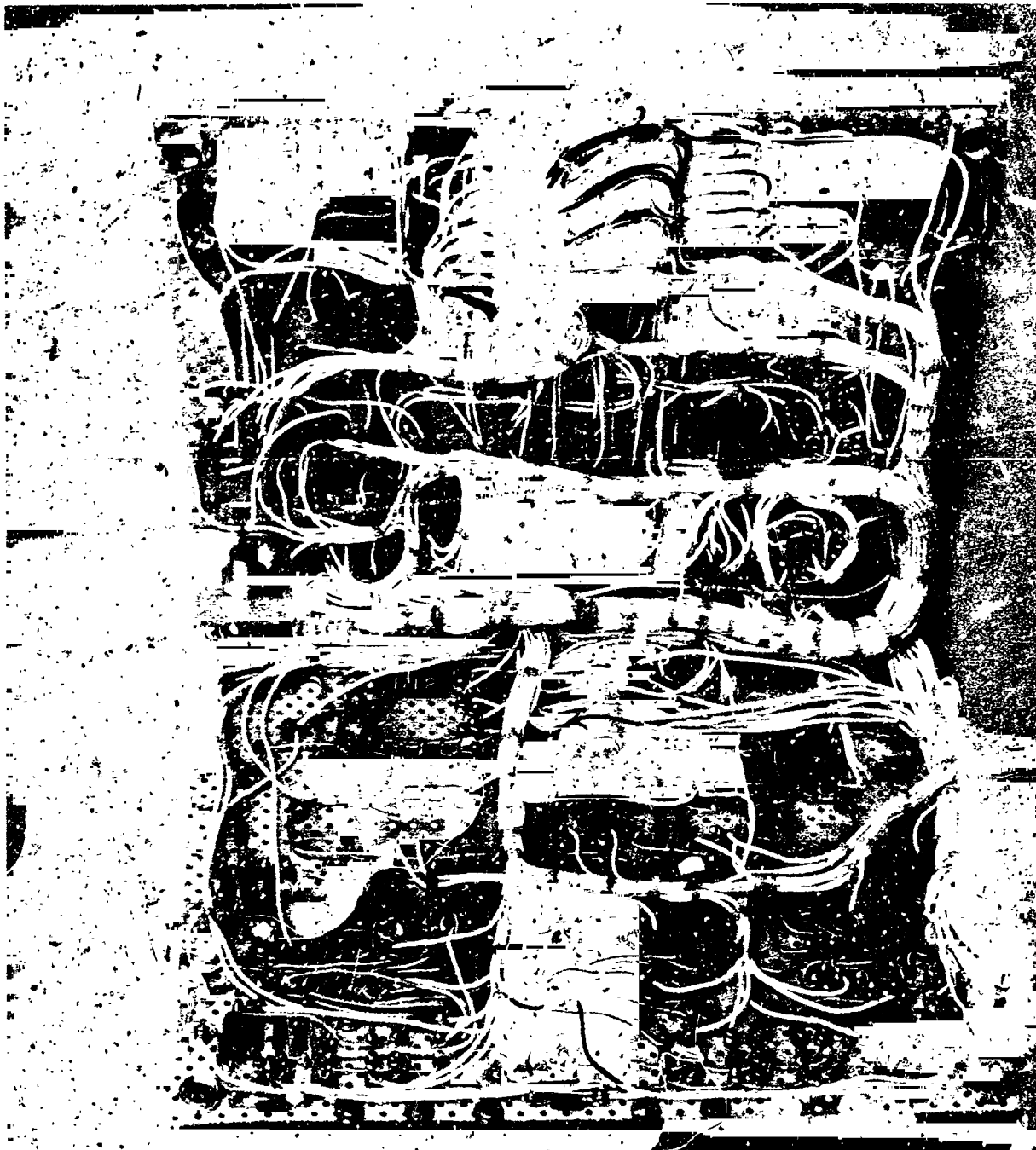
#### 3.4.6 TELEMETRY SIGNAL CONDITIONER

The telemetry signal conditioning subassembly provides pre-telemetry conditioning of all monitored signals from the FACS. All outputs from this unit are conditioned zero to +5 VDC (with the exception of the 400-cycle frequency monitor which is fed directly to the transmitter of the telemetry system being used) for ready use by most telemetry systems in general use.

Photographs of the Telemetry Signal Conditioning subassembly are shown in Figures 22 and 23. A complete calibration procedure of this unit is presented in Appendix VI.

#### 3.4.7 JUNCTION BOX

All of the FACS subassemblies are interconnected in the "J" box shown in the lower compartment of Figure 9. The "J" box is the central distribution point of all system power and contains the power switchover relay for transferring from external to internal +28-VDC battery power.



742/014

Figure 18. Breadboard IACS Control Electronics Subassembly, Front View

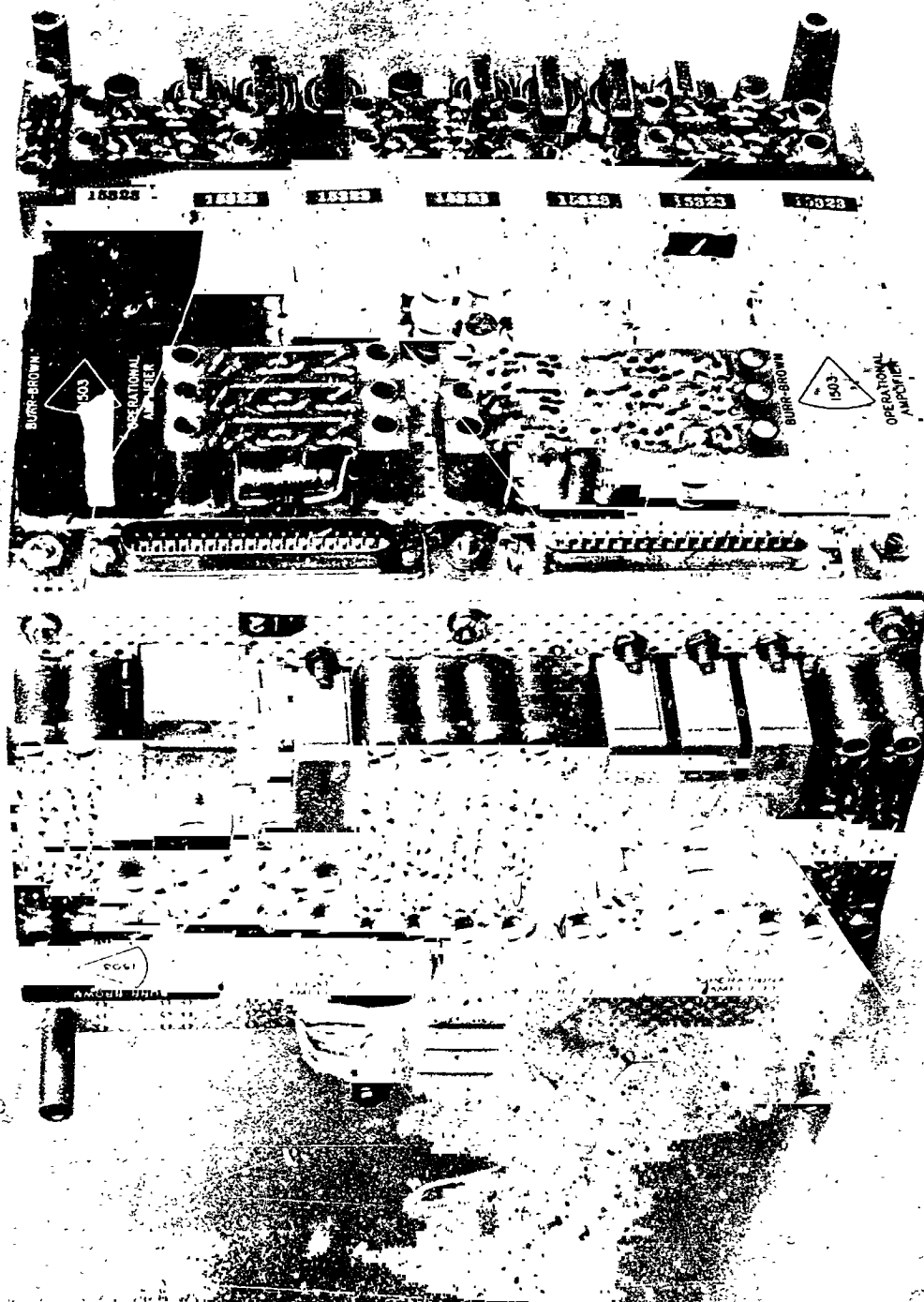
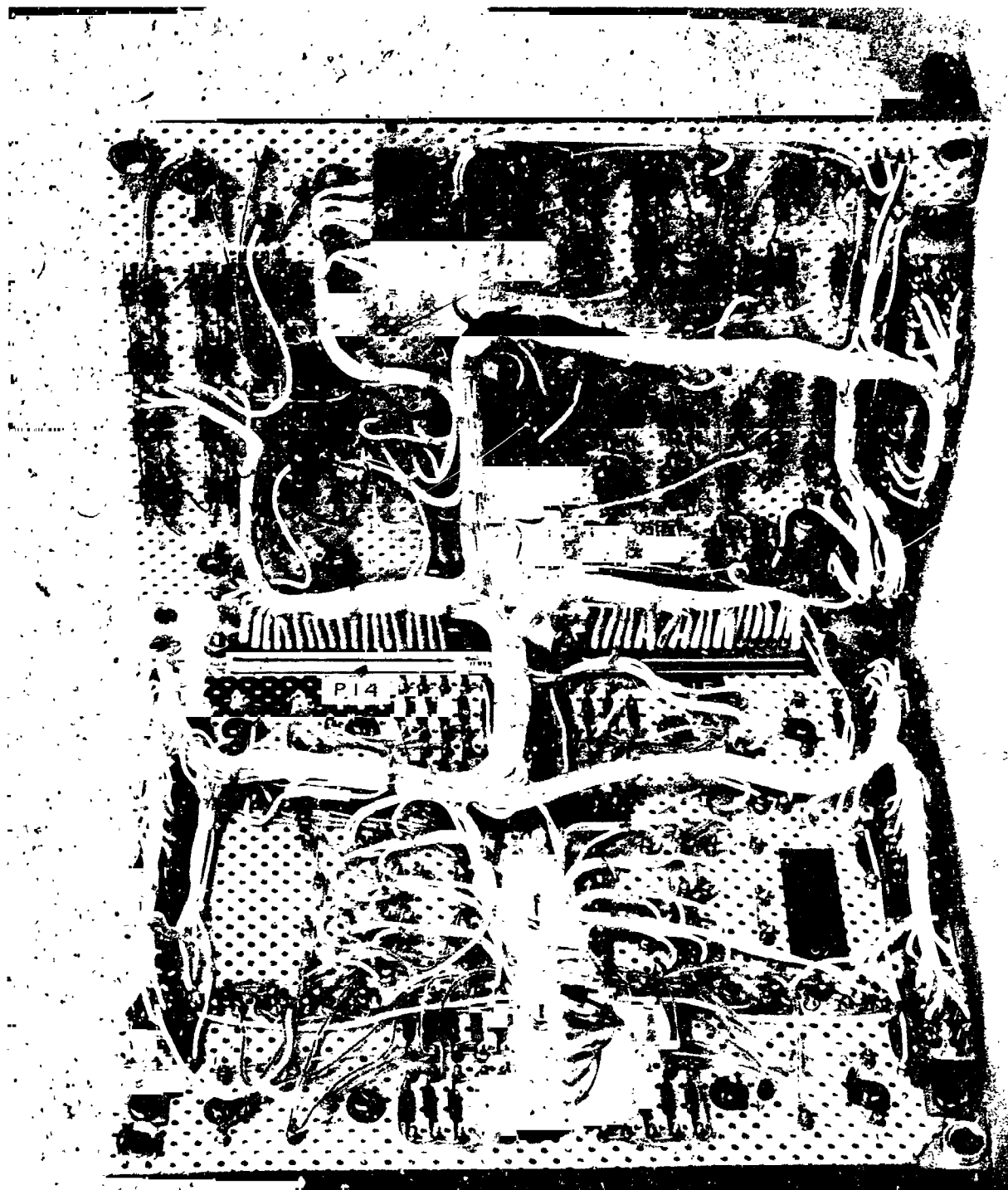


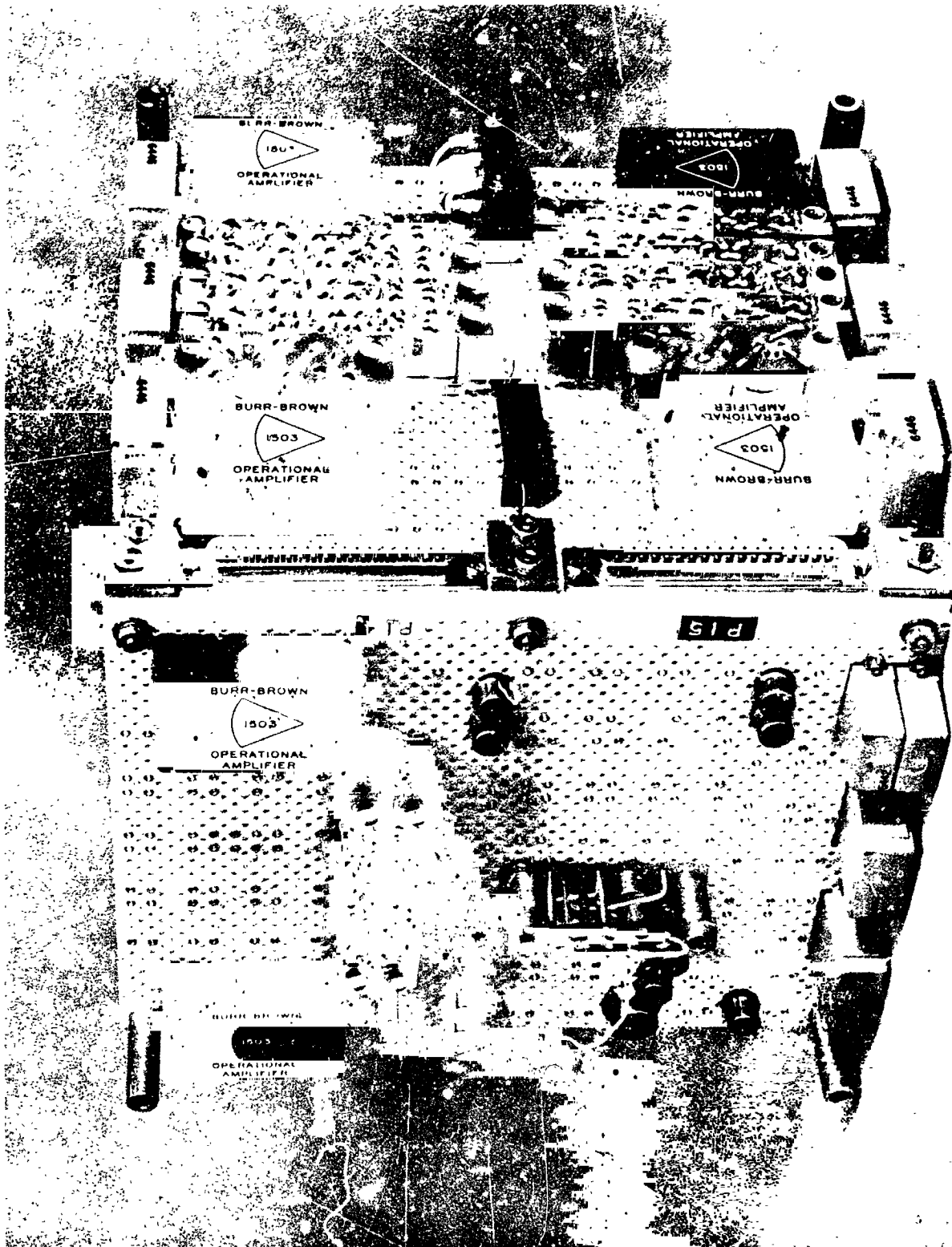
Figure 19. Breadboard IACS Control Electronics Subassembly, Rear View

742/C.5



742/013

Figure 20. Breadboard SACS Control Electronics Subassembly, Front View



742/016

Figure 21. Breadboard SACS Control Electronics Subassembly, Rear View

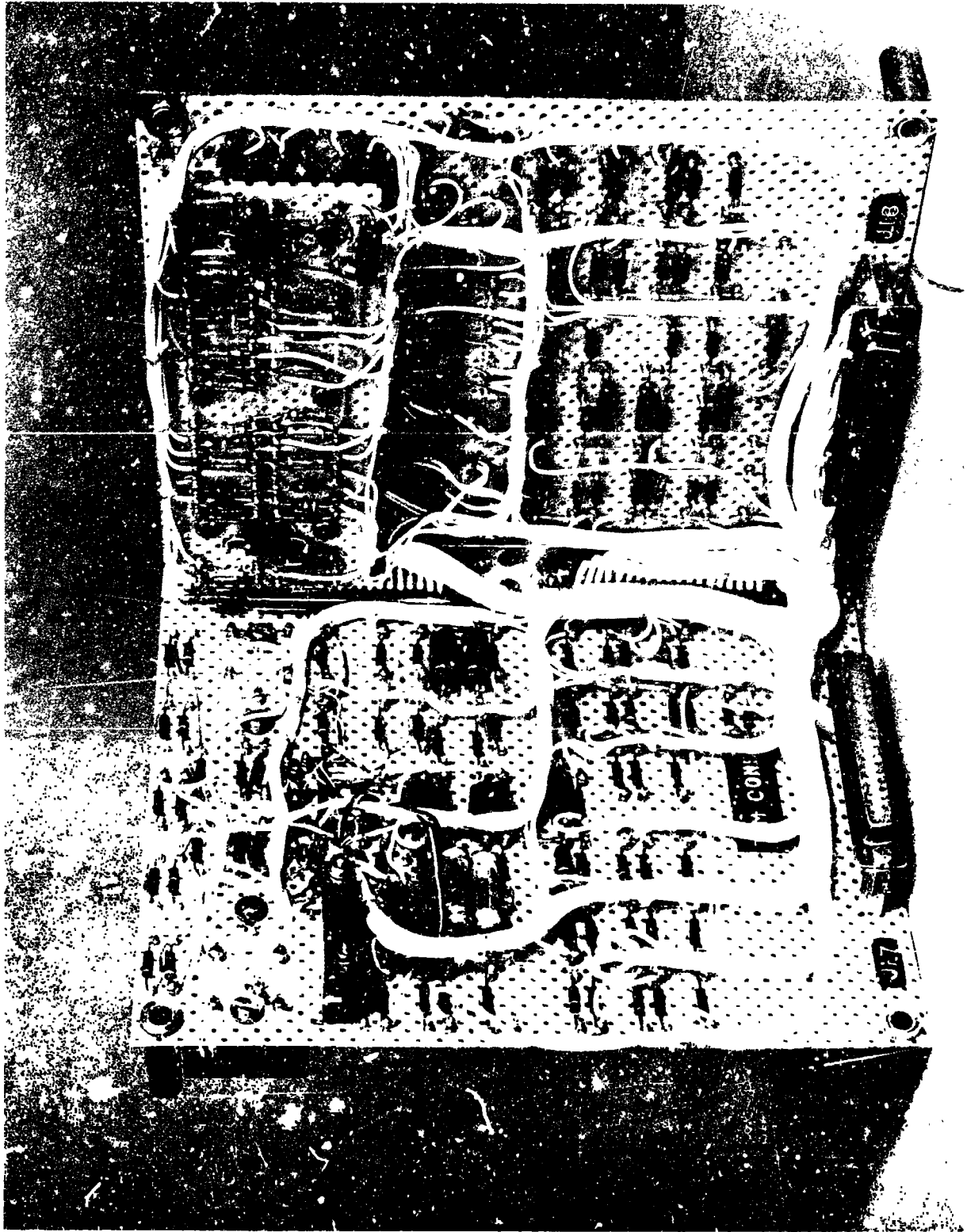


Figure 22. Breadboard Telemetry Conditioning Subassembly, Front View

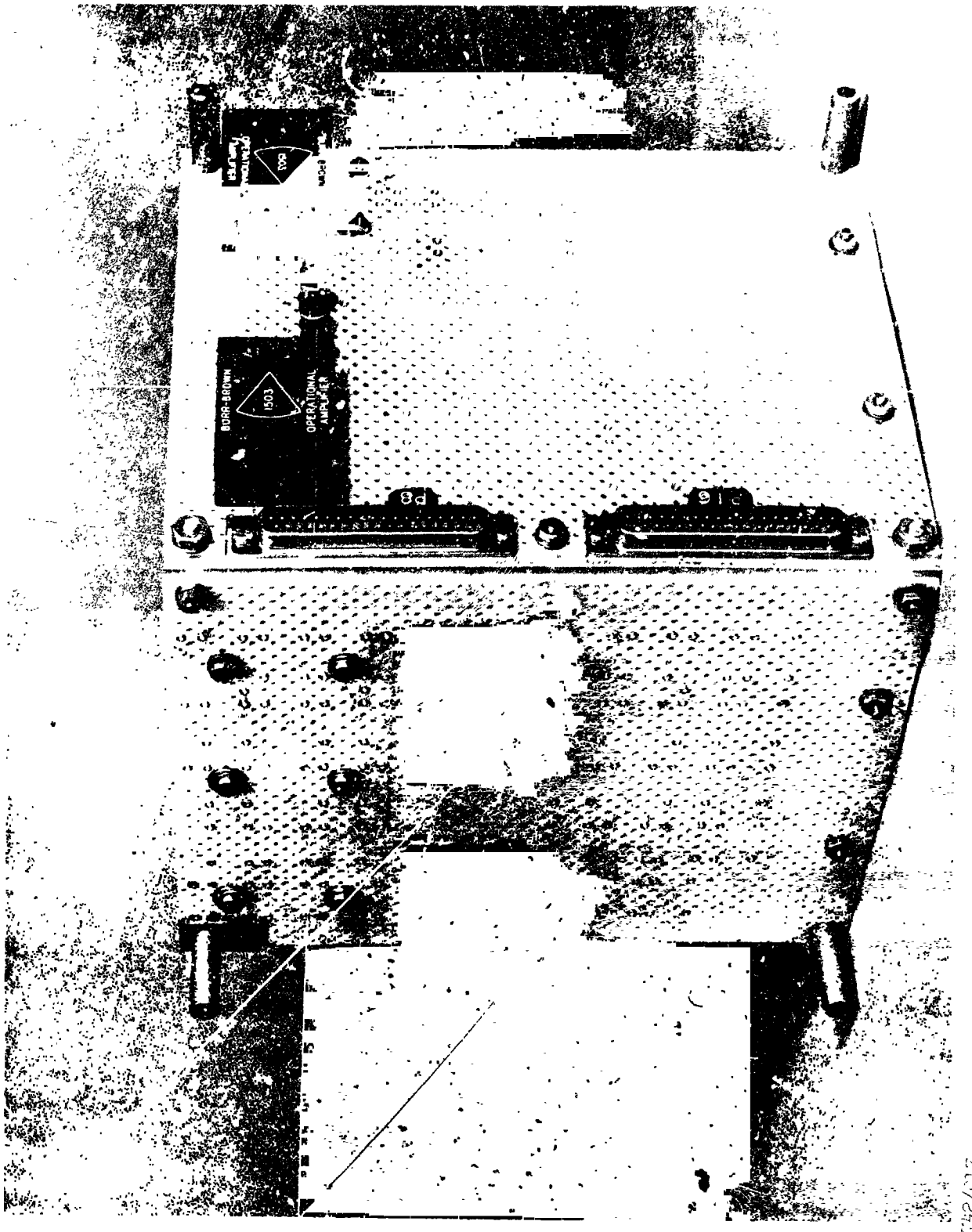


Figure 23. Breadboard Telemetry Conditioning Subassembly, Rear View

#### 3.4.8 ROLL STABILIZED PLATFORM

The roll stabilized platform (RSP) incorporates two free gyros which provide the inertial reference for the IACS. This subassembly has undergone successful development and flight test. A photograph of the RSP is shown in Figure 24.

The platform mount is servo driven to continually null the output of the roll gyro synchro, thereby maintaining an essentially stable roll platform for vehicle spin rates up to 3.0 rps. A tachometer, which senses platform rate relative to the vehicle, provides the necessary damping. Vehicle roll position error is obtained by combining the output signals from the roll gyro synchro and from a platform position synchro. This technique effectively eliminates any platform dynamics from the vehicle roll-control loop and the roll-gyro caging loop. The inner gimbals of the two gyros provide the pitch and yaw reference. The FACS RSP will meet all of the requirements specified in Section 2 of this report.

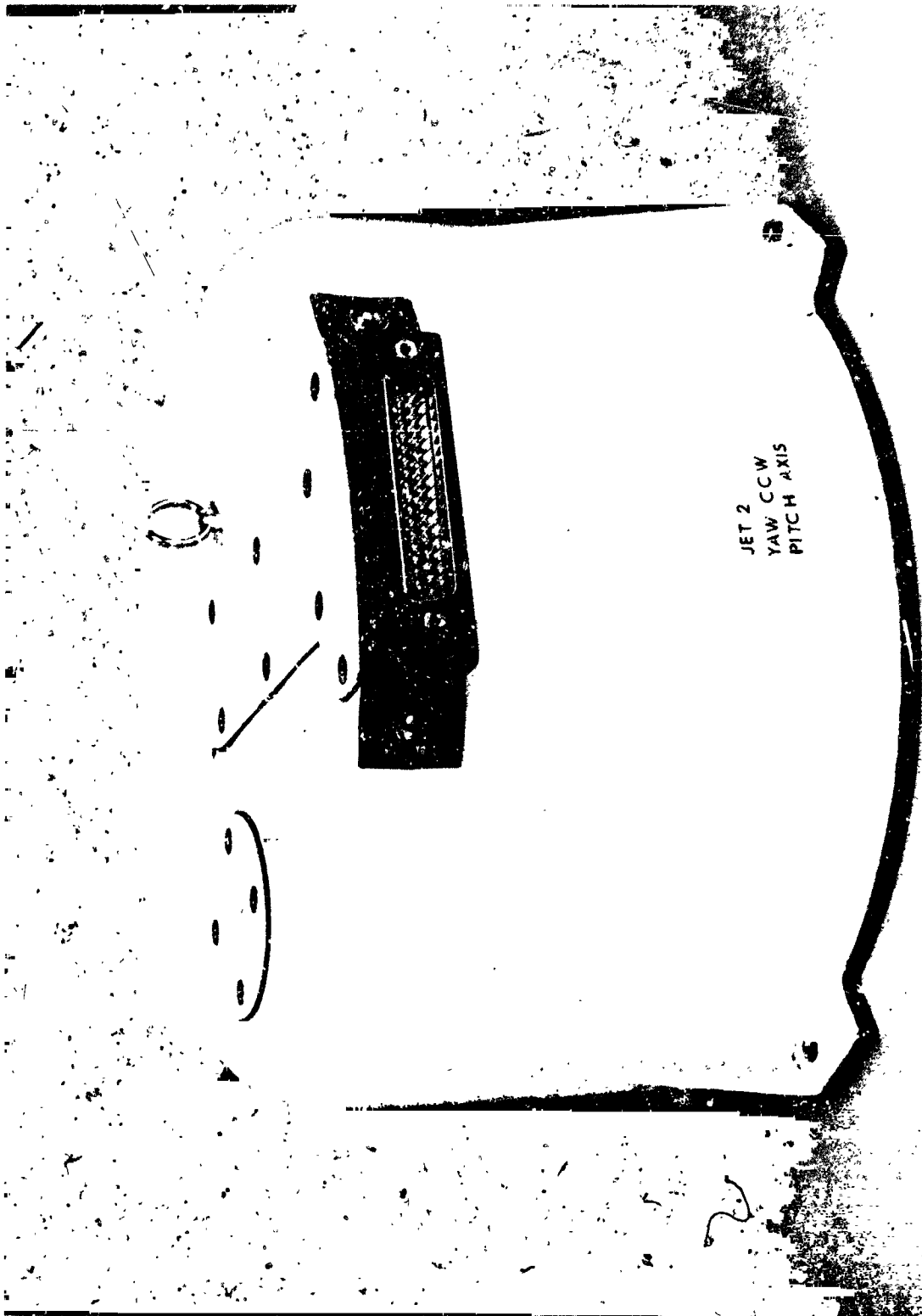
#### 3.4.9 RATE GYROS

The rate gyro subassembly contains the roll, pitch and yaw rate gyros that are used for rate feedback stabilization of the IACS control loops. The three rate gyros form a single subassembly similar to that shown in Figure 25.

#### 3.5 SENSOR

The FACS is designed to be suitable either as a solar pointing or stellar pointing system. Under separate procurement, GSFC has contracted for development of a suitable stellar sensor. To permit earlier flight tests of the FACS, the Phase I and Phase II FACS programs utilize a solar sensor developed by GSFC. The solar sensor has been designed to have a similar output characteristic to that of the planned stellar sensor, thus facilitating conversion from a solar pointing to a stellar pointing FACS, and vice-versa.

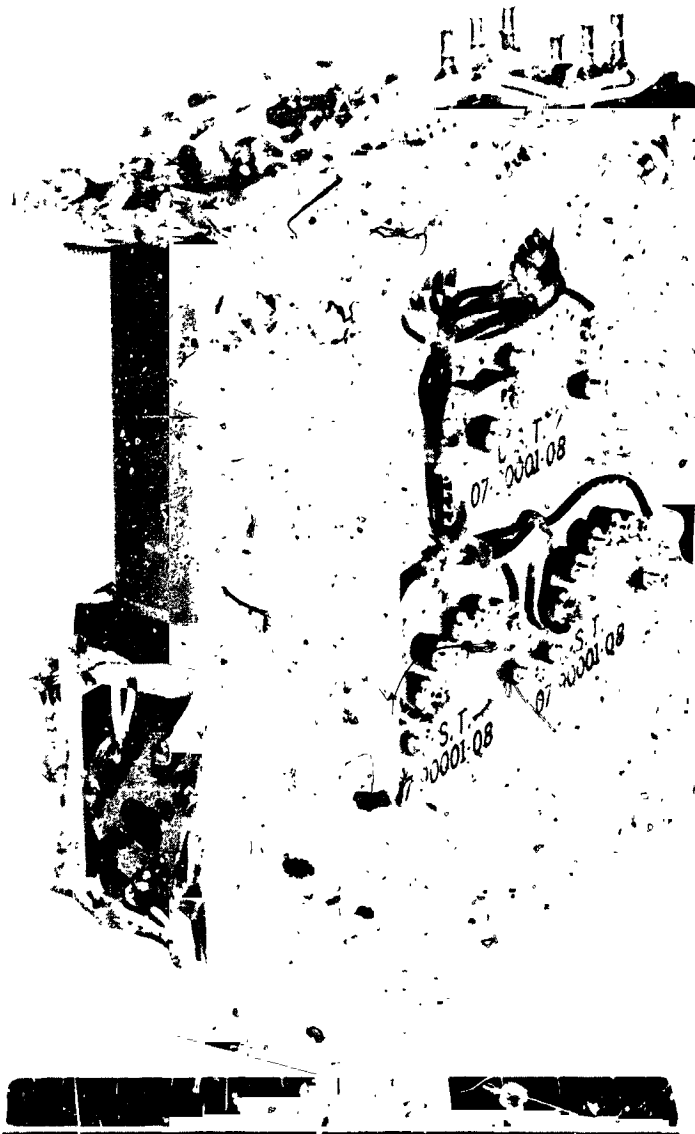




JET 2  
YAW CCW  
PITCH AXIS

05/125

Figure 24. Roll Stabilized Platform Subassembly



SGC/704

Figure 25. Rate Gyro Subassembly

The GSFC solar sensor utilizes four Ball Brothers type FE-5 calibrated silicon photo-voltaic cells as the basic sensing elements. These four photo-voltaic cells are mounted on a solid metal block. The block establishes the necessary relative alignment of the four cells, and provides a heat sink to keep the sensor at minimum drift when the cells are connected in pairs of opposing polarity.

The output of each cell-pair is amplified in a Burr Brown Model 1503 operational amplifier. In the breadboard version, amplifier gain was adjusted to provide the desired output sensitivity near null of 5.0 mv/arc sec when operated with a Melpar, Inc., Model SS-4 Solar-Source Simulator, which has an intensity of approximately 1/60 that of the sun in space.

The linear field is approximately  $\pm 15$  arc minutes wide. Saturated signals persist out to about  $\pm 10^\circ$ . The useful range of the sensor during three axis simulator tests was about  $\pm 1^\circ$ . This limitation was imposed by the 5-inch diameter of the collimated solar source simulator.

## Section 4

### FACS PHASE I PROGRAM

#### 4.1 WORK STATEMENT ITEMS

SGC shall provide the facilities, materials, and personnel necessary to furnish the following items:

- Item 1 - SGC shall prepare a complete set of electrical schematic diagrams and a test outline covering planned tests for the major components and subassemblies of the proposed Fine Attitude Control System (FACS) for the Aerobee 150 sounding rocket. SGC shall also prepare a complete functional description that ties in with the schematic diagrams and which covers the step-by-step operation of the system. The schematic diagrams and functional description must be approved by GSFC prior to construction of the breadboard FACS. However, procurement of key components in the breadboard FACS can be initiated prior to such approval. The test outline must be approved by GSFC prior to actual testing of components of the FACS.
- Item 2 - SGC shall conduct an analysis of the present IACS flight pneumatics.
- Item 3 - SGC shall conduct a comprehensive single-axis analog simulation of the FACS. SGC shall prepare a report covering the analog study.
- Item 4 - SGC shall procure a solar simulator to permit checkout of the integrated FACS.
- Item 5 - SGC shall construct a breadboard FACS in accordance with the GSFC approved design using the control parameter values determined from the analog optimization study.
- Item 6a - SGC shall conduct bench checks of the breadboard FACS at SGC in accordance with the approved test outline.
- Item 6b - SGC shall deliver the bench-tested breadboard FACS to GSFC.
- Item 6c - The FACS three-axis simulator final acceptance testing shall be at GSFC on the Aerobee simulator. SGC shall provide the necessary liaison and technical services during the period of the three-axis simulator tests and acceptance testing at GSFC.

Item 7 - Task deleted.

Item 8 - SGC shall prepare a final report on the breadboard FACS.

#### 4.2

#### DESIGN

The basic structure that houses the FACS electronics in an all welded and machined aluminum cruciform and ring-deck arrangement, as shown in Figure 8. This type of structure maintains acceptable dimensional stability and rigidity to insure that the sensing elements and the attitude-control references are accurately aligned at all times, and that the balance of the entire FACS-Simulator assembly is not disturbed on the air bearing. Machined surfaces and alignment marks were used to provide the alignment of the solar sensor, roll-stabilized platform, and rate-gyro package, in relation to each other and to the FACS-Simulator interface. The open cruciform mounting compartments incorporate excellent access and serviceability in a rigid configuration. All equipment and unit attachments, as well as cabling tiedowns, are machined into the structure. The resulting FACS package .5 inches in diameter, and 20 inches long, not including the fine sensor.

The breadboard packaging design was based on a modular concept, as specified by the requirements of Section 2.3, incorporating each of the subassemblies described in Section 3.4. The programmer, IACS control electronics, and SACS control electronics subassembly breadboard packaging was partially implemented by the use of several small printed circuit board modules that were modified from another SGC program. These modules included the full triggers, half triggers, absolute valve circuits, valve drivers and the demodulators. In addition, the programmer used several other modified modules.

An example of the subassembly packaging technique is shown in Figures 18 and 19. The latter shows the rear view of the subassembly and illustrates the mounting stand-offs and plug-in technique used for attaching to the main FACS structure both mechanically and electrically. This rear view also shows the mounting of the modules. The leads of the modules, transformers, relays, transistors, and amplifiers all extend through the vector boards to the front side of the subassembly shown in Figure 18.

The umbilical connector for electrical interface with the GSE is shown in the lower compartment of the photograph presented in Figure 7. The photograph also shows one of the four access holes (one in each quadrant) in the rear mounting ring for electrical interface cables interconnecting the FACS and GSFC Simulator.

The breadboard FACS design conforms to or surpasses the GSFC specification requirements of Section 2.3 of this report. Schematic diagrams of all the breadboard FACS subassemblies are presented in Appendix I. A complete parts list of the subassemblies is presented in Appendix II.

#### 4.3 ANALYSIS

The FACS Phase I program included extensive analysis carried out on the analog computer covering all aspects of system performance. An analysis was also made of the reaction jet pneumatic circuits now used with Space-General's Aerobee 150-150A Attitude Control System.

##### 4.3.1 PNEUMATICS ANALYSIS

As required by Work Statement Item 3, an analysis was made of the pneumatic circuits used in the Aerobee 150-150A. The resulting report was submitted to GSFC and is included herein as Appendix III.

Pneumatic circuits for the FACS will be designed during Phase II of this program. The material presented in Appendix III defines the characteristics of presently used systems. The "high thrust" circuits of the FACS will probably be similar. However, some changes may be expected due to addition of the "low-thrust" circuits and to repackaging of the roll control valve-nozzle hardware.

##### 4.3.2 ANALOG COMPUTER STUDY

Computer studies were carried out in support of the FACS design effort. These studies formed the basis for assessing the suitability of design features and were used to establish settings for all parameters. A report covering this work was submitted to GSFC (Reference 1). The findings were

closely examined at GSFC by computer studies reported in Reference 2. Good correlation was obtained between the two studies.

An objective of the program was to examine the correlation between the analog simulation and tests conducted with the FACS on a three-axis simulator. These tests are described in Section 4.5. Tests results led to some changes which were subsequently incorporated into the analog simulation. A series of analog computer runs was then made which duplicated the conditions examined on the three-axis simulator. A comparison of results is discussed in Section 4.5.7. Specific changes from the analog simulation of Reference 1 are described below. Also included is a description of the mechanization for each change.

#### 4.3.2.1 POSITION GYRO SIGNAL LIMITING

During three-axis simulator tests, Zener diode limiters were installed to produce voltage limiting of the position gyro output signals in the IACS. This permitted a reduction in the setting of rate gain and thereby alleviated overdamping during maneuvers made at high control moment acceleration levels. Section 4.5 treats this in detail and includes a definition of the limiter characteristics.

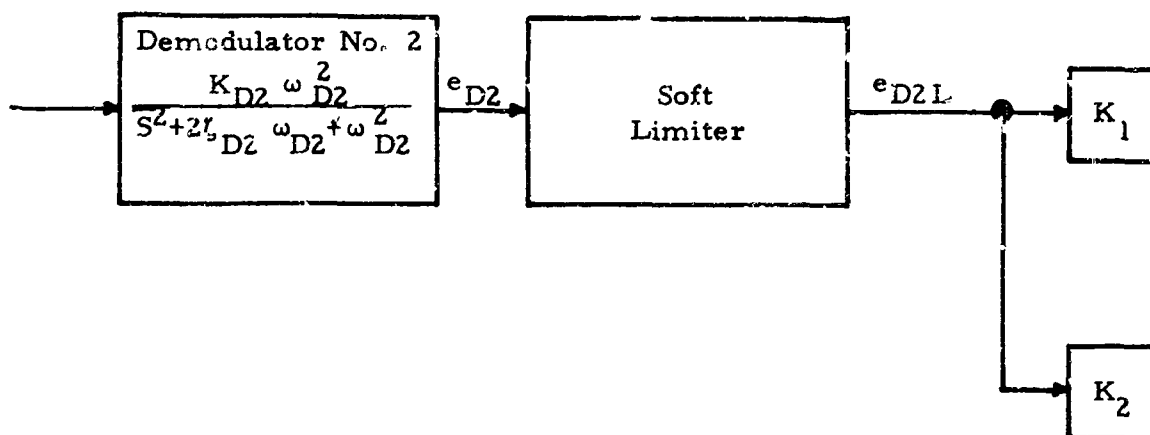
The computer mechanization of this change is shown in Figure 26 (block diagram) and Figure 27 (computer circuit diagram). A diode function generator was employed to duplicate the limiter characteristics; DFG settings are shown in Table 3.

#### 4.3.2.2 MANEUVER RATE GAIN

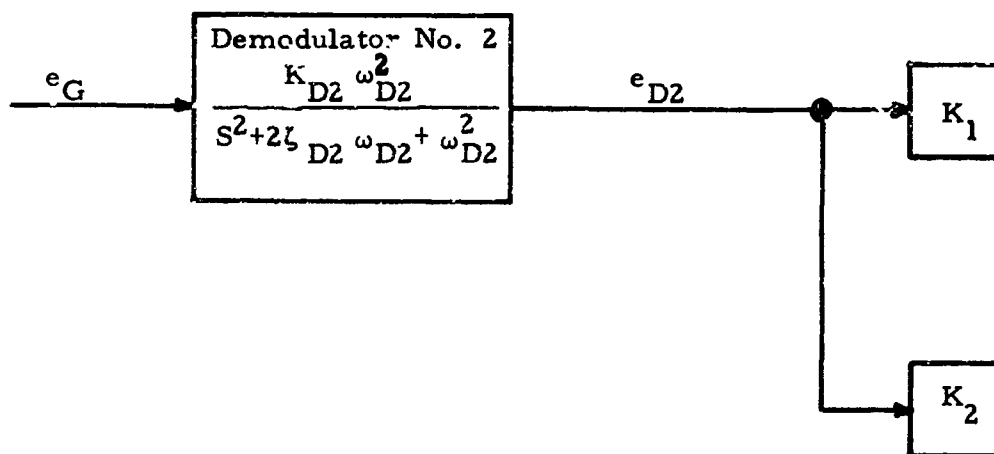
Three-axis simulator tests led to selection of maneuver (high) rate gain = 1.55 sec in the IACS pitch and yaw circuits. This change was incorporated in the final computer simulation where:

$$K_1''/K_1 = 1.55 \text{ seconds} \quad (\text{Potentiometer Q24 set at } .0690)$$

The effective rate gain is increased substantially above this level by the signal limiter as the lag angle increases beyond the break point of the limiter.



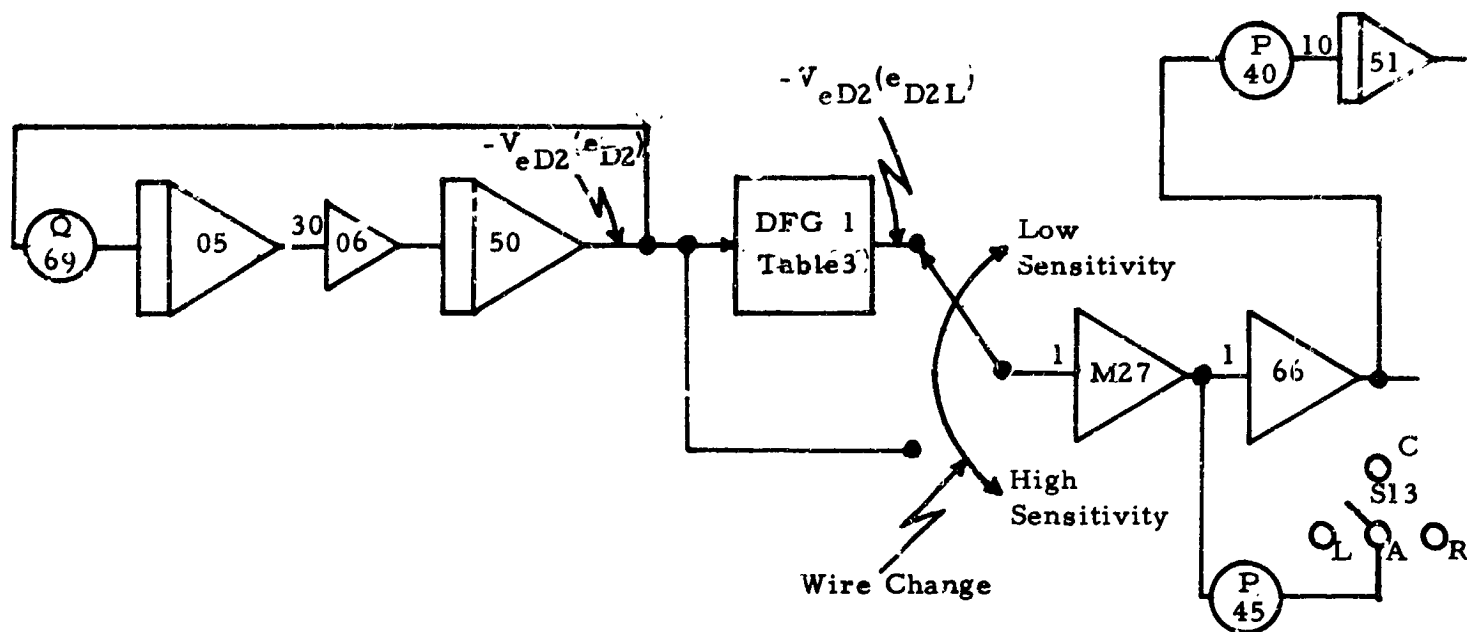
Modified Arrangement



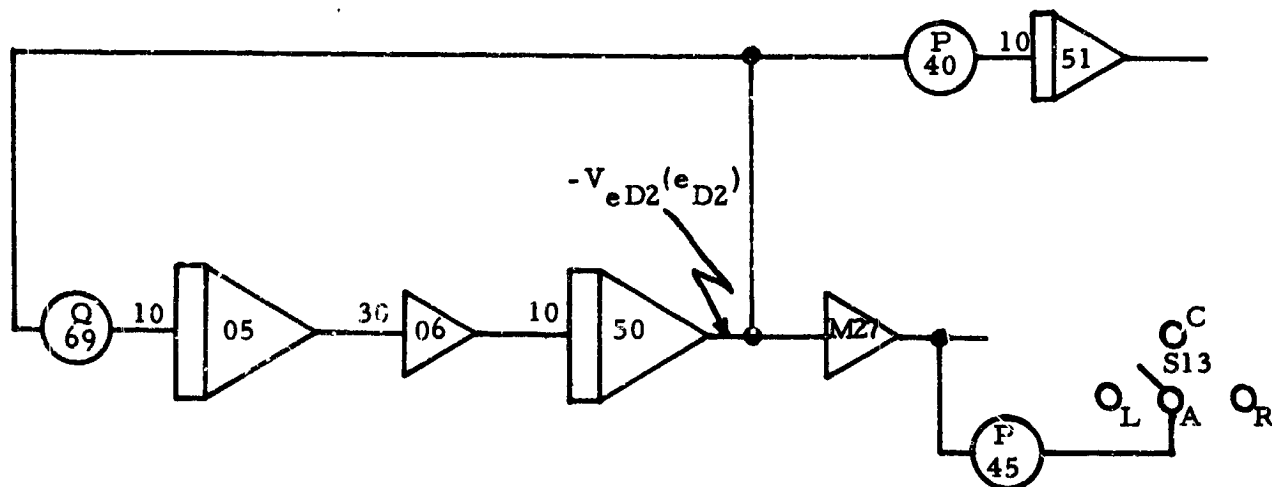
Reference 1 Arrangement

Figure 26. IACS Position Signal Limiter Change, Servo Block Diagram





Modified Circuit



Reference 1 Circuit

Figure 27. IACS Position Signal Limiter Change, Analog Computer Circuit

Table 3

DFG SETTINGS FOR POSITION SIGNAL  
LIMITER SIMULATION

Segment	Quadrant	Gain	Breakpoint	Slope
1	CS	--	--	8.2
3	2	Low	8.2	11.4
4	2	Low	14.0	17.3
5	2	Low	33.2	28.0
6	2	Low	75.4	--
11	-CS	--	--	-8.2
13	2	Low	-8.2	-11.4
14	2	Low	-14.0	-17.3
15	2	Low	-33.2	-28.0
16	2	Low	-75.4	--

Parallax = 0

#### 4.3.2.3 VALVE CHARACTERISTICS

The high-thrust (coarse) valve characteristics were adjusted into closer correspondence with valves used on the GSFC simulator. The low thrust (fine) valves were set to the "C" characteristics of Reference 1. Response characteristics and potentiometer settings were as follows:

	<u>Fine Valves</u>	<u>Course Valves</u>
Time to energize (sec)	.012	.010
Time to de-energize (sec)	.017	.019
Potentiometer Settings:		
Q25 = .0094		Q03 = .0194
Q29 = .0094		Q12 = .0194
Q27 = .2000		Q04 = .0178
Q15 = .2000		Q11 = .0178

#### 4.3.2.4 MANEUVER TORQUING

Initial tests on the three-axis simulator indicated a discrepancy in maneuver characteristics as compared to analog results. Maneuvers on the simulator did not produce a steady-state condition (constant rate, constant lag angle) in mid-maneuver. This was attributed to an incorrect simulation of gyro-torquing characteristics on the computer.

The computer simulation was corrected by modifying the gyro-torquing characteristics from

$$\dot{\psi}_c = (\dot{\psi}_c)_{\text{man}} = \text{constant}$$

to the following:

$$\dot{\psi}_c = (\dot{\psi}_c)_{\text{man}} \frac{1}{\cos \psi_e}$$

Mechanization of this change is shown in Figure 28 (block diagram) and Figure 29 (computer circuit diagram).

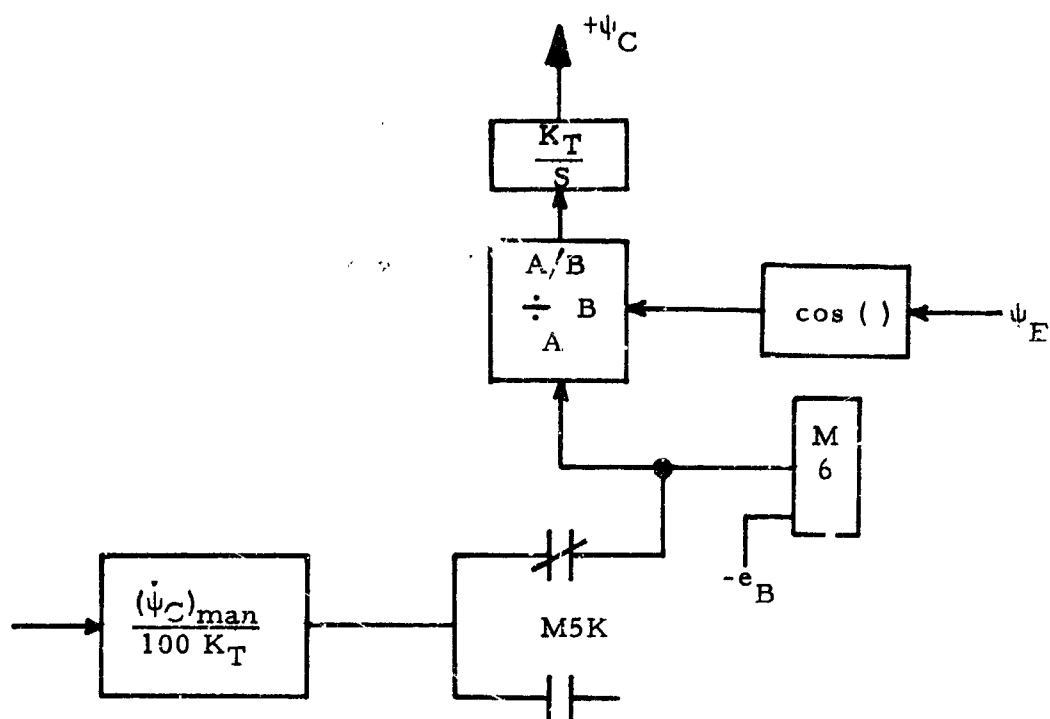
A technical note discussing the effect of gyro torquing characteristics on maneuver characteristics was submitted to GSFC. This note is reproduced in Appendix VIII. It does not include the position limiter effects. Therefore, the recommended change in rate gain was superseded by the introduction of limiting.

#### 4.3.3 ROLL SLAVING ANALYSIS

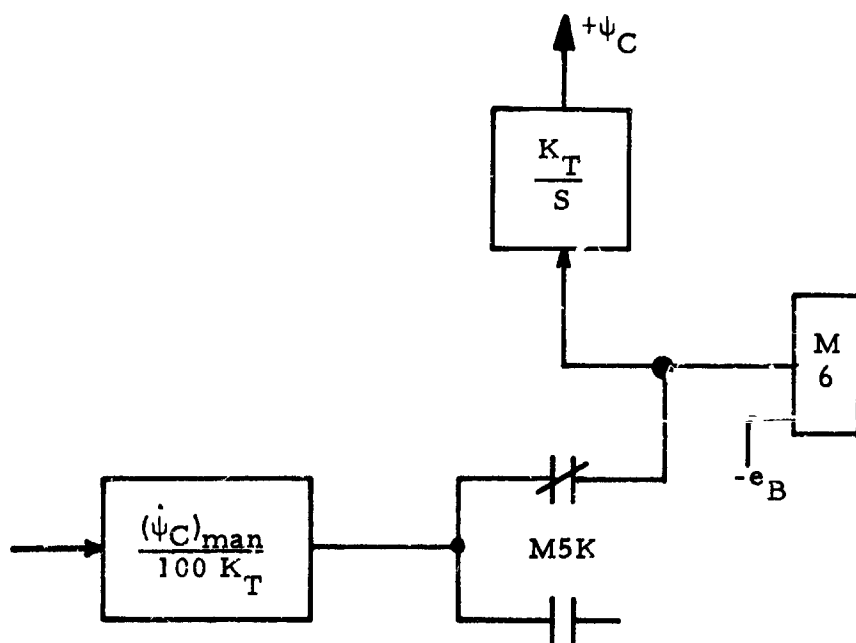
In the FACS, slaving of the redundant gimbal of the yaw gyro is deferred until three-axis capture is complete. This method was questioned at the time of proposing. An analysis was prepared to justify the approach. For completeness, the analysis is included in Appendix IX.

#### 4.4 BENCH TEST

Bench checkout of the breadboard FACS was performed in three phases. The first phase involved testing of the electronic modules to insure compliance with design requirements prior to installation into subassemblies. Phase two of the bench test was a subassembly calibration and functional

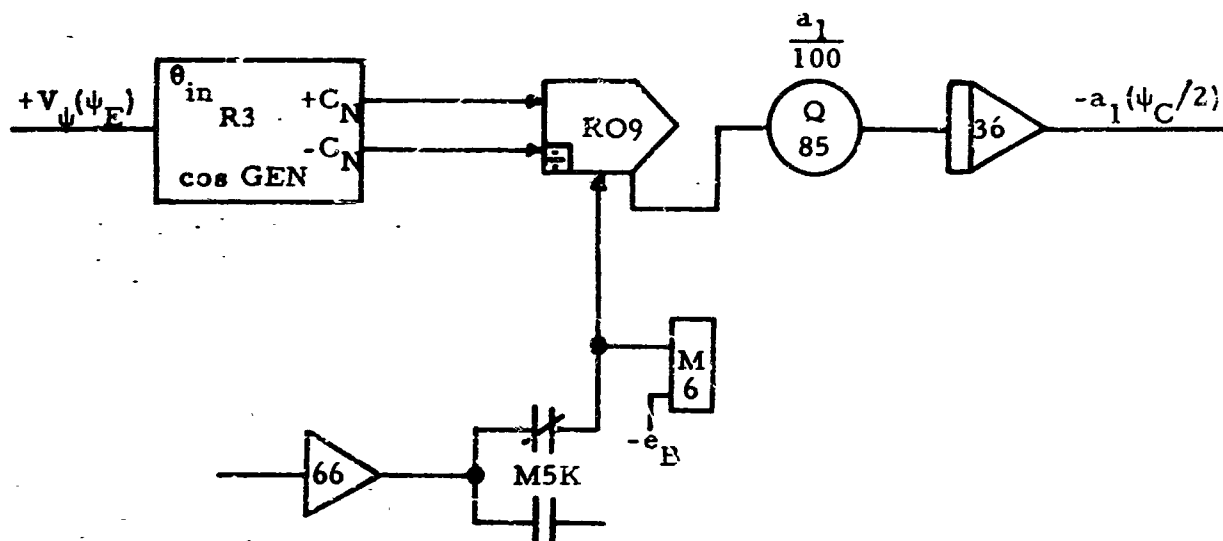


Modified Arrangement

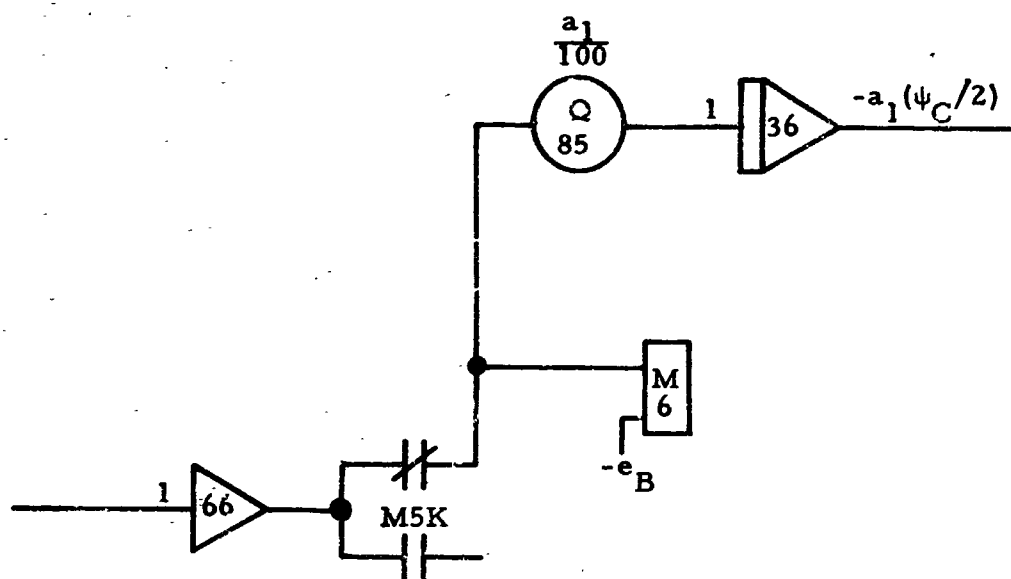


Reference 1 Arrangement

Figure 28. Maneuver Torquing Change, Servo Block Diagram



Modified Circuit



Reference 1 Circuit

Figure 29. Maneuver Torquing Change, Servo Block Diagram

checkout at the environmental temperature extremes. Phase three involved the functional checkout of the completely integrated breadboard FACS at the environmental temperature extremes. Also included in the systems bench test of phase three were functional tests performed on a single-axis simulator and on the SGC 3-axis simulator. A solar simulator was used, during the single-axis tests, to functionally test the fine sensor while operating with the breadboard FACS. The 3-axis tests performed at SGC were limited to functional operating tests to assure proper operation upon arrival at GSFC.

#### 4.4.1 SUBASSEMBLY AND MODULE TESTS

Each of the FACS breadboard subassemblies was individually tested to verify its stability of calibration and proper functional operational behavior under a variety of operating conditions (e.g., varying supply voltage, loading, signal level, temperature, etc.). Each subassembly was subjected to, and tested over, a temperature range from +40°F to 120°F in accordance with a test outline submitted to, and approved by GSFC. The bench test data for all of the subassemblies is presented in Appendix IV.

All of the pre-fabricated modified modules used in the subassemblies were functionally tested prior to installation. The full trigger, half trigger, absolute valve circuit, and demodulator modules were fully tested for stability and functional operation at the temperature extremes. The test data for these modules is included in Appendix IV.

#### 4.4.2 SYSTEM TEST AND CALIBRATION

Calibration of the breadboard FACS was performed without the roll stabilized platform, rate gyro package, or the fine sensor connected to the system. The connectors normally inserted into these sensors were used to apply input signals for static calibration of the various gains and trip levels throughout the system. Tests were conducted to verify the stability of calibration and proper functional operation through the temperature range. Calibration of the telemetry signal conditioning circuits is presented in Appendix VI. The breadboard FACS calibration and system bench test data is presented in Appendix V.

After calibration and temperature testing the breadboard FACS, the system was tested on a single-axis simulator in conjunction with a solar simulator to verify proper operation of the fine sensor with the completely integrated breadboard FACS.

The final test at SGC, prior to shipment to GSFC, was performed on the SGC air bearing simulator. Two test runs were made. The first run was conducted with the system in the "IACS only" mode of operation to examine the basic system operation. The second run on the simulator was designed to establish that the system would transfer from IACS to SACS control of the vehicle. Neither solar source nor fine valves were implemented for this test run. The object of the second run was to verify overall system readiness for shipment.

#### 4.4.3 VTT TEST

The FACS incorporates an improved technique for maneuver angle control. This technique is based upon an automatic adjustment of the gyro-torquing time to compensate for temperature and voltage variations. The approach has come to be known as the "Variable-Time Torquing" concept (VTT).

As implemented in the breadboard FACS, both current and voltage at both windings of the gyro torquer are monitored. DC voltages proportional to these quantities are summed together with a DC reference voltage and integrated while gyro torquing is in process. The integrator output is compared to an adjustable voltage which is set to provide the desired maneuver angle and torquing is terminated when the integrator output exceeds this voltage.

GSFC breadboarded and tested the VTT circuits. Excellent results were achieved with a modified circuit which utilized only the current-monitoring, and reference-voltage portions of the circuit. This modification (the "current-only" mode) results in simplification of circuitry. SGC was directed to conduct tests thereof and to make recommendations for the final form of VTT circuits.

A series of tests using four FM10G-2 gyros was made. The results of these tests were reported in Reference 3. During GSFC-SGC coordination meetings at the end of Phase I, the "current-only" mode was selected for incorporation in the prototype FACS.

Final acceptability of the breadboard FACS was demonstrated in the three-axis simulator facility at GSFC, Greenbelt, Md. Figure 30 shows a photograph of this recently-completed facility. The central gas-bearing supported structure is housed within a light tight enclosure. A Melpar, Inc., Model SS-4 Solar-Source Simulator provides an image of the simulated sun in a 5-inch collimated light beam which is directed toward the forward end of the structure. The FACS was mounted upon the structure and the solar source simulator was aligned with the FACS solar sensor. The gas-bearing-supported structure incorporated a 25-VDC battery pack, telemetry equipment, solenoid valves and nozzles for reaction jet control of attitude, and nitrogen gas storage for the reaction jets. The facility also included auto-collimator equipment for monitoring pitch or yaw angular position near the target-pointing null region.

This facility provided the capability for evaluation of FACS performance, essentially free of restraint, through despin, maneuvering, acquisition, and limit cycle operation.

#### 4.5.1 TEST DESCRIPTION

The objective of the three-axis simulator tests was to show conformance with all requirements for FACS operation. Additionally, a comparative evaluation was carried out to permit selection of the best of the four alternate configurations examined during the analog study.

A fixed program, suitable for all tests, was incorporated in the FACS programmer. This program is outlined in Table 4. It provides for maneuvers in both directions in each control axis, four on-target holds periods, and four target-acquisition sequences. Since only a single solar-source "target" was employed, all acquisitions subsequent to the first were accomplished by programming, in sequence, maneuvers away from and returning to the target pointing orientation.

In the target-pointing orientation, the FACS controlled pitch and yaw attitude to maintain the vehicle roll axis pointed at the solar source.





SGC/705

Figure 30. GSFC Three-Axis Simulator Facility

Table 4

BREADBOARD FACE PROGRAMMER SEQUENCE  
FOR 3-AXIS SIMULATOR TEST

Program Position	Time Delay (sec)	Maneuver Axis and Direction	Maneuver Magnitude (Deg)
1	0	Yaw CW	75
2	65	Yaw CW	30
3	0	Yaw CCW	30
4	65	Pitch CW	15
5	0	Pitch CCW	15
6	65	Pitch CCW	20
7	0	Pitch CW	20
8	270 or 65 (adjusted)	Roll CW	30
9	0	Roll CCW	30
10	0	Yaw CCW	75
11	0	----	--

Roll attitude control maintained the yaw axis vertical (i.e., the yaw plane was horizontal). In this orientation, activity in the yaw plane was essentially free of gravity effects whereas the pitch plane activity was occasionally influenced by a less-than-perfect balance of the simulator.

The typical operating sequence for each test was as follows:

- a. Vehicle oriented approximately  $75^{\circ}$  yaw displacement from target.
- b. All systems on, remove umbilical.
- c. Manual roll spin-up (this step was frequently omitted to reduce gas consumption).
- d. Automatic start signal to FACS programmer.

- e. "Coast-Time" delay.
- f. Despin and roll capture.
- g. Pitch and yaw capture.
- h. Yaw  $75^{\circ}$  maneuver.
- i. Target acquisition.
- j. Target-pointing limit cycle.
- k. Maneuver and hold sequence (as outlined by Table 4) culminating in final  $75^{\circ}$  yaw maneuver return to initial orientation.
- l. IACS limit cycle.
- m. Insert umbilical and shutdown.

During each test, telemetry data were transmitted to a receiving station located outside the facility enclosure. A listing of telemetered functions is shown in Table 5. Real-time recording of eight selected functions provided means for quick look interpretation of results. All functions were recorded on magnetic tape and replay recordings were made as desired.

Continuous recordings were made during each test utilizing an autocollimator in conjunction with a mirror mounted on the aft end of the simulator structure. These data were used to correlate the actual yaw angular displacement with the displacement indicated by the corresponding output signal from the solar sensor.

The solenoid valves used for reaction jet control exhibited the following characteristics at 200 psig inlet pressure:

<u>Valve</u>	<u>Open Response Time - ms</u>	<u>Close Response Time - ms</u>
Pitch and Yaw High Thrust	8	17
Pitch and Yaw Low Thrust	10	17
Roll	16	14

Table 5

TELEMETRY MEASUREMENTS FOR THREE-AXIS SIMULATOR  
TEST OF FACS

<u>Channel</u>	<u>Measurement</u>
1	+5 VDC Telemetry Reference
2	Electrical Ground
3	Yaw High-Thrust Values
4	Program Position
5	"G" Switch and Arm Roll
6	Pitch Low-Thrust Values
7	Yaw Low-Thrust Values
8	+15-VDC Monitor
9	-15-VDC Monitor
10	26-V $\angle 0^\circ$ Monitor
11	26-V $\angle 90^\circ$ Monitor
12	Pitch Position Blowup
13	+28-VDC Monitor
14	Roll Valves
15	Slave Roll Torquer
16	Yaw Torquer
17	Pitch Torquer
18	Roll Torquer
19	Roll Position
20	Slave Roll Position
21	Pitch Position
22	Yaw Position
23	Roll Rate
24	Pitch Rate
25	Yaw Rate
26	SACS State
27	Yaw Valve Switchover

Table 5 (Continued)

TELEMETRY MEASUREMENTS FOR THREE-AXIS SIMULATOR  
TEST OF FACS

<u>Channel</u>	<u>Measurement</u>
28	Torque Loop Closure
29	Pitch Valve Switchover
30	Sensor Pitch X 10
31	Sensor Pitch
32	Sensor Yaw X 10
33	Sensor Yaw
34	Pitch High Thrust Valves
35	Roll Capture
36	Pitch Capture
37	Yaw Capture
38	Yaw Position Blowup
44	400-cps Frequency Monitor
47	28 VDC for "G" Switch
48	"G" Switch
49	+28-VDC Power
50	Ground Power

Measured moment arms for the reaction jets were:

Pitch and Yaw High Thrust	5.55 ft
Pitch and Yaw Low Thrust	5.74 ft
Roll	1.25 ft (between nozzles)

Measured moments of inertia were:

Pitch and Yaw	322 ft-lb-sec <sup>2</sup>
Roll	6.09 ft-lb-sec <sup>2</sup>

The simulator included provisions for setting reaction jet thrust levels (and therefore, acceleration levels) by pneumatic regulator adjustment. Independent adjustment was available for pitch and yaw high thrust, pitch and yaw low thrust, roll thrust, and despin thrust. The adjusting regulators exhibited a rising characteristic. That is, the regulated pressure increased slightly as the supply tank pressure decreased. Thus, typically, the preset acceleration level was observed to increase by approximately 10% in the course of a single run. In the discussions to follow, the indicated values for acceleration refer to the levels existing at the start of a run.

One of the simulator test objectives was to select the best of four FACS system configurations. Differences between configurations were minor and involved only the method of implementation of IACS pitch and yaw rate gain and the method of position error level detection. The configurations were categorized as follows:

<u>Configuration</u>	<u>Description</u>
I	Dual Detector, Bi-level Rate Gain
II	Dual Detector, Single Rate Gain
III	Single Detector, Bi-level Rate Gain
IV	Single Detector, Single Rate Gain

When dual detectors are used, one initiates rate gain change and the other initiates SACS Enable.

When a single detector is used, both functions are initiated by the same detector.

When bi-level rate gain is used, a higher value of rate gain is made effective during maneuvers than during limit cycle.

#### 4.5.2

#### MANEUVER EVALUATION

The character of maneuvers is established by parameters associated with IACS operation and by the control acceleration ( $\alpha_c$ ) produced by the high thrust reaction jets. The selection of IACS rate gain provides the principle means for adjustment of maneuver behavior. When bi-level rate gain is utilized (Configuration I), then the level at which rate gain change occurs exercises influence over the terminal portion of the maneuver.

The range of acceleration examined during three-axis simulator tests was from  $\alpha_c = 1.4$  to  $4.0 \text{ deg/sec}^2$ . This corresponds to a pitch (or yaw) thrust variation from 1.75 to 5.0 lb for a moment of inertia of  $900 \text{ ft-lb-sec}^2$ . These values are representative of operation in an Aerobee 150 where blowdown operation results in a decreasing thrust level as gas is used. As previously noted, the simulator reaction jet typically showed a 10% increase in thrust, and acceleration, from run beginning to end. Thus the maximum acceleration runs were usually conducted with  $\alpha_c = 3.6 \text{ deg/sec}^2$  at run start. Roll control acceleration was generally fixed at  $7.0 \text{ deg/sec}^2$  and the evaluation of maneuver characteristics was based on observations of behavior in pitch and yaw. This value of roll acceleration is representative of operation in an Aerobee 150 during the initial period of ACS control. Despin was accomplished with an acceleration level of  $70 \text{ deg/sec}^2$ .

##### 4.5.2.1

##### INITIAL EVALUATION

The initial selection of IACS rate gain was based on the requirement for critical damping at the lowest level of acceleration. Computer studies led to selection of high rate gain = 3.3 sec to satisfy this requirement. Operation at higher levels of acceleration is then overdamped. The initial simulator tests substantiated that very high frequency jet action occurred at maximum acceleration. The "hammering" imposed on the solenoid valves was cause for concern. Therefore a remedy was introduced in the form of voltage limiting in the IACS pitch and yaw position channels at the demodulator output. Figure 31 shows the experimentally-determined result of this limiting. It then became possible to reduce the high rate gain and thereby substantially smooth reaction jet activity.

NOTE: New CV Characteristics shown at 1.2109.  
See Appendix IV.

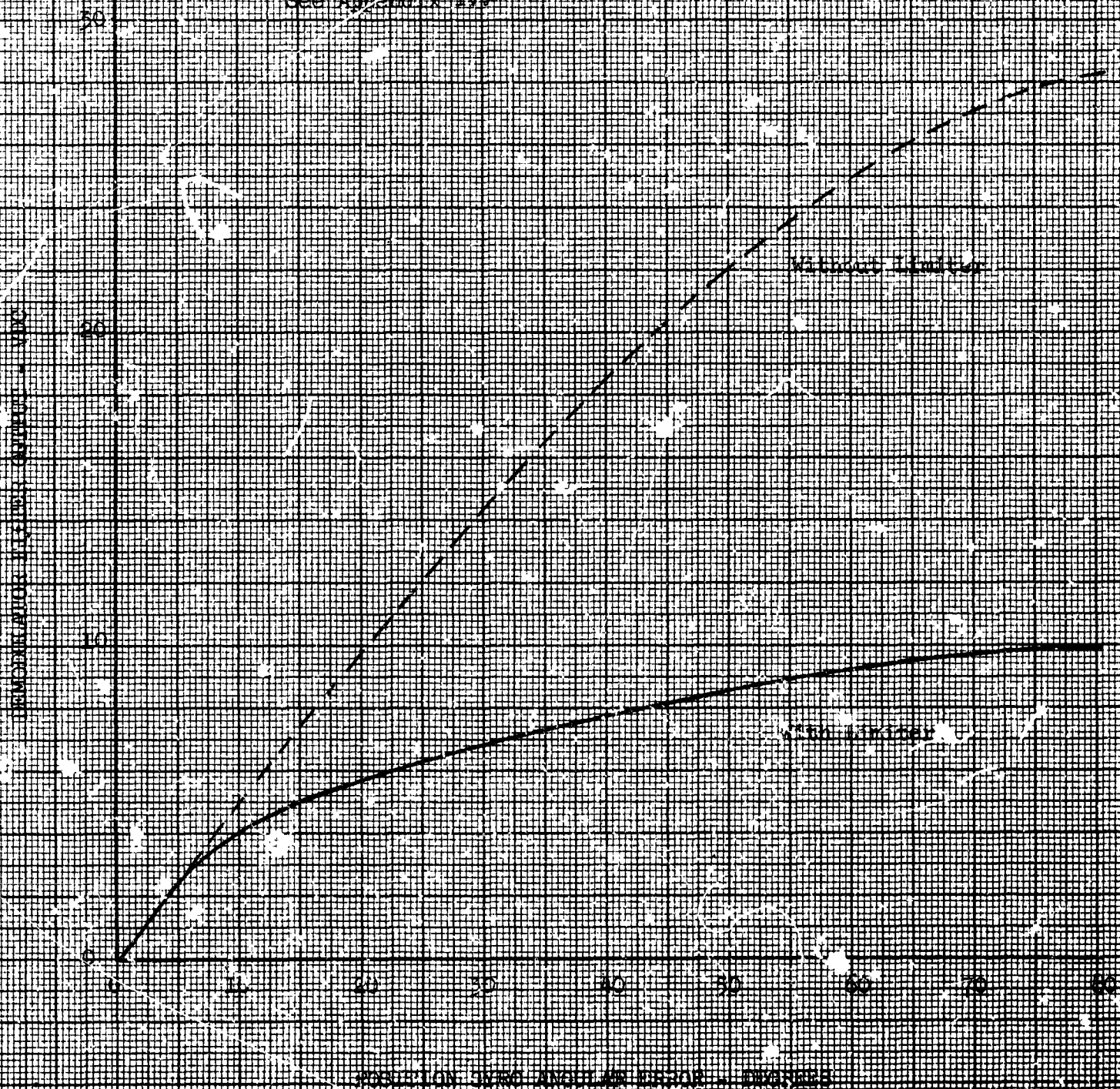


Figure 31. Position Channel "Soft Limiting" Characteristic



#### 4.5.2.2 MANEUVER EVALUATION RUNS

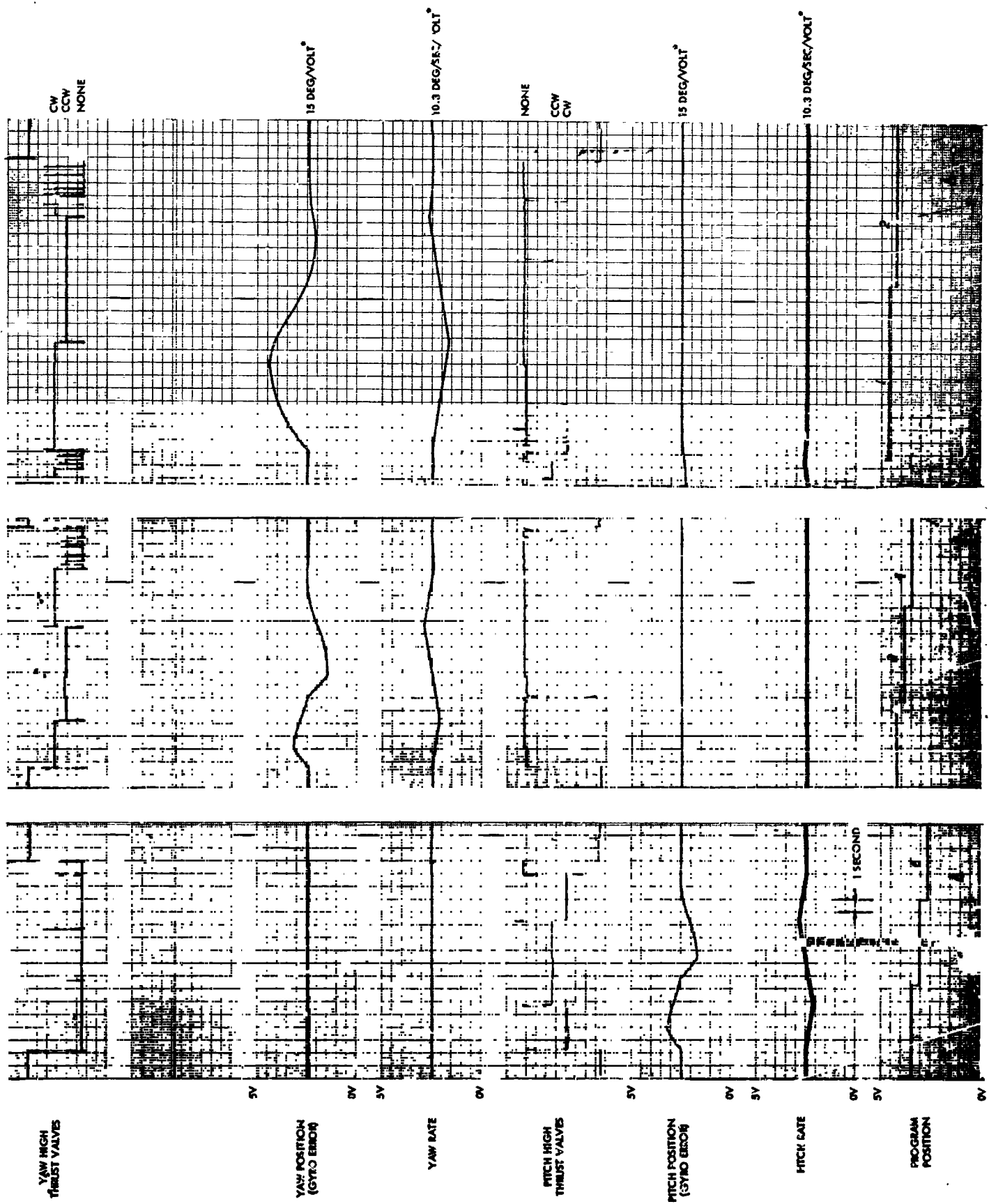
After incorporation of pitch and yaw position signal limiting, the high rate gain was reduced to 1.55 sec. Low rate gain remained unchanged at 1.25 sec. An overshoot of 5 to 7° was then seen after a 75° maneuver at  $\alpha_c = 1.4 \text{ deg/sec}^2$ . This was accepted as tolerable since testing established that premature enabling of the SACS does not occur under such conditions of overshoot.

Figures 32, 33, 34, 35, 36, and 37 show maneuver characteristics with configuration I for  $\alpha_c = 1.4, 1.9, 3.0$ , and  $3.6 \text{ deg/sec}^2$ , respectively. A comparison of Figures 32 and 33 reveals that a seven degree overshoot occurred after the first 75° yaw maneuver, where  $\alpha_c = 1.4 \text{ deg/sec}^2$ , and that no overshoot occurred after the last yaw maneuver when  $\alpha_c$  was measured (post-run) at  $\alpha_c = 1.7 \text{ deg/sec}^2$ . Observation of Figure 32 also shows that SACS enabling (i.e. torque loop closure) does not occur until settling is complete.

At higher acceleration levels, overdamped characteristics prevail. Figures 36 and 37 show maneuvers from simulator run 51 which was conducted at the maximum acceleration level. Although overdamping is clearly evident, jet action is essentially one-sided and thus rate removal is accomplished without waste of impulse.

Parameters which are useful for comparison of maneuver characteristics include maximum lag angle (maximum gyro-to-vehicle angular error), maximum vehicle rate, and maneuver time. These parameters are shown in Table 6 for the first 75° yaw maneuver and the first 20° pitch maneuver at various levels of acceleration. This table includes data for both configurations I and IV. In configuration I, a change from high rate gain (1.55 sec) to low rate gain (1.25 sec) occurs during terminal maneuver when the gyro error is less than 2°. In configuration IV, high rate gain is retained at all times. This minor difference has no significant effect on maneuver characteristics.

Test results from the 75° maneuver did demonstrate significant variations in lag angle when operating at  $\alpha_c = 1.4 \text{ deg/sec}^2$ . In Table 6, a comparison between runs 40 and 47 (with all conditions presumably identical) shows a difference in maximum lag angle of more than 9°. It appears that this



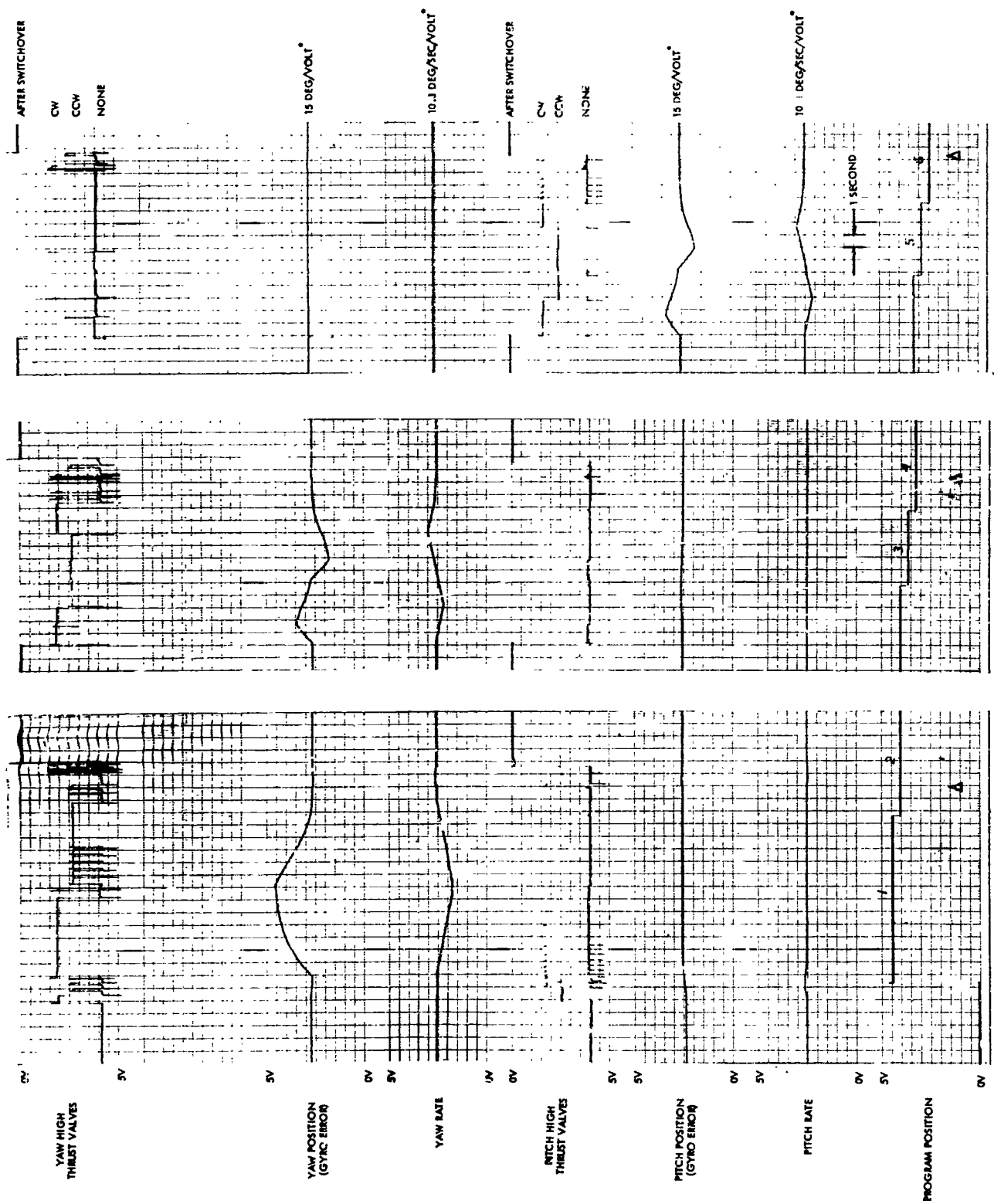
Notes: \* Approximate 1/10th error near roll (0.5V NOM)  
See Appendix VI for telemetry calibration data

A. Torque loop closure

Figure 32. FACS Maneuver Characteristics for Acceleration = 1 g



Figure 33. FACS Maneuver Characteristics for Acceleration = 1.4 deg/sec<sup>2</sup> (Three-Axis Simulator Run 47 Continued)



Note:  
 \* Approximate 10 Hz range near null (2.5V NOM)  
 See Appendix VI for Telemetry Calibration Data  
 A Torque loop closure

Figure 34. FACS Maneuver Characteristics for Acceleration = 1.9 deg/sec<sup>2</sup> (Three-Axis Simulator Run 48)

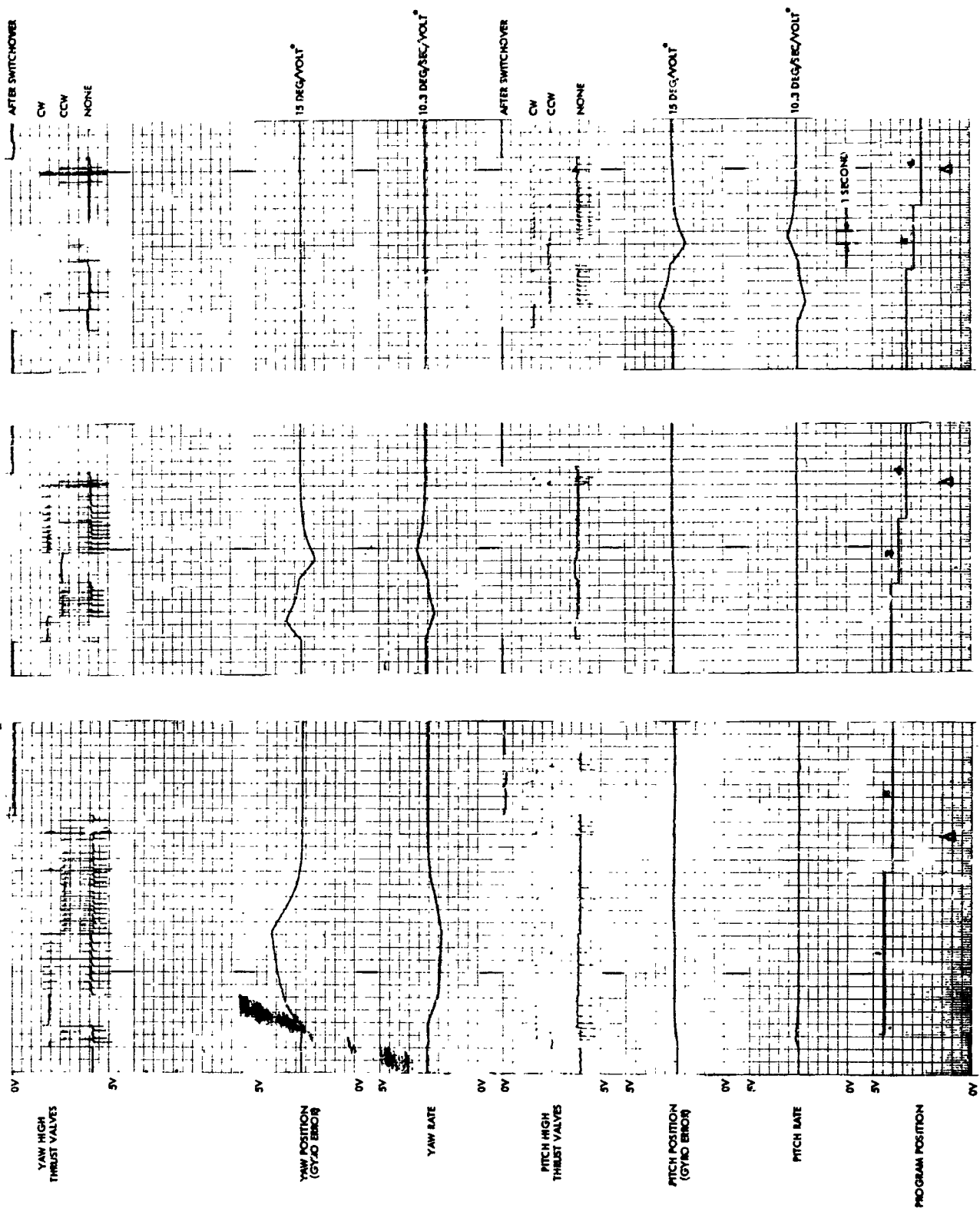
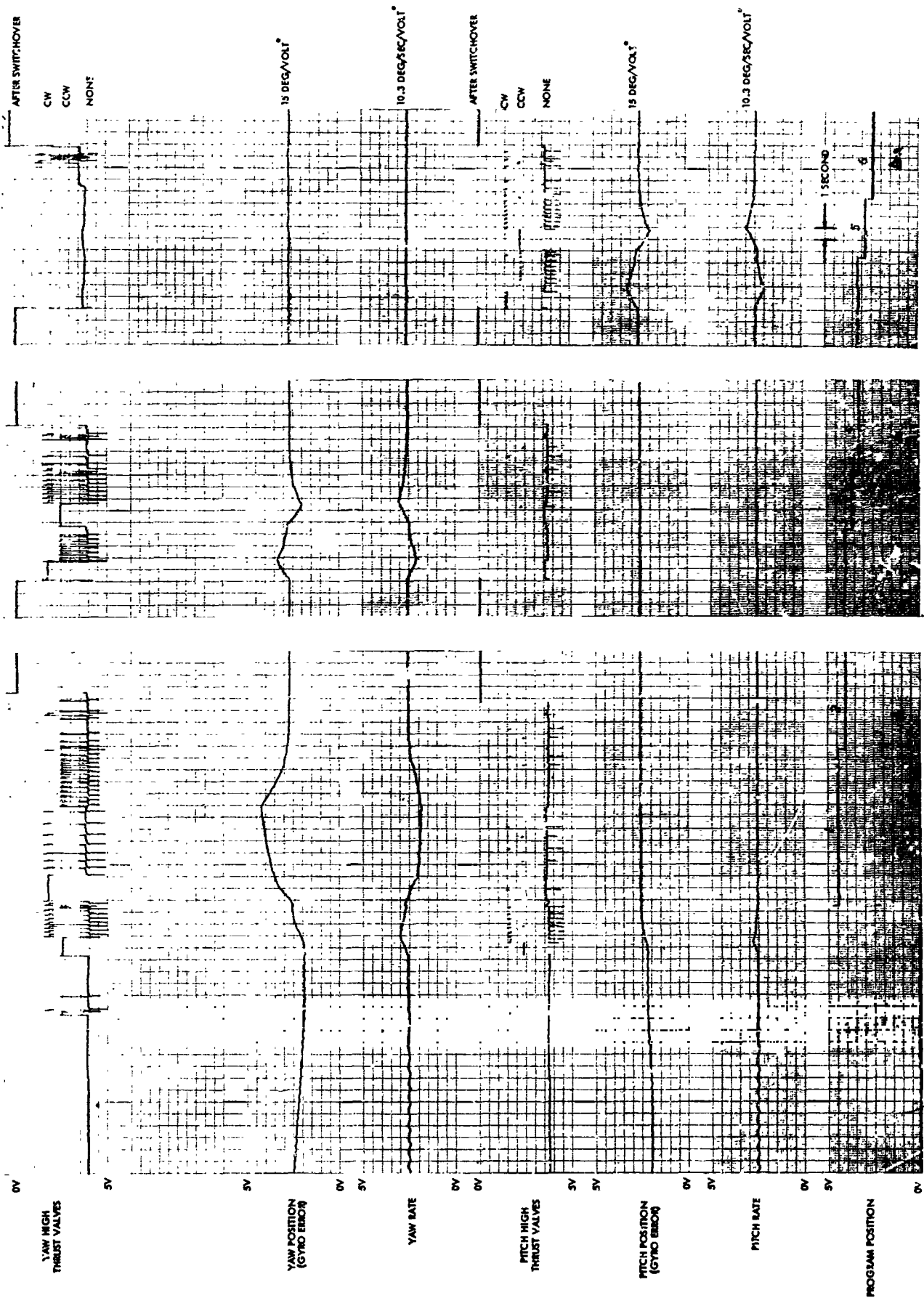
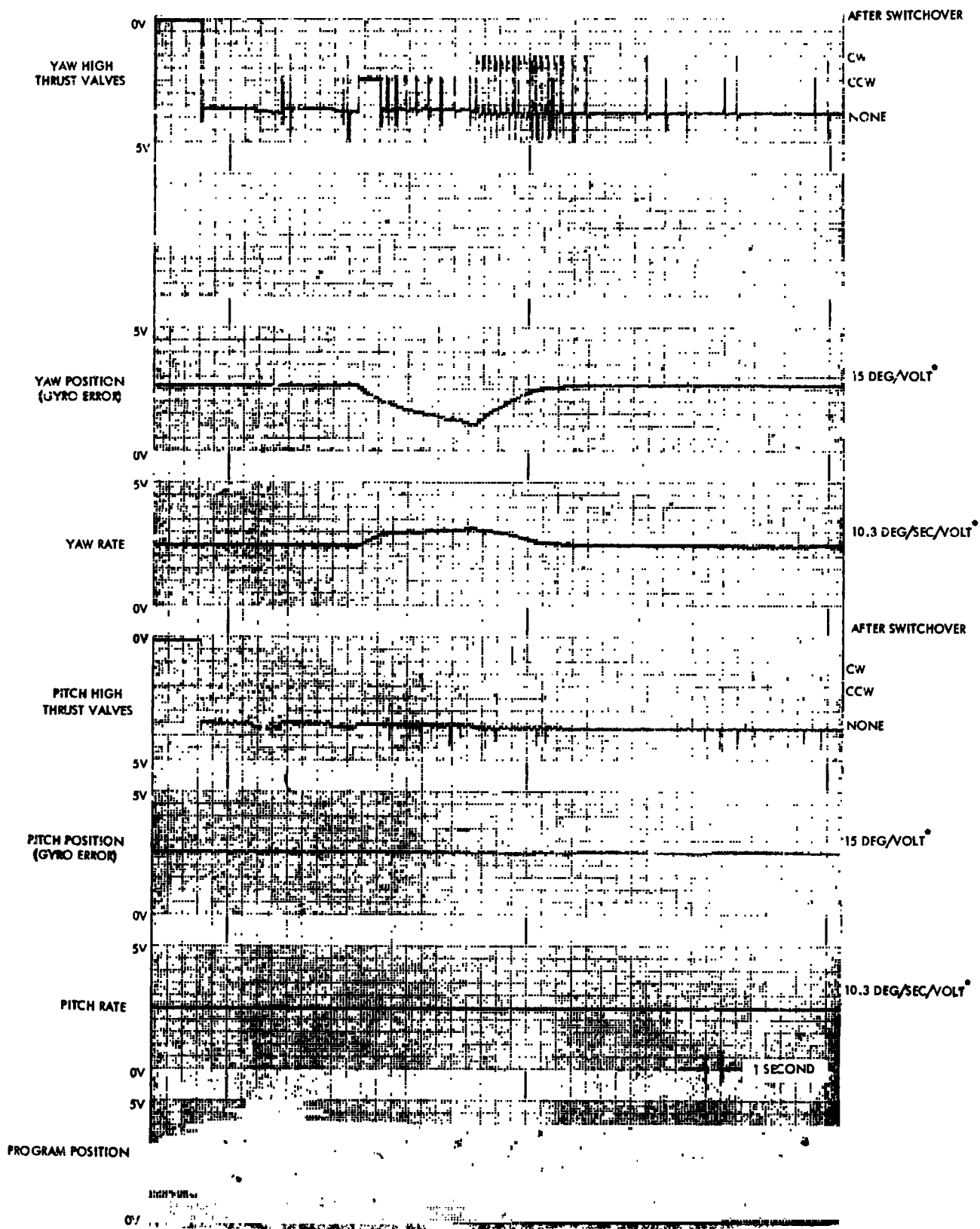


Figure 35. FACS Maneuver Characteristics for Acceleration = 3.0 deg/sec<sup>2</sup> (Three-Axis Simulator Run 49)



Note: \* Approximate to linear range near null (2.5V NOW)  
 See Appendix VI for Telemetry Calibration Data  
 A Torque Loop closure

Figure 36. FACS Maneuver Characteristics for Acceleration = 3.6 deg/sec<sup>2</sup> (Three-Axis Simulator Run 51)



Note: \*Approximate in linear range near null (2.5V NOM)  
See Appendix VI for Telemetry Calibration Data

Figure 37. FACS Maneuver Characteristics for Acceleration =  $3.6 \text{ deg/sec}^2$  (Three-Axis Simulator Run 51 Continued)

Table 6

MANEUVER PARAMETERS  
FROM THREE-AXIS SIMULATOR TESTS

FOR 75 DEGREE YAW MANEUVER

<u>High Thrust Acceleration (Deg/Sec<sup>2</sup>)</u>	<u>Configuration</u>	<u>Maneuver Time (Sec)</u>	<u>Maximum Lag Angle (Deg)</u>	<u>Maximum Vehicle Rate (Deg/Sec)</u>	<u>Ref Run No.</u>
1.4	I	24.0	> 45	10.6	40
1.4	I	21.4	36	8.6	47
1.9	I	15.0	33	8.2	48
3.0	I	15.2	33	7.5	49
3.6	I	15.6	33	7.0	51
1.4	IV	21.9	46	9.5	45
3.6	IV	16.6	32	8.1	41

FOR 20 DEGREE PITCH MANEUVER

1.4	I	-	12	6.5	40
1.4	I	-	13	4.4	47
1.9	I	-	12	5.9	48
3.0	I	-	12	5.9	49
3.6	I	-	10.5	5.9	51



parameter is very sensitive to acceleration variation when operating at low levels of acceleration.

Maneuver time is essentially the same at all acceleration levels except when overshoot occurs. Thus the runs at  $\alpha_c = 1.4 \text{ deg/sec}^2$  show an increase of  $\bar{t}$  to 9 seconds in  $75^\circ$  maneuver time. As noted, this condition does not result in premature enabling of the SACS.

#### 4.5.3 ACQUISITION EVALUATION

The process of acquisition is considered to start at the end of an IACS maneuver when the pitch and yaw position gyro error signals have been reduced to a value lower than that established by the SACS-enable level detector. When this condition exists for one second, torque loop closure is initiated.

The acquisition sequence typically requires removal of large ( $0.4^\circ$  to  $4.0^\circ$ ) line-of-sight errors. This is accomplished by torquing the position gyros toward the target and thus producing high-thrust jet action as the vehicle follows. When the position gyro errors are again reduced to a low value for one second, switchover to the low-thrust jets occurs and the fine-pointing limit cycle is established.

When acquisition is accomplished smoothly, valve changeover occurs only once without subsequent dropout and repeat. For this type of action, body rates established by IACS high-thrust jet control must be low enough so that the low-thrust jets can slow the vehicle without overshoot beyond the SACS-enable detector level.

Thus most runs were made using a combination of high acceleration settings for the high-thrust jets and low acceleration settings for the low-thrust jets. After satisfactory acquisition was shown for this "worst case" combination, acquisition behavior was evaluated over the range  $\alpha_c = 1.4$  to  $3.6 \text{ deg/sec}^2$  and  $\alpha_f = .04$  to  $0.18 \text{ deg/sec}^2$ .

Mixing ratio ( $K_M$ ) also influences acquisition. This is the ratio of gyro error signal to sensor error signal maintained by the SACS torquing loop. For a given sensor line-of-sight error, higher values of  $K_M$  result in

larger position gyro error signals. This tends to produce heavier high-thrust valve action. It is possible to raise  $K_M$  to a level where acquisition cannot occur, or to reduce  $K_M$  so low that acquisition times are too long. A range of  $K_M$  from 2.0 to 4.0 was examined.

The setting of the SACS-enable level detector also influences acquisition. Position gyro errors must be greater than this level to produce high-thrust valve action. Thus it is possible to set this level so high that, for a given  $K_M$ , no high-thrust valve action occurs and thus acquisition is slowed. The detector level can be reduced so low that the time available for removal of rates by the low-thrust valves is too short and excessive repetition of switchover occurs, which also slows acquisition.

#### 4.5.3.1 INITIAL EVALUATION

Early tests indicated that satisfactory acquisition could be achieved for  $K_M = 2.0$  and with the SACS-enable level detector at  $0.4^\circ$ . However, a difference in acquisition behavior between pitch and yaw was observed with yaw exhibiting a more oscillatory tendency. Although gravity effects sometimes affected pitch, it was established that this did not explain the differences in behavior. Test records showed higher residual rates in yaw at switchover. An interchange of pitch and yaw rate gyros resulted in transfer of the effect and thus established rate gyro performance as the cause.

The rate gyros used in the FACS breadboard had been used for laboratory checkout and in flight. To determine whether the yaw rate gyro had become defective, the rate gyros were tested on a single-axis simulator. The simulator was driven so as to apply step changes in rate input to the gyros. All three gyros exhibited satisfactory performance for large signals. (This was to be expected since maneuver control of the FACS had been satisfactory.) However, at lower rates corresponding to levels characteristic of target acquisition, the yaw gyro showed a sluggish response. Figure 38 shows the comparative behavior of pitch and yaw rate gyros at 0.2 deg/sec; Figure 39 is similar, but at 0.1 deg/sec. They show that the yaw gyro response to a step change is much slower and that its output amplitude is reduced.

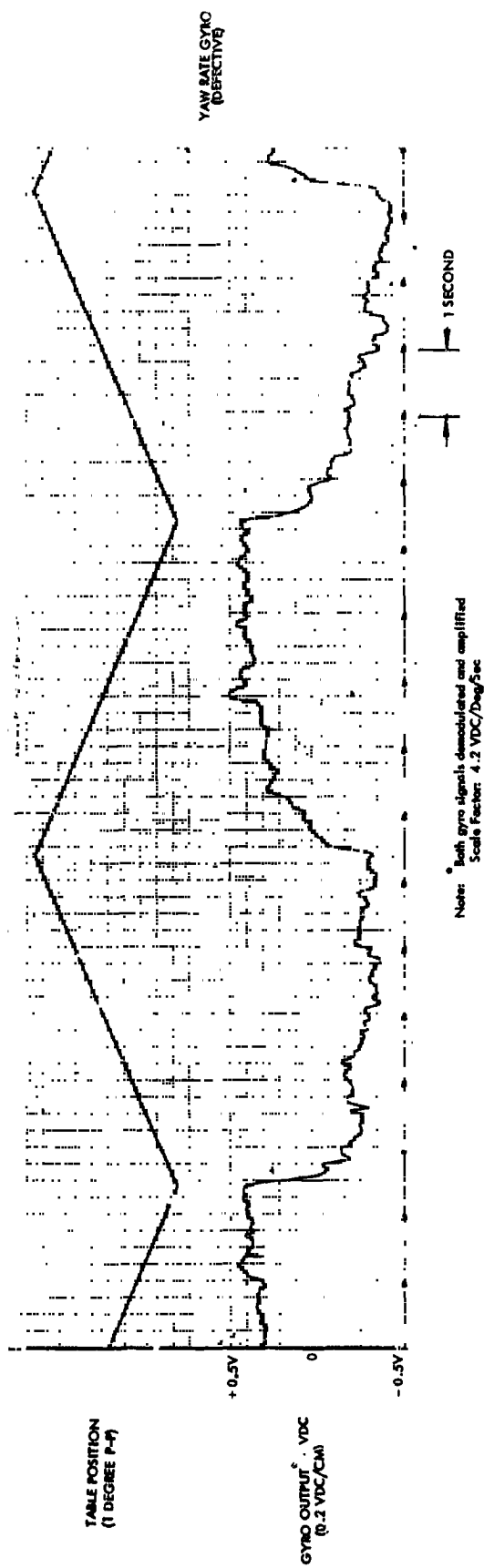
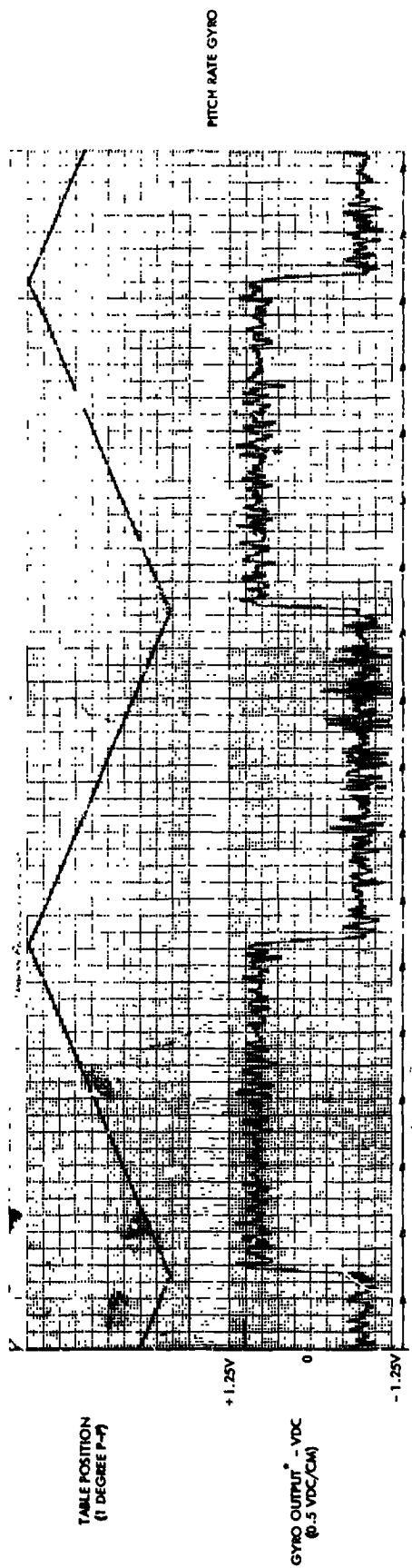


Figure 38. Comparison - Rate Gyro Performance at 0.2 deg/sec

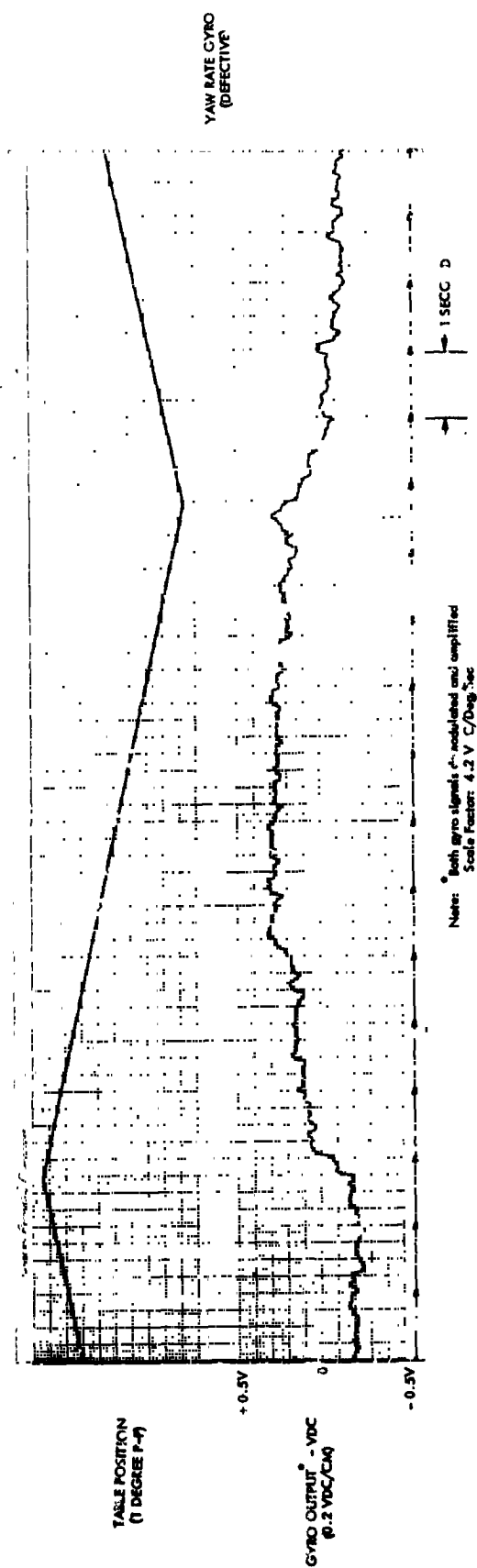
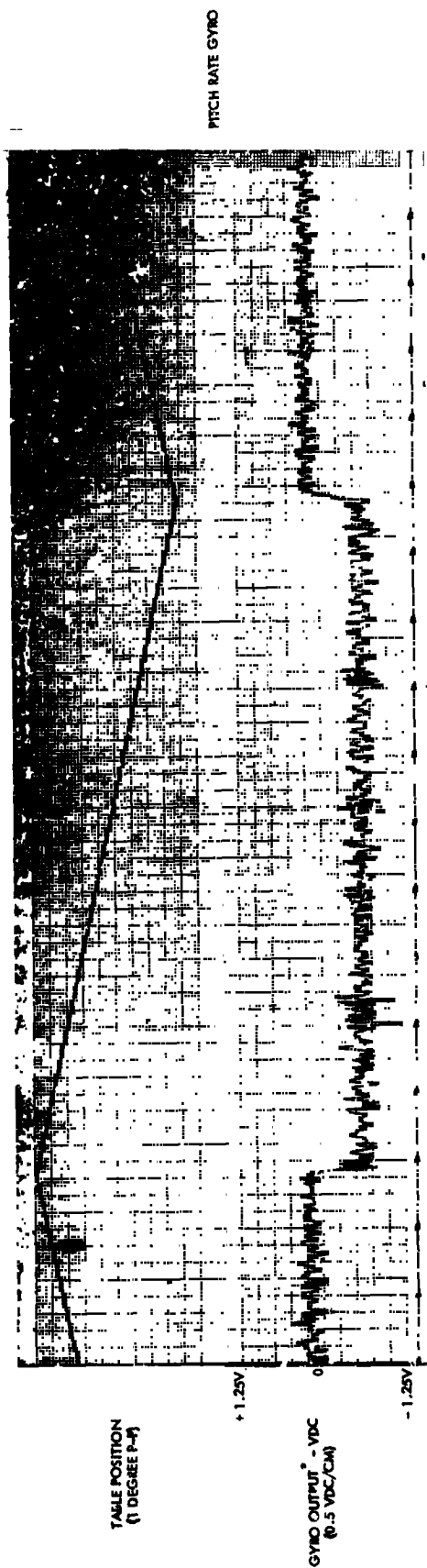


Figure 39. Comparison - Rate Gyro Performance at 0.1 deg/sec

The roll rate gyro was also checked and appeared comparable to the pitch rate gyro. A similar satisfactory check was obtained with three rate gyros obtained GFE from GSFC. One of these gyros was used to replace the defective yaw rate gyro.

Subsequent FACS tests on the three-axis simulator verified that the deficiency in acquisition was corrected by replacement of the yaw rate gyro.

#### 4.5.3.2 ACQUISITION EVALUATION RUNS

The effect of parameter changes on acquisition was somewhat difficult to quantize. The time required for acquisition and the number of switchovers accompanying acquisition were employed as indicators. The line-of-sight error existing at the time of torque loop closure was not determinable. Random variations in this quantity were sufficient to produce a similar random variation in acquisition performance. Nevertheless, by observation of several acquisitions, the effect of a given parameter change was sufficiently discernable to permit selection of appropriate settings.

The line-of-sight error was never greater than  $1.0^{\circ}$ . This was because the geometrical relationship of solar source collimated beam width and sensor distance-from-ball required a pointing error of less than  $1.0^{\circ}$  if the sensor was to be illuminated by the source.

Each simulator run involved four acquisitions. Occasionally, due to an improper initial alignment condition, the line-of-sight error at torque loop closure after the first  $75^{\circ}$  yaw maneuver was greater than  $1.0^{\circ}$  and the sensor was therefore not illuminated. In these cases the vehicle was moved until the sensor entered the collimated beam and normal acquisition followed.

#### 4.5.3.3 EFFECT OF MIXING RATIO ON ACQUISITION

Mixing ratio was varied from 2.0 to 4.0 for Configurations I and IV. Table 7 summarizes the result. For ease of presentation, an average time for the four acquisitions of each run is shown. (The average neglects the first acquisition in those cases where a manual assist was necessary.) Also, the

Table 7

## EFFECT OF MIXING RATIO ON ACQUISITION

( $\alpha_c = 3.6 \text{ deg/sec}^2$ ,  $\alpha_F = .06 \text{ deg/sec}^2$ , SACS-Enable Detector at  $0.4^\circ$ )

Config.	$K_M$	Average Acquisition Time (Sec)		Average Number of Changeovers		Ref. Run
		<u>Yaw</u>	<u>Pitch</u>	<u>Yaw</u>	<u>Pitch</u>	
I	2	5.8	4.9	1.3	1.0	35
	3	6.6	4.9	1.7	1.2	37
	4	6.5	6.8	2.0	2.7	36
IV	2	7.3	6.4	1.2	1.5	41
	3	5.7	6.0	1.5	1.5	43
	4	3.5	4.5	1.0	1.3	42

number of switchovers is averaged. It is, of course, not possible to produce a fractional switchover; nevertheless, the averaged value does provide an indicator of the stability of acquisition.

The averaged data show that Configuration IV is more suited to operation at higher mixing ratios than is Configuration I. Configuration I produced fastest acquisitions with minimum changeover when  $K_M = 2$ . The advantage of higher mixing ratios with Configuration I had been shown during analog computer studies. Although the simulator tests confirmed this (Configuration IV showed best performance at  $K_M = 4$ ), the selection between Configurations I and IV was based on both operating at  $K_M = 2$ . The decision to avoid use of higher mixing ratios took cognizance of the fact that mixing ratio is dependent upon the sensitivity of the solar sensor. Some uncertainty is expected to exist prior to flight. If the actual sensitivity is greater than predicted, the effect is equivalent to an increase in mixing ratio. Thus a mixing ratio of  $K_M = 2$  was selected. Both configurations produce acceptable acquisition at this setting and both make acquisition even if mixing ratio is doubled.

#### 4.5.3.4 EFFECT OF LEVEL DETECTOR ON ACQUISITION

SACS-enable level detector settings of  $0.3^\circ$  and  $0.4^\circ$  were examined. Little difference in acquisition behavior results from so small a change in detector level. A setting of  $0.4^\circ$  was selected on the basis of providing a margin of safety in the event of out-of-tolerance performance of rate gyros or low thrust jets.

#### 4.5.3.5 EFFECT OF CONTROL ACCELERATION ON ACQUISITION

After selection of Configuration I as the preferred configuration (see Section 4.5.5), satisfactory acquisition was demonstrated over the expected range of high-thrust acceleration ( $\alpha_c = 1.4$  to  $3.6 \text{ deg/sec}^2$ ). Table 8 presents a summary of averaged acquisition data. Also shown is the effect of low-thrust acceleration,  $\alpha_F$ .

Figures 40, 41, and 42 show a series of yaw acquisitions from simulator runs made at  $\alpha_c = 1.9, 3.0, \text{ and } 3.6 \text{ deg/sec}^2$ , respectively. These run records show position gyro and sensor signals, both high- and low-thrust jet action, and torque loop closure and torquer action. The runs were made with  $\alpha_F = 0.12 \text{ deg/sec}^2$ .

Figure 43 is a similar record showing yaw acquisition with  $\alpha_F$  reduced to  $0.06 \text{ deg/sec}^2$ .

This testing demonstrated satisfactory acquisition performance from Configuration I with principal parameters varied over the following range:

Mixing Ratio - 2.0 to 4.0

SACS-Enable Level Detector -  $0.3$  to  $0.4^\circ$

Low Thrust Valve Switching Threshold - 5.0 to 22.5 arc sec

High Thrust Acceleration - 1.4 to  $3.6 \text{ deg/sec}^2$

Low Thrust Acceleration - 0.06 to  $0.12 \text{ deg/sec}^2$

The parameter values selected for the prototype FACS were:

Mixing Ratio - 2.0

SACS-Enable Level Detector -  $0.4^\circ$

Table 8

EFFECT OF ACCELERATION ON ACQUISITION  
FROM THREE-AXIS SIMULATOR TESTS

Configuration I

Mixing Ratio = 2

SACS-Enable Detector at  $0.4^\circ$

Variation - High-Thrust Acceleration

(Low-Thrust Jet Switching at  $\pm 22.5$  arc seconds)

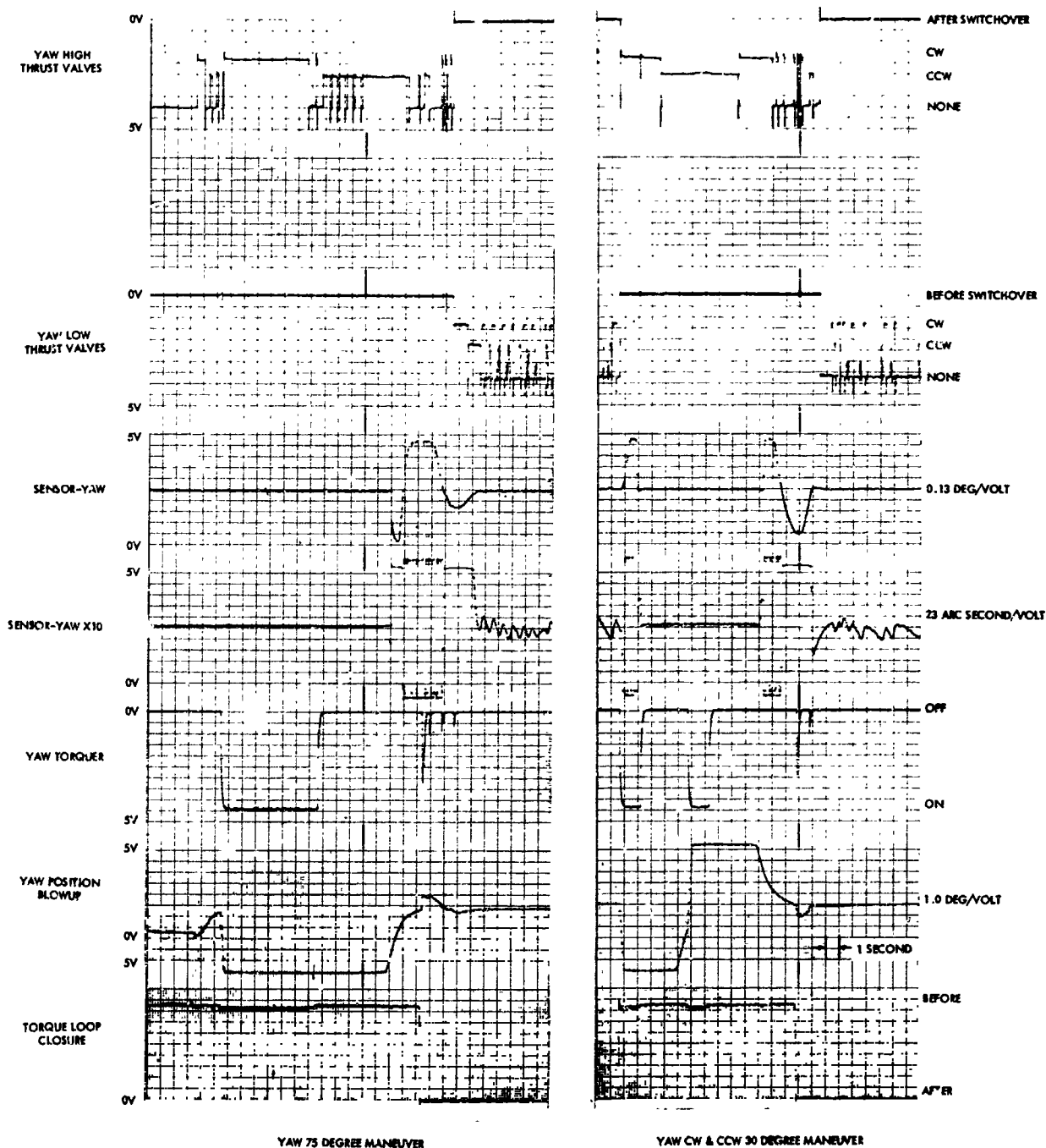
<u>Control Acceleration (Deg/Sec<sup>2</sup>)</u>		<u>Average Acquisition Time (Sec)</u>		<u>Average Number of Changeovers</u>		<u>Reference Run</u>
<u>High Thrust</u>	<u>Low Thrust</u>	<u>Yaw</u>	<u>Pitch</u>	<u>Yaw</u>	<u>Pitch</u>	
1.4	.12	4.3	4.3	1.0	1.0	47
1.9	.12	2.8	3.2	1.0	1.0	48
3.0	.12	3.1	3.4	1.0	1.2	49
3.6	.12	6.9	4.6	1.2	1.0	50

Variation - Low Thrust Acceleration

(Low-Thrust Jet Switching at  $\pm 10$  arc seconds)

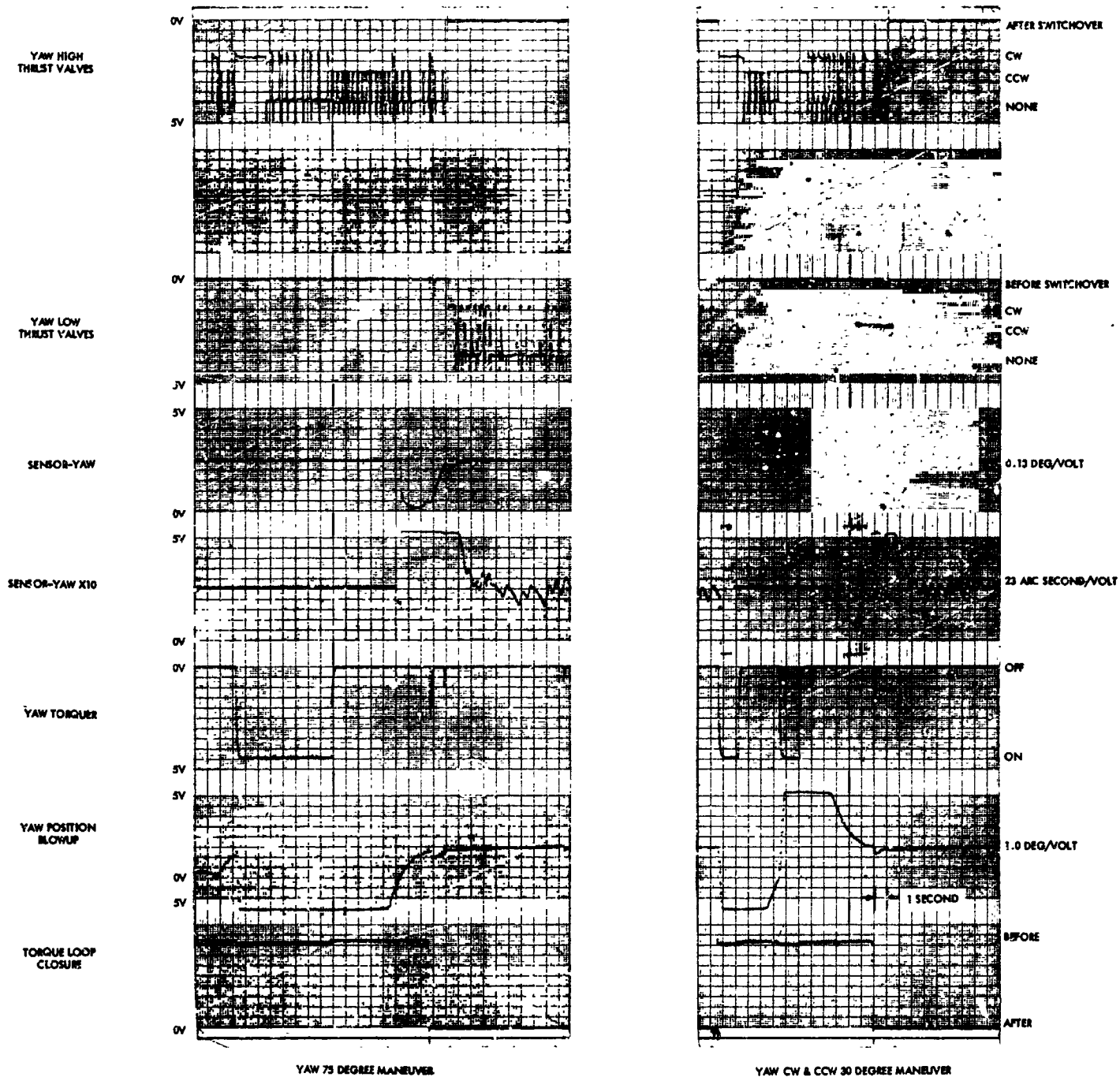
<u>Control Acceleration (Deg/Sec<sup>2</sup>)</u>		<u>Average Acquisition Time (Sec)</u>		<u>Average Number of Changeovers</u>		<u>Reference Run</u>
<u>High Thrust</u>	<u>Low Thrust</u>	<u>Yaw</u>	<u>Pitch</u>	<u>Yaw</u>	<u>Pitch</u>	
3.6	.12	3.2	3.8	1.0	1.0	51
3.6	.06	5.1	5.8	1.0	1.0	52





Notes: 1. See Appendix VI for Telemetry Calibration Data  
 2. Low thrust acceleration,  $a_p = 0.12 \text{ Deg/Sec}^2$

Figure 40. FACS Acquisition Characteristics for  $\alpha_c = 1.9 \text{ deg/sec}^2$   
 (Three-Axis Simulator Run 40)



Notes: 1. See Appendix VI for Telemetry Calibration Data  
2. Low thrust acceleration,  $a_p = 0.12 \text{ Deg/Sec}^2$

Figure 41. FACS Acquisition Characteristics for  $\alpha_c = 3.0 \text{ deg/sec}^2$   
(Three-Axis Simulator Run 49)

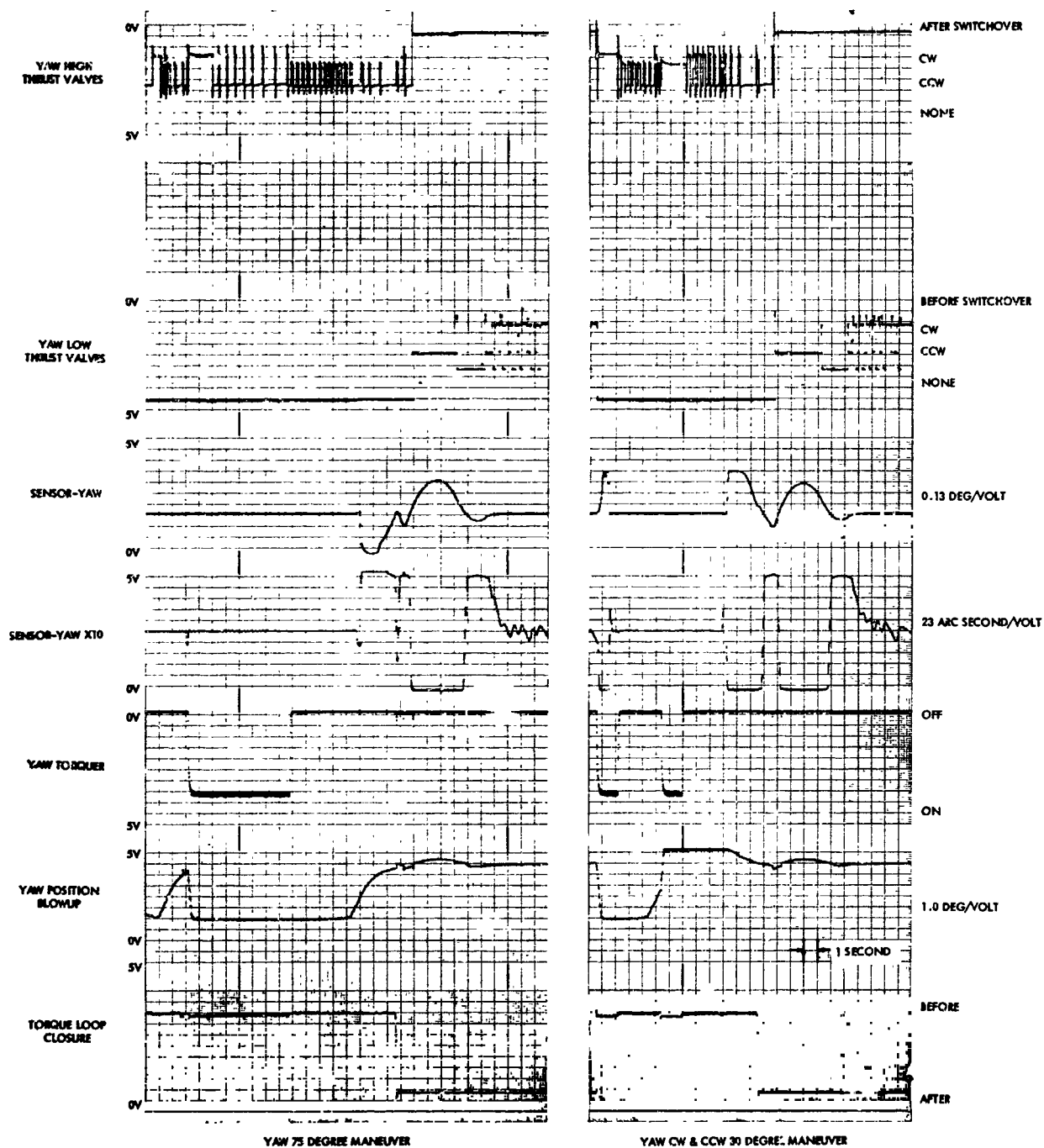
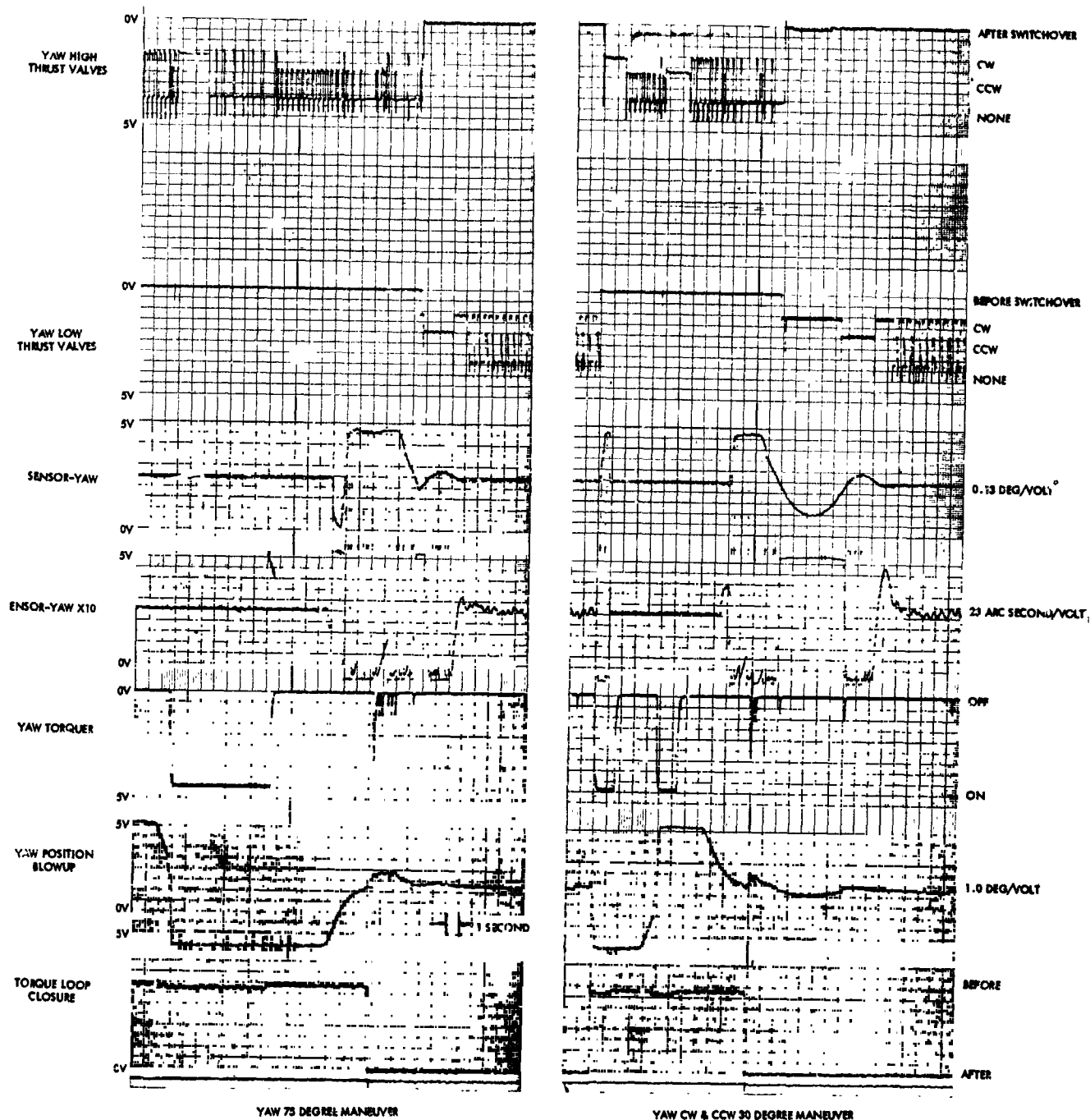


Figure 42. FACS Acquisition Characteristics for  $\alpha_c = 3.6 \text{ deg/sec}^2$   
(Three-Axis Simulator Run 50)



Notes: 1. See Appendix VI for Telemetry Calibration Data  
 2. Low thrust acceleration,  $a_p = .06 \text{ Deg/Sec}$

Figure 43. FACS Acquisition Characteristics for Reduced  $\alpha_F$   
 (Three-Axis Simulator Run 52)

## 4.5.4

## LIMIT CYCLE EVALUATION

During testing on the three-axis simulator, attention was directed primarily to evaluation of the on-target limit cycle control established by the SACS circuits operating on signals from the solar sensor. The programmer sequence did, however, permit observation of IACS limit cycle characteristics after the final yaw maneuver.

## 4.5.4.1

## IACS LIMIT CYCLE

The IACS limit cycle is established by the IACS control circuits operating on signals provided by the position and rate gyros. The limit cycle characteristics are sensitive to rate gain and to the acceleration produced by the high-thrust reaction jets. A suitable value for pitch and yaw low rate gain ( $K_R = 1.25$  sec) had been established by analog computer studies and was retained throughout testing of Configuration I on the simulator. Also, the switching threshold was set at  $\pm 0.25^\circ$  and was not changed.

The following tabulation indicates the effect of yaw high thrust acceleration ( $\alpha_c$ ) on the IACS limit cycle period. It should be noted that the limit cycle periods shown are only generally indicative of performance. Irregularities in the limit cycle make a precise determination unfeasible. This may be seen by observation of the high-thrust jet action shown during program position 11 in Figures 33 and 37. In the former figure, for  $\alpha_c = 1.4$  deg/sec<sup>2</sup>, the yaw high-thrust jet action shows a point at which an external disturbance was required to excite a limit cycle.

## IACS LIMIT CYCLE CHARACTERISTIC

<u>Ref Run No.</u>	<u>High Thrust Acceleration - Deg/Sec<sup>2</sup></u>	<u>Yaw Limit Cycle Period - Seconds</u>
47	1.4	8
48	1.9	8
49	3.0	6
51	3.6	4

Control acceleration levels in the roll channel were set to  $7.0 \text{ deg/sec}^2$  for most runs, with a few runs made at  $1.0 \text{ deg/sec}^2$ . Three-axis simulator run 51 was conducted at  $7.0 \text{ deg/sec}^2$  with rate gain  $K_R = 0.88 \text{ sec}$ . The limit cycle period in roll was observed to be approximately 2.0 seconds. Unfortunately, the runs made with the lower roll acceleration level ( $1.0 \text{ deg/sec}^2$ ) exhibited roll unbalance which prevented determination of the characteristic limit cycle.

When operated with the Aerobee 150-150A, the IACS control acceleration is dependent upon the pressure of residual helium in the vehicle tanks. The system is operated in a blowdown fashion and a gradually decreasing thrust level results from gas usage. The intent of testing here was to show satisfactory limit cycle behavior over the anticipated range of acceleration level.

#### 4.5.4.2 SACS LIMIT CYCLE

Tests were conducted to evaluate the SACS limit cycle sensitivity to variations in low-thrust acceleration and to valve-switching threshold level. The effect of variations in derived rate gain was not examined. A suitable value for the lead time constant (0.6 second) had been established by analog computer studies and was used throughout the tests.

Acceleration levels were varied over a range of  $0.04$  to  $0.18 \text{ deg/sec}^2$ . When operated in an Aerobee 150, the SACS reaction jet thrust level will be fixed by use of a pneumatic regulator. The objective of testing here was to establish a preferred level. Acquisition was shown to be reliable over the indicated range; the effect on limit cycle is discussed below.

The SACS valve-switching threshold level was varied over a range from  $\pm 22.5$  arc seconds down to  $\pm 5.0$  arc seconds. The switching threshold corresponds to the angular error which will produce valve-control-trigger action for zero body rate. When the limit cycle is established, the characteristic body rates tend to produce jet turn-on at lower position errors.

Setting of threshold level for switching at a desired angular error is dependent upon calibration of the solar sensor. The sensor characteristic is in turn dependent upon the illumination level provided by the solar source simulator. Prior to three-axis simulator tests, sensor calibrations had

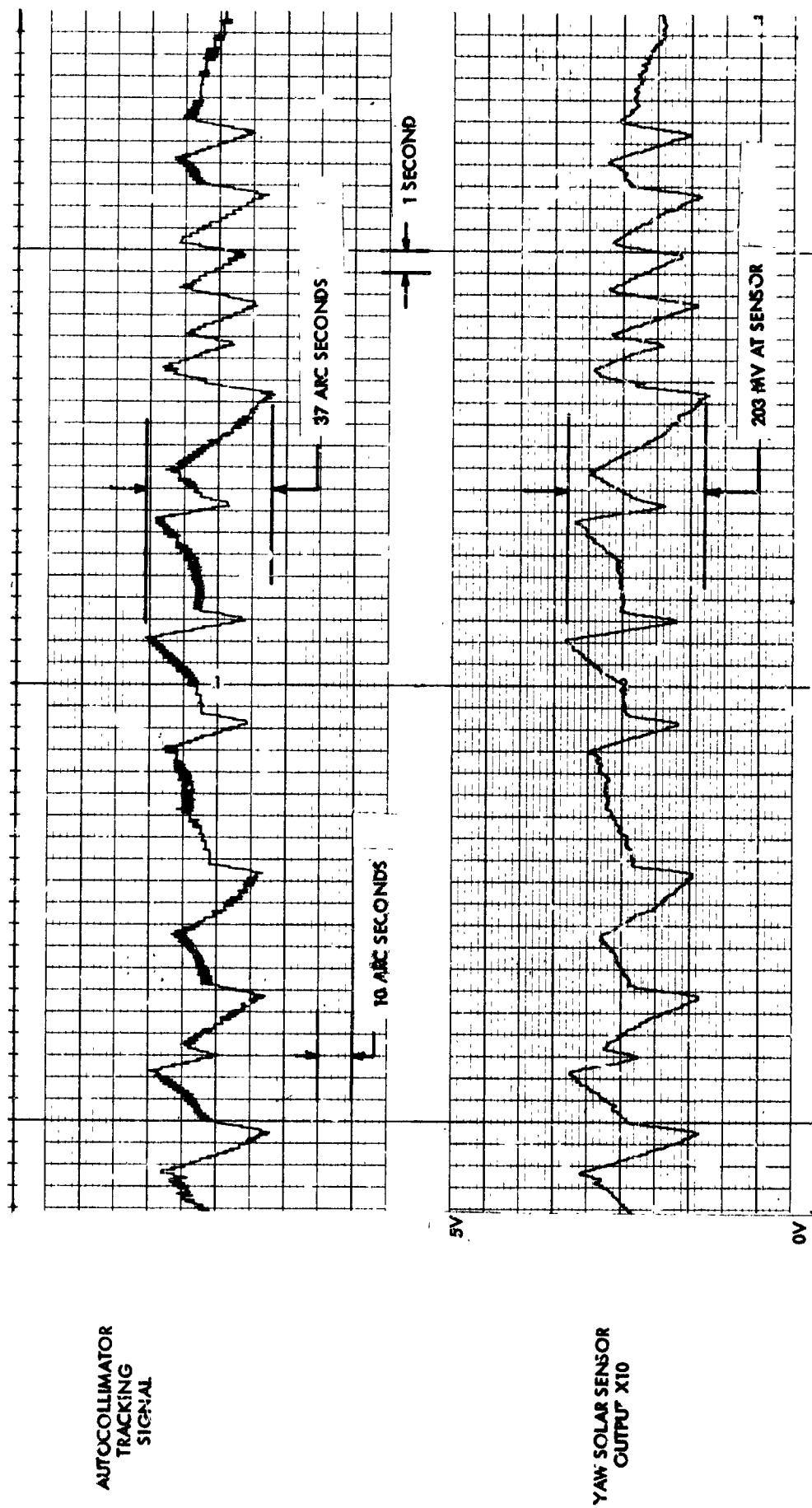
been made using a photo-voltaic cell as a reference for source intensity. The reference cell was utilized to establish the solar-source intensity at the GSFC facility so as to provide a desired solar sensor sensitivity of 5 mv/arc second. Autocollimator measurements during limit cycle indicate that the actual sensitivity was slightly higher near null. However, since all settings were made on the basis of 5 mv/arc second, this scale factor has been used for all data reduction involved in the following discussions.

The examination of the lower amplitude limit cycles is related to the anticipated requirements of solar pointing experimenters. A target goal here is to maintain limit cycle amplitude within  $\pm 10$  arc seconds while holding body rates below 5 arc second/second. The FACS tests demonstrated the capability of producing the low-amplitude limit cycle. However, body rates were significantly higher than the desired 5 arc seconds/second.

Preliminary evaluation tests were conducted using a promising technique for approaching this goal proposed and implemented by GSFC. The technique herein referred to as "delayed feedback", represents a simple form of pulse-width control. Results of these tests are discussed in Section 4.5.8. The following discussion is concerned with limit cycle characteristics of the FACS without delayed-feedback circuits incorporated.

#### 4.5.4.2.1 SACS LIMIT CYCLE - CORRELATION OF SENSOR AND AUTOCOLLIMATOR

Figure 44, showing data obtained from three-axis simulator run 40, is typical of the correspondance shown between the autocollimator tracking signal and the output signal from the solar sensor. Close agreement is seen in the transient behavior of the two signals. This quality of agreement lends confidence as to the dynamic-tracking capability of the autocollimator. There is, however, an apparent small discrepancy between angular displacement as indicated by sensor and autocollimator. That is, based on a sensor sensitivity of 5 mv/arc second, the angular displacement indicated by the sensor is greater by approximately 10% than the displacement indicated by the collimator. It appears quite likely that (at least for this run) the sensor-source combination was such as to produce a sensitivity at the sensor output of 5.5 mv/arc second when operating near null.



- Note:
1. Low thrust acceleration =  $0.6 \text{ Deg/sec}^2$  ; Switching threshold =  $22.5 \text{ arc sec (1/2\sigma)}$ .
  2. Indicated solar sensor sensitivity:  $5.5 \text{ mv/arc second}$ .
  3. Data from three-axis simulator Run 49

Figure 44. SACS Limit Cycle - Correlation of Sensor to Autocollimator



The sensor-source calibration data obtained prior to three-axis simulator tests was achieved by measuring sensor output with line-of-sight errors of several arc minutes. The day-to-day setting of source intensity was also subject to slight error. Under these circumstances the correlation is considered quite good. Also, errors in the order of 10% do not seriously affect any of the findings from the simulator tests.

#### 4.5.4.2.2 SACS LIMIT CYCLE DESCRIPTION

Portions of nine three-axis simulator tests have been excerpted to show the effect on limit cycle of variations in low-thrust acceleration ( $\alpha_f$ ) and valve-switching threshold.

Figure 45 shows operation at a threshold setting of  $\pm 22.5$  arc seconds for  $\alpha_f = 0.18, 0.12, 0.08$ , and  $0.04 \text{ deg/sec}^2$ . Clearly shown is the reduction in limit cycle frequency, and increase in angular displacement as  $\alpha_f$  is reduced.

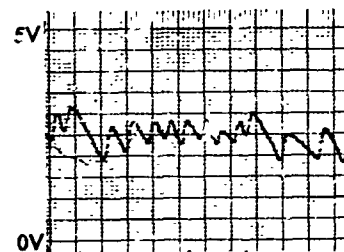
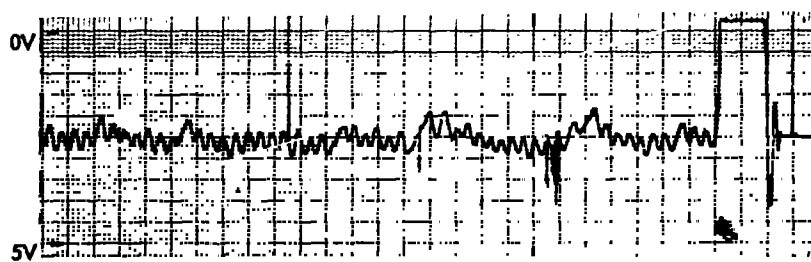
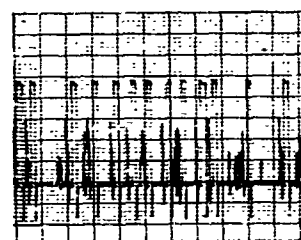
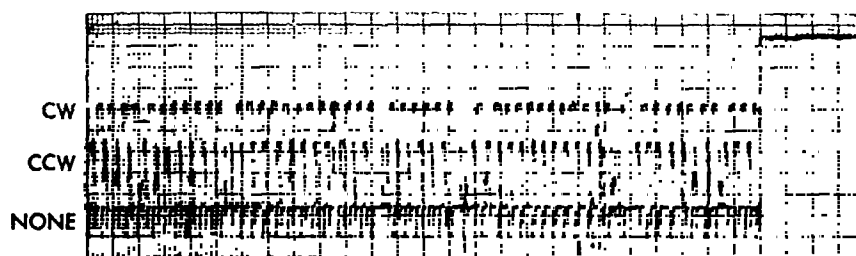
Figure 46 shows similar records for a threshold setting of  $\pm 10$  arc seconds, and Figure 47 shows records obtained with a threshold of  $\pm 5.0$  arc seconds.

A summary of results is shown in Table 9. It is seen that the amplitude of limit cycle was held satisfactorily low. The indicated vehicle rates represent the highest values observed over a period of approximately 25 seconds. In all cases examined they were higher than desirable for solar pointing. For example, Table 9 shows a maximum rate of  $58 \text{ arc sec/sec}$  with the threshold at  $\pm 10 \text{ arc sec}$  and  $\alpha_f = 0.06 \text{ deg/sec}^2$ ; this is an order of magnitude greater than desired. Incorporation of delayed-feedback produced considerable improvement as discussed in Section 4.5.8 below.

Testing indicates that for operation without delayed feedback, a low-thrust acceleration of  $0.08 \text{ deg/sec}^2$  represents the best selection. This value is low enough to provide reasonable limit cycle characteristics, and high enough to produce reliable acquisition. The tests demonstrate that limit cycle amplitudes as low as  $\pm 9 \text{ arc seconds}$  can be achieved at this thrust level.

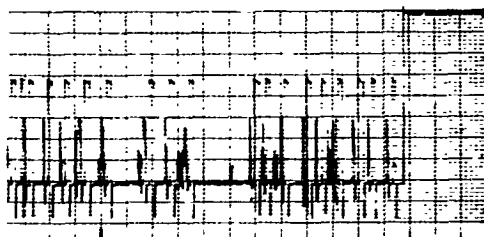
$a_F = 0.18 \text{ DEG/SEC}^2$   
 (THREE-AXIS SIMULATOR RUN 7J)

(THR

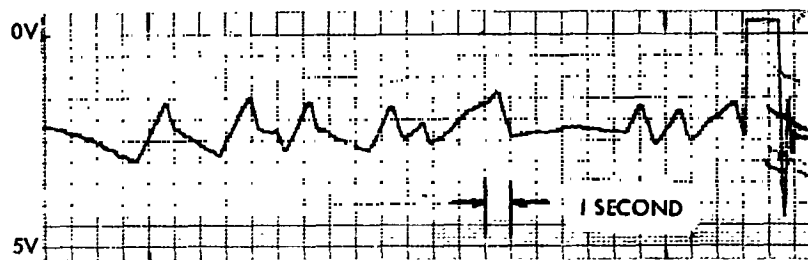
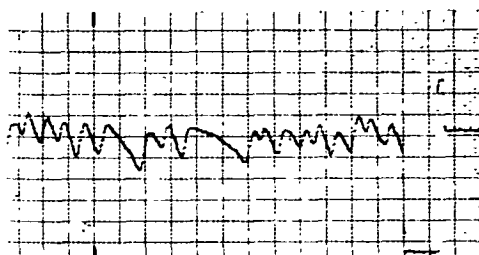
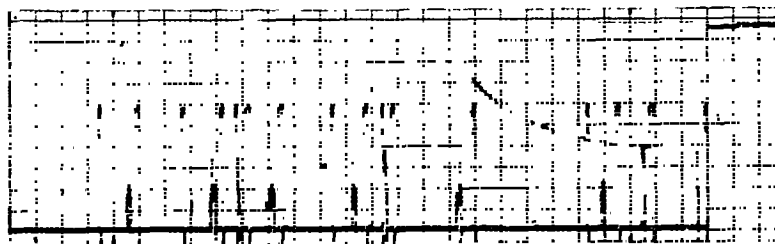


94-1

$a_F = 0.12 \text{ DEG/SEC}^2$   
 EE-AXIS SIMULATOR RUN 47)



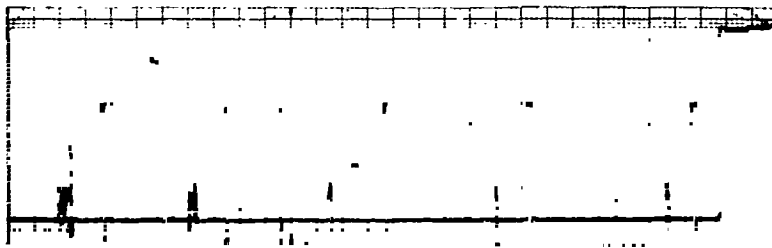
$a_F = .08 \text{ DEG/SEC}^2$   
 (THREE-AXIS SIMULATOR RUN 21)



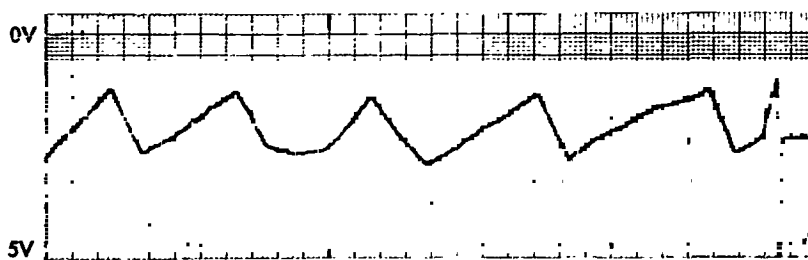
- Note:
1.  $a_F$  is low-thrust acceleration
  2. Yaw Sensor Output X10: 1.0 VDC = 23 arc seconds
  3. Lag Feedback not installed

Figure 45. SACS Limit Cycle Characteristics for Switching  
 Threshold  $\pm 22.5$  Arc Seconds

$a_F = .04 \text{ DEG/SEC}^2$   
(THREE-AXIS SIMULATOR RUN 23)

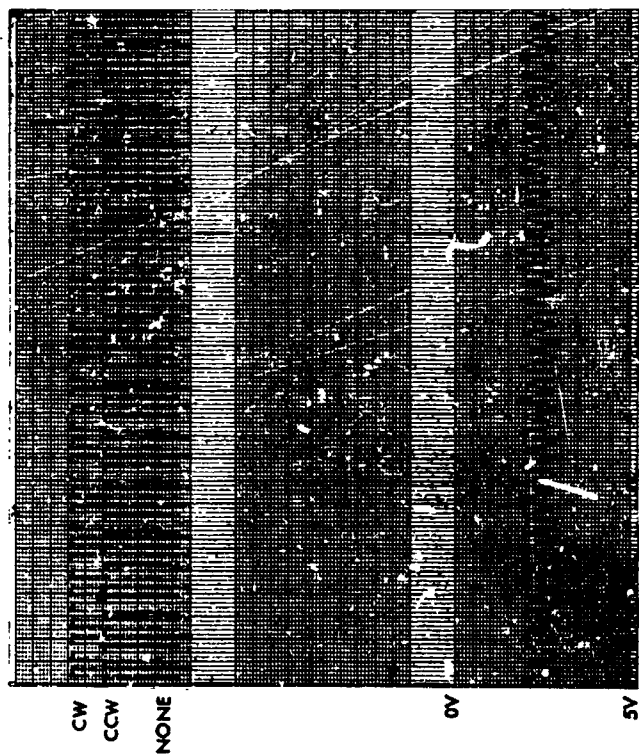


YAW LOW THRUST  
VALVES

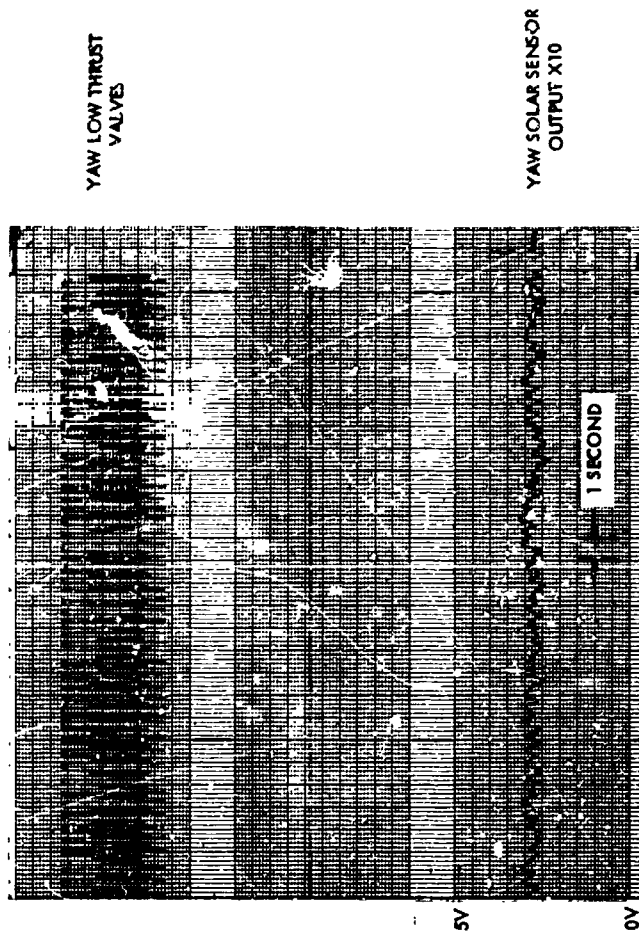


YAW SOLAR SENSOR  
OUTPUT X10

$a_F = 0.12 \text{ DEG/SEC}^2$   
(THREE-AXIS SIMULATOR RUN 54)



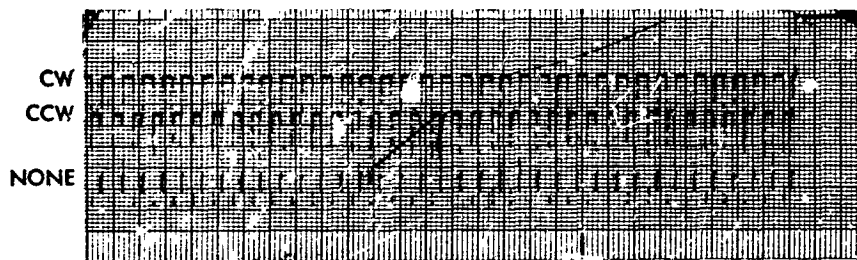
$a_F = .06 \text{ DEG/SEC}^2$   
(THREE-AXIS SIMULATOR RUN 52)



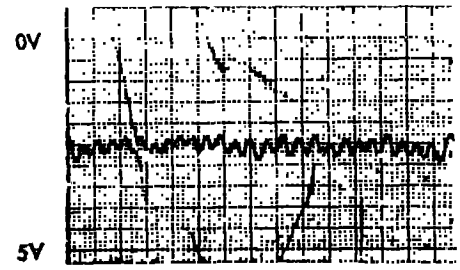
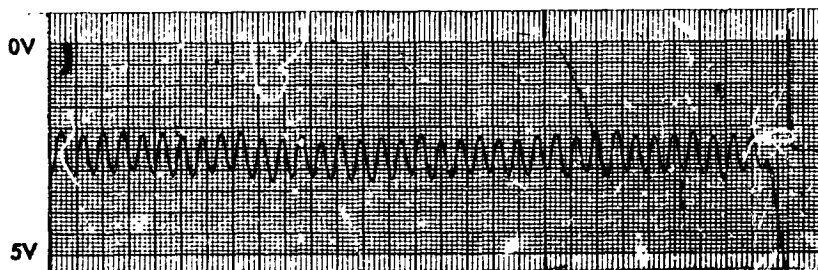
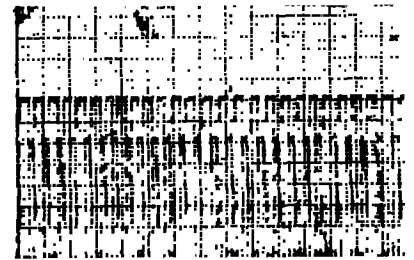
Note: 1.  $a_F$  is low-thrust acceleration  
2. Yaw Sensor Output X10; 1.0 VDC = 23 arc seconds  
3. Lag Feedback not Installed

Figure 46. SACS Limit Cycle Characteristics for Switching  
Threshold + 10 Arc Seconds

$a_F = 0.12 \text{ DEG/SEC}^2$   
(THREE-AXIS SIMULATOR RUN 57)



$a_F = .08 \text{ DEG/S}$   
(THREE-AXIS SIMULATC)

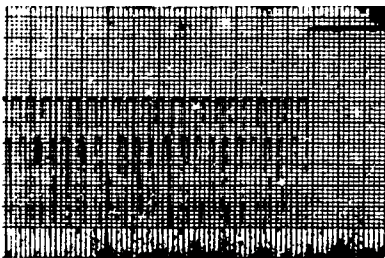


Note: 1.  $a_F$  is low-thrust c  
2. Yaw Sensor Output  
3. Lag feedback not

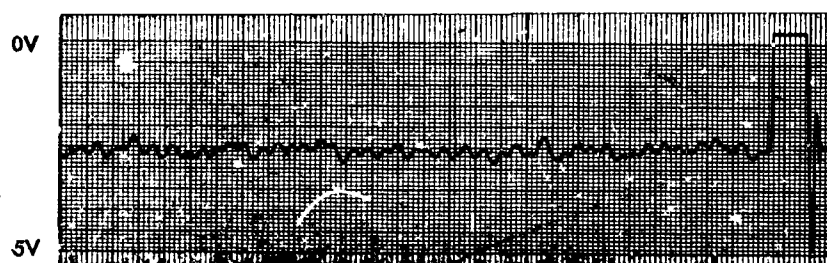
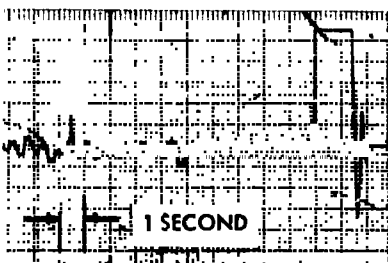
Figure 47. SACS Limit Cycle  
Threshold  $\pm 5$

SEC<sup>2</sup>  
 OR RUN 80

$a_F = .01 \text{ DEG/SEC}^2$   
 (THREE-AXIS LATOR RUN 80)



YAW LOW THRUST  
 VALVES



YAW SOLAR SENS  
 OUTPUT X10

acceleration  
 at X10: 1.0 VDC = 23 arc seconds  
 installed

Characteristics for Switching  
 Arc Seconds

Table 9

SACS LIMIT CYCLE CHARACTERISTICS  
 (Without Delayed-Feedback)  
 FROM THREE-AXIS SIMULATOR TESTS

<u>Switching Threshold Level (arc sec)</u>	<u>Low Thrust Acceleration (deg/sec<sup>2</sup>)</u>	<u>Max. Peak-to-Peak Amplitude (arc sec)</u>	<u>Avg. Period (sec)</u>	<u>Max. Vehicle Rate (arc sec/sec)</u>	<u>Ref. Run No.</u>
± 22.5	.18	21	0.5	116	7J
	.12	33	0.9	96	47
	.08	39	3.0	50	21
	.04	42	5.4	29	23
± 10.0	.12	32	0.74	145	54
	.04	16	0.54	58	52
± 5.0	.12	28	0.77	129	57
	.08	17	0.55	77	8E
	.04	12	0.53	42	8G



Simulator test findings resulted in selection of FACS Configuration I for follow-on design. Although four configurations were checked, the final selection was based upon a comparison of Configurations I and IV. This was because the differences between configurations were so minor that each exhibited closely similar performance. Therefore the advantages of dual vs single detector and single-level vs bi-level rate gain could be ascertained by a direct comparison of Configurations I and IV.

As discussed in Section 4.5.2, the configuration change produced no significant effect on maneuver characteristics.

Inherently, the configuration change produces no effect on SACS limit cycle. Single level vs bi-level rate gain can influence the IACS limit cycle but testing did not demonstrate a discernable difference.

As discussed in Section 4.5.3, the configuration change did influence acquisition behavior. Although both exhibited satisfactory behavior, Configuration I was shown to be better suited to operation at low mixing ratio. A comparison was made of vehicle body rate at the time of switchover to the low-thrust jets. The following tabulation shows the result of averaging this value for four acquisitions:

	<u>Configuration I</u>		<u>Configuration IV</u>	
High Thrust Acceleration - $\text{deg/sec}^2$	3.6	1.4	3.5	1.4
Mixing Ratio	2.0	2.0	2.0	2.0
Body Rate at First Switchover - $\text{deg/sec}$	0.085	0.062	0.150	0.117
Ref. Runs	35	40	41	45

Configuration I characteristically produces the lowest rates at changeover. This attribute is advantageous for a smooth transition to SACS operation.

Although some component simplification would have been possible by selection of Configuration IV, the acquisition behavior of Configuration I was judged sufficiently superior to warrant its selection.

#### 4.5.6 FINAL CONFIGURATION SUMMARY

Simulator tests were conducted at various levels of high-thrust acceleration for the selected Configuration I.

Maneuver characteristics have been shown in Figures 32 through 37.

Acquisition characteristics have been shown in Figures 40, 41, 42, and 43.

SACS limit cycle characteristics have been shown in Figures 45, 46 and 47.

Of the parameters and configuration features evaluated during simulator tests, the following selections were made:

- a. Configuration I, dual detector, bi-level rate gain was selected.
- b. Position signal limiting was incorporated in the IACS pitch and yaw channels.
- c. Roll rate gain switching accomplished at roll capture and locked thereafter.
- d. IACS pitch and yaw rate gains set at 1.55 sec (high) and 1.25 sec (low). Roll rate gain set at 1.54 sec (high) and 0.88 sec (low).
- e. Mixing ratio set at 2.0.
- f. SACS-enable detector set at  $0.4^{\circ}$ .
- g. Low-thrust acceleration at  $0.08 \text{ deg/sec}^2$  preferred unless delayed feedback incorporated.
- h. SACS valve-switching threshold settings between 22.5 and 5.0 arc seconds found acceptable; can be adjusted to suit mission requirements.

#### 4.5.7

#### CORRELATION WITH ANALOG COMPUTER STUDIES

Analog computer runs were made for the purpose of assessing the degree of correlation with 3-axis simulator tests.

##### 4.5.7.1

##### MANEUVER CHARACTERISTICS

Maneuver runs made on the analog computer show the same general characteristics as observed during 3-axis simulator tests. Sample analog records for a  $75^\circ$  maneuver are shown in Figures 48 and 49 for high thrust acceleration levels of 1.4 and 3.6 deg/sec<sup>2</sup>, respectively. Similar records are shown for a  $20^\circ$  maneuver in Figures 50 and 51. (Note: The configuration and parameter values applicable to each of the analog computer records reproduced herein have been tabulated in the run index of Table 10.)

Table 11 shows a tabulation of maneuver parameters obtained from analog records. This may be compared directly with the similar tabulation for 3-axis simulator tests shown in Table 6. A comparison will show that analog results generally yield:

- ♦ Slightly shorter maneuver time,  $T_M$
- ♦ Lower values of maximum lag angle,  $\psi_{E_{max}}$
- ♦ Slightly higher maximum vehicle rates,  $\dot{\psi}_{max}$

To account for the differences, the correspondence between the two simulations with respect to several parameters which significantly affect maneuver characteristics has been examined. The parameters considered significant are high thrust acceleration,  $\alpha_c$ , gyro torquing rate,  $\dot{\psi}_c$ , and effective rate gain,  $K_{RE}$ . The time constants associated with the valves and amplifiers are thought to be sufficiently small to have negligible effects on  $T_M$ ,  $\psi_{E_{max}}$ , and  $\dot{\psi}_{max}$  \*.

The effect of a difference in  $\alpha_c$ , alone, between the two simulations can be assessed from the results obtained. As  $\alpha_c$  increases from 1.4 deg/sec<sup>2</sup> to 3.6 deg/sec<sup>2</sup>, the trends of  $T_M$ ,  $\psi_{E_{max}}$ , and  $\dot{\psi}_{max}$  characteristically vary

---

\* It is recognized, however, that these time constants can have a significant influence on impulse expended during maneuver (c.f. Reference 1, Section 6).

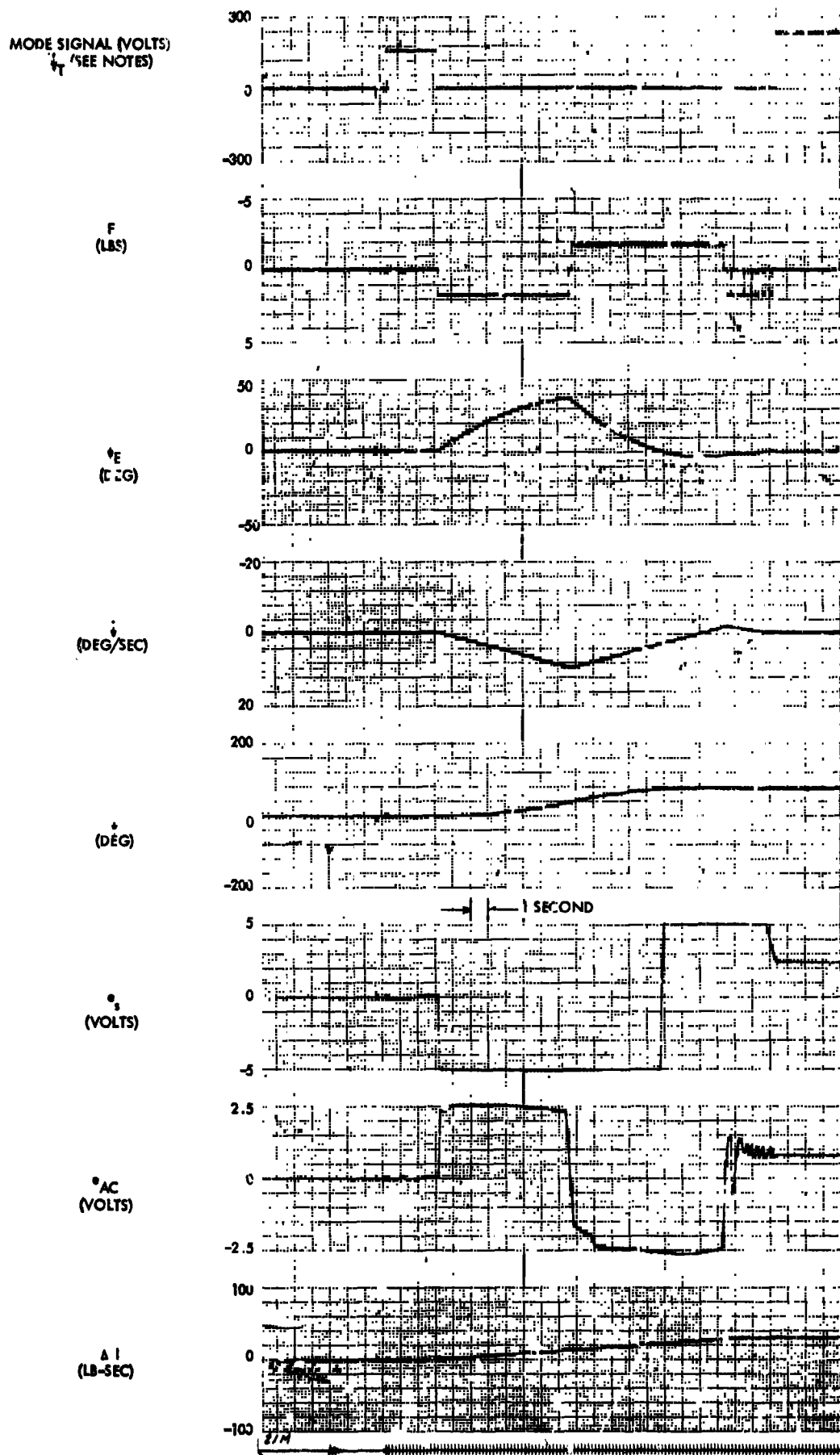


Figure 48.  $75^\circ$  Maneuver at  $\alpha_c = 1.4 \text{ deg/sec}^2$  (Analog Run 21M)

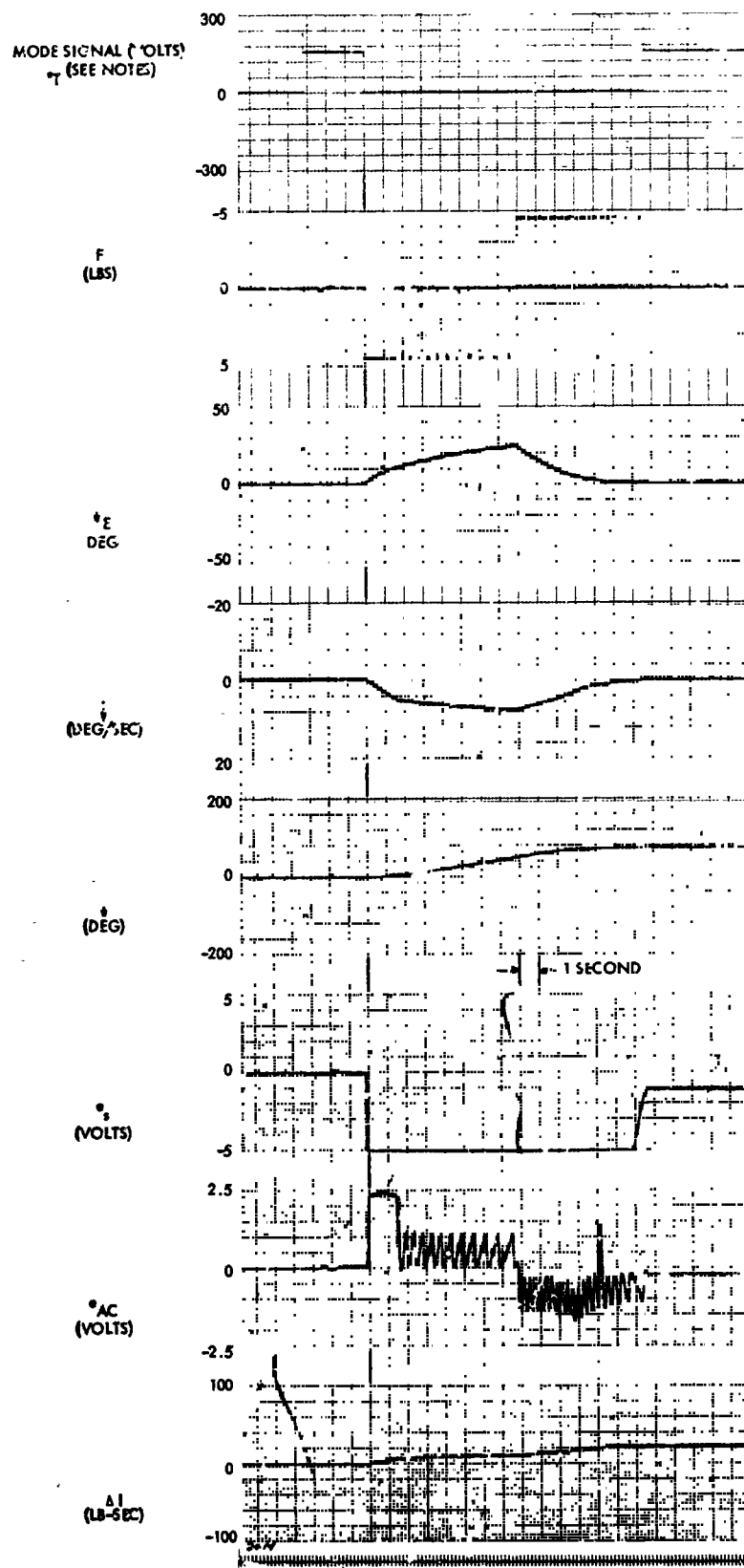


Figure 49.  $75^\circ$  Maneuver at  $\alpha_c = 3.6 \text{ deg/sec}^2$  (Analog Run 24M)

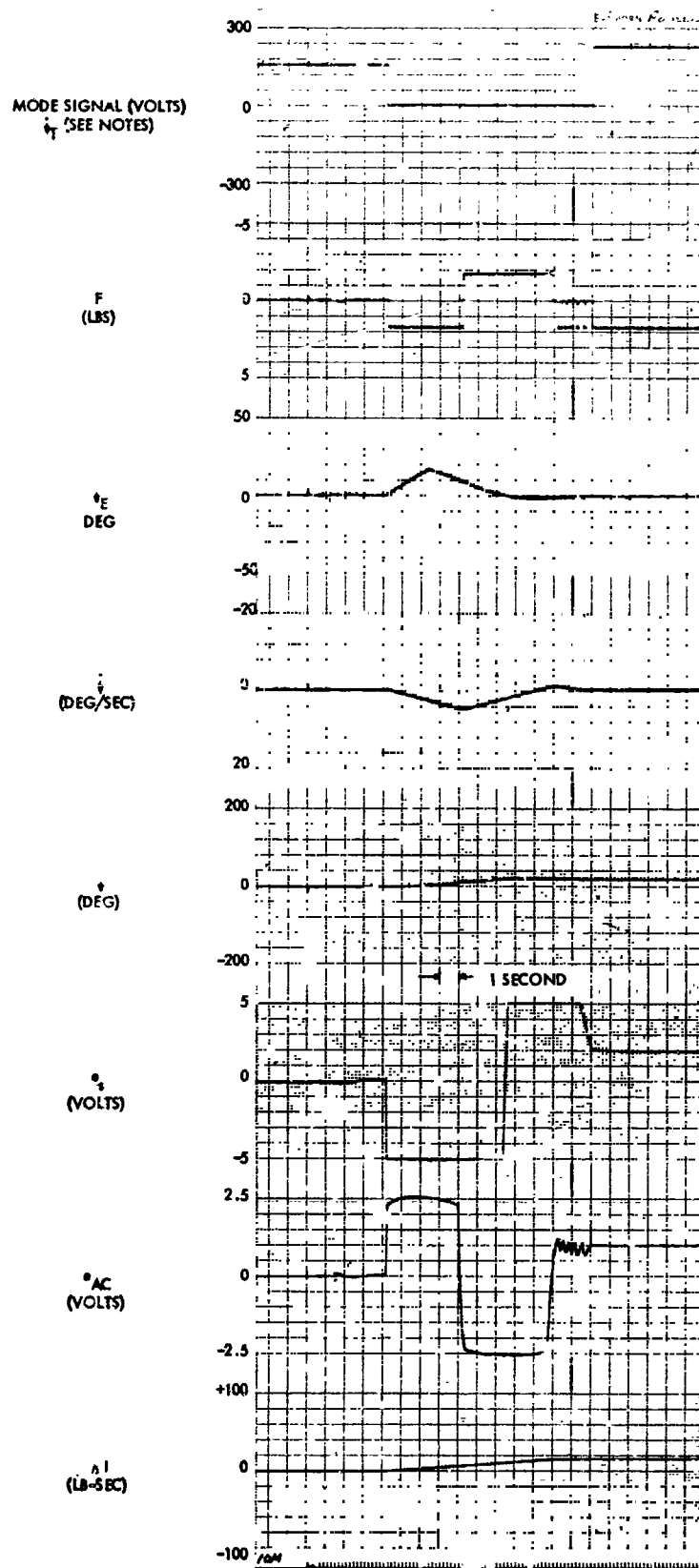


Figure 50.  $20^\circ$  Maneuver at  $\alpha_c = 1.4 \text{ deg/sec}^2$  (Analog Run 10M)

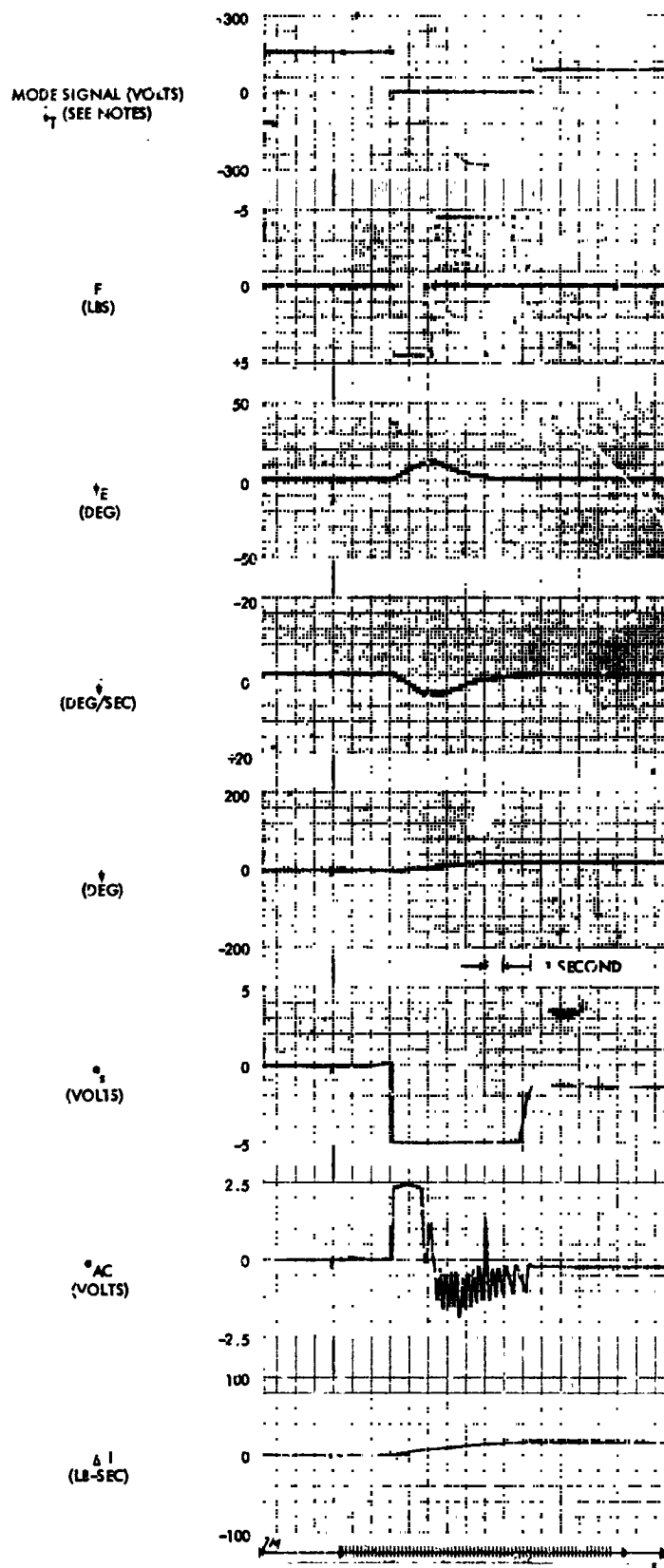


Figure 51.  $20^\circ$  Maneuver at  $\alpha_c = 3.6 \text{ deg/sec}^2$  (Analog Run 7M)

Table 10

## INDEX OF SELECTED RUNS

Figure Number	Type	Configuration	Maneuver Angle (deg)	$\psi_{EO}$ (deg)	$\alpha_c$ (deg/sec <sup>2</sup> )	$\alpha_f$ (deg/sec <sup>2</sup> )	$e_{TP}$ (arc-sec)	$e_{T1}$ (deg)	$e_{T2}$ (deg)	$K_M$ (1/1)	Run Number
48	M	I	75	0	1.4	.12	22.5	.4	2.0	2	21M
49	M	I	75	0	3.6	.12	22.5	.4	2.0	2	24M
50	M	I	20	0	1.4	.06	22.5	.4	2.0	4	10M
51	M	I	20	0	3.6	.06	22.5	.4	2.0	4	7M
54	A	I	75	0	1.4	.12	22.5	.4	2.0	2	21A-1
55	A	I	75	+3	1.4	.12	22.5	.4	2.0	2	21A-2
56	A	I	75	-3	1.4	.12	22.5	.4	2.0	2	21A-3
57	A	I	75	0	3.6	.12	22.5	.4	2.0	2	24A-1
58	A	IV	75	0	3.6	.06	22.5	.4	.4	2	11A-1
59	A	I	75	0	3.6	.12	10	.4	2.0	2	25A-1

NOTE: Parameter values not shown are as given in Reference 1 except for specific changes discussed in Section 4.3.2 of this report.



Table 11

ANALOG SIMULATION MANEUVER PARAMETERS  
FOR 75 DEGREES YAW MANEUVER

<u>High Thrust Acceleration (deg/sec<sup>2</sup>)</u>	<u>Configuration</u>	<u>Maneuver Time (sec)</u>	<u>Maximum Lag Angle (deg)</u>	<u>Maximum Vehicle Rate (deg/sec)</u>	<u>Analog Run Number</u>
1.4	I	19.3	37	9.4	21M
1.9	I	14.5	29	8.8	22M
3.0	I	14.8	25	8.0	23M
3.6	I	14.7	25	8.2	24M
1.4	IV	19.5	37	10.0	15M
3.6	IV	15.0	25	8.4	11M

FOR 20 DEGREES YAW MANEUVER

1.4	I	10.8	17	5.2	10M
3.6	I	7.4	13	5.6	7M

from their highest values at  $\alpha_c = 1.4 \text{ deg/sec}^2$  to relatively constant values as  $\alpha_c$  increases toward  $3.6 \text{ deg/sec}^2$ . If  $\alpha_c$ , alone, were the difference, the maneuver characteristics obtained from both simulations should then be the same at the high acceleration level. However, a comparison of the results shows significant differences at  $\alpha_c = 3.6 \text{ deg/sec}^2$ . This indicates that differences in  $\alpha_c$  alone cannot account for the differences in maneuver results.

The steady state lag angle in a ramp command, position-plus-rate, system is proportional to both the effective rate gain,  $K_{RE}$ , and the gyro torquing rate,  $\dot{\psi}_C$ . The gyro sine pick-off and position signal limiter are nonlinearities in the FACS which cause  $K_{RE}$  to be a function of the lag angle,  $\psi_E$ . The steady state condition is not realized for  $75^\circ$  (and smaller) maneuvers. This is true of both simulations. Both simulations also show that for  $75^\circ$  maneuvers  $\dot{\psi}_{max}$  is attained nearly simultaneously with  $\psi_{E_{max}}$  and a thrust-off state. Thus, operation at this point is on the switching line.

If  $\dot{\psi}_C$  were less in the analog simulation than in the air bearing simulation, the generally lower  $\psi_{E_{max}}$  obtained in the analog simulation could be attributed to a  $\dot{\psi}_C$  difference. However, if  $\dot{\psi}_C$  were less in the analog simulation,  $T_M$  should be greater and  $\dot{\psi}_{max}$  should be less, in general, for the analog simulation. The results show the converse to be true. Therefore, the differences in results cannot be attributed, in a consistent manner, to differences in  $\dot{\psi}_C$  alone.

The possibility that the switching logic and corresponding  $K_{RE}$  in the analog simulation differed from that in the 3-axis simulation was examined. First, the compliance of the analog switching logic with the hardware test results was checked. Figure 52 shows the results. The switching line with limiting was derived from the position-limiter calibration test results for a rate gain setting,  $K_1''/K_1 = 1.55$  seconds. (The switching line without limiting is shown for reference only. It is the logic used in Reference 1 adjusted for rate gain.) Then yaw rate,  $\dot{\psi}$ , and lag angle,  $\psi_E$ , were read from the analog traces at thrust-off conditions. These values were superimposed on the switching line graph. It is evident that the hardware test results were properly simulated on the analog computer. A comparison of analog simulation and 3-axis

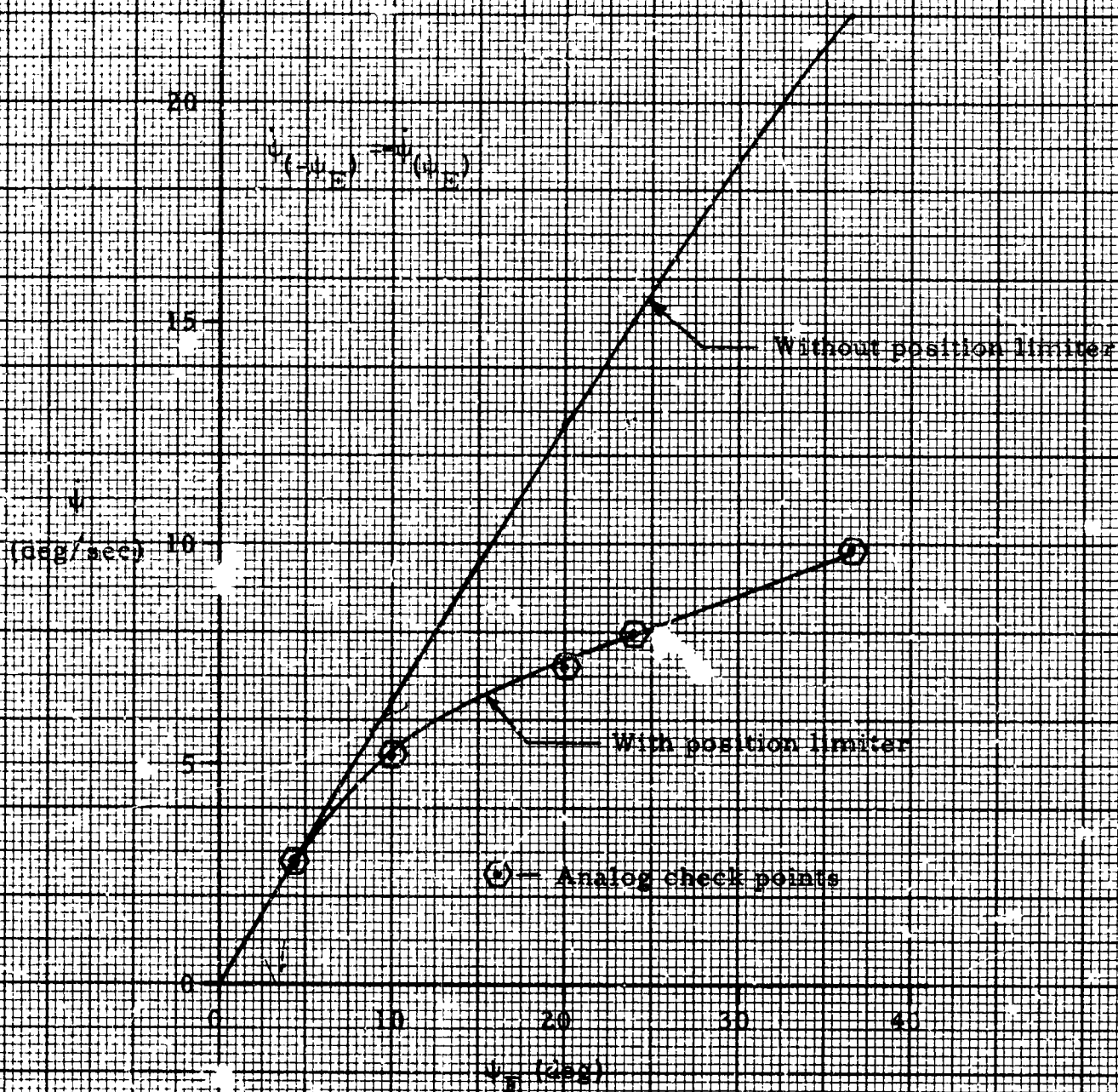


Figure 52. IACS Switching Logic Derived from Position-Limiter Calibration ( $K_1''/K_1 = 1.55$  sec)

simulation switch points was made based on the  $\psi_{E_{max}}$  and  $\psi_{max}$  values shown in Tables 6 and 11. As previously stated, these values occur simultaneously and with thrust-off for a  $75^\circ$  maneuver. The comparison is shown in Figure 53. It is seen that the indicated switch points from the air bearing simulation lie below the reference switch line, whereas those from the analog simulation are distributed along the reference switch line. The dispersion of the switch points suggests that a statistical treatment of the data is appropriate. A statistical approach is further justified in consideration of the uncertainties in the accuracies of both the analog and 3-axis simulator data and uncertainties concerning external disturbances which existed during the air bearing tests (air disturbances and c.g. offset torques, for example). A quasi-statistical comparison of the results from the two simulations is presented in Table 12. Deviations are given as a percentage of the reference as indicated. The effective rate gain comparison is based on the data shown in Figure 53. Here, effective rate gain is defined as

$$K_{RE} = \frac{\psi_{E_{max}}}{\psi_{max}}$$

It is seen that the  $K_{RE}$  for the analog simulation nearly coincides with that derived from hardware test data; the percentage deviation has an average value of -0.08% and an rms value of 2.7%. The 3-axis simulator data yields a  $K_{RE}$  which has an 18.4% higher value and this compares fairly well with the 22.1% higher average value for  $\psi_E$  obtained. The longer  $T_M$  (-7.7%) and lower  $\psi_M$  (-7.5%) obtained from 3-axis simulator data are consistent with the indicated higher  $K_{RE}$ . These results strongly suggest that, during the 3-axis simulator tests, the position signal limiter had an output in the limited range approximately 20% below that indicated by the position-limiter calibration tests. Substantiating but not conclusive evidence of this could be obtained by a rerun of several conditions on the analog computer with the position signal limiter set, in the limited range, to limit 20% lower than previously.

The foregoing comparison of analog with three-axis simulator results refers to the  $75^\circ$  maneuver condition. The results from two  $20^\circ$  analog simulation maneuvers are shown in Table 11 for comparison with results in

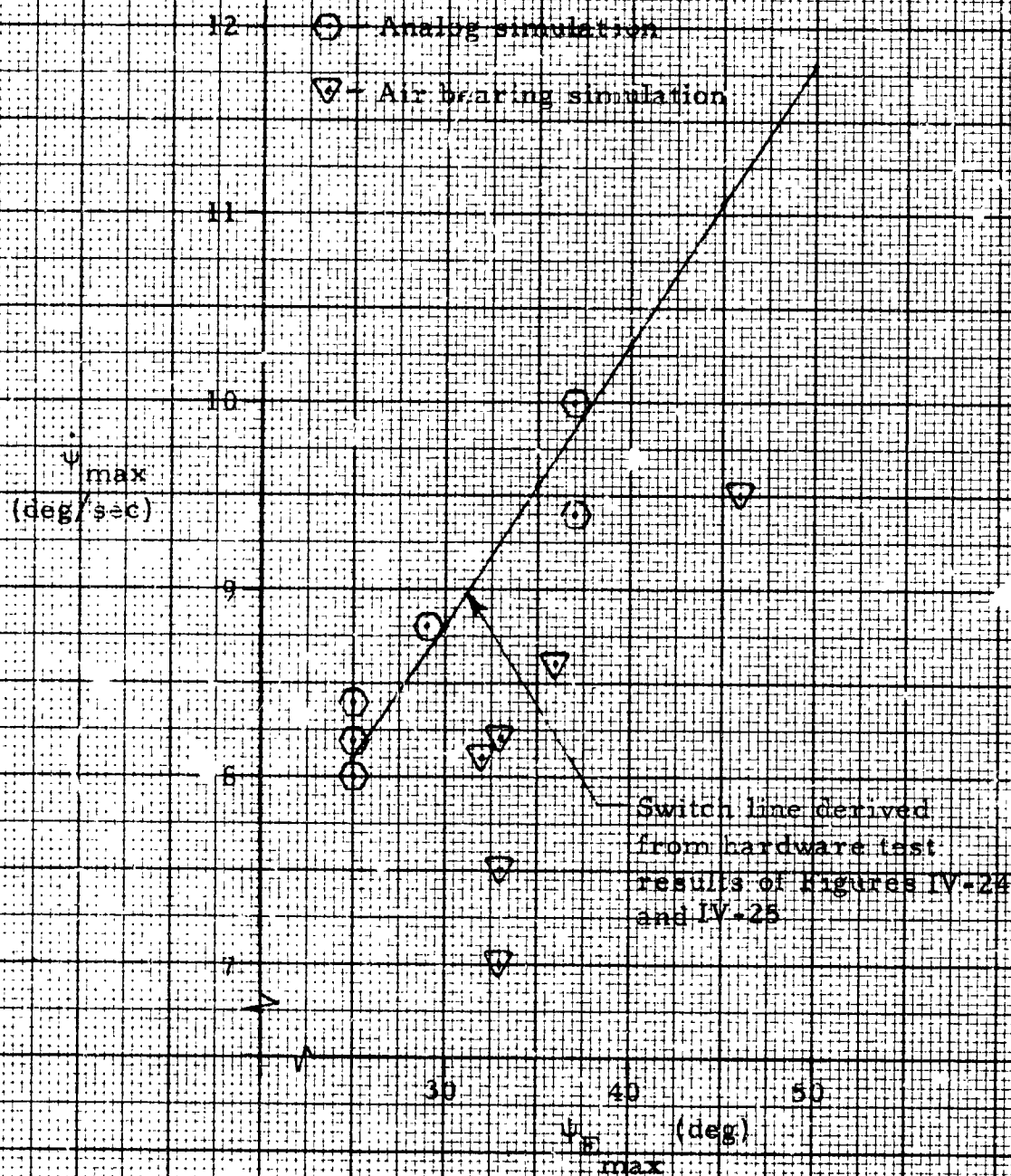


Figure 5 Comparison Between Analog Simulation and Air Bearing Simulation Switch Points (75 deg maneuver)

Table 12

COMPARISON OF ANALOG AND 3-AXIS SIMULATOR  
MANEUVER RESULTS FOR 75 DEGREE MANEUVER

Percent Deviation from "Hardware Test" Switch  
Line Effective Rate Gain

	Average Deviation	RMS Deviation
Analog	-0.08	2.7
3-Axis Simulator	+18.4	19.7

Percent Deviations of 3-Axis Simulation Results  
from Analog Simulation Results

Maneuver Time		Maximum Lag Angle		Maximum Vehicle Rate	
Average	RMS	Average	RMS	Average	RMS
+7.7	8.6	+22.1	24.2	-7.5	8.3

Table 13

MAXIMUM LAG ANGLE COMPARISON  
FOR 20 DEGREE MANEUVER

High Thrust Acceleration, $\alpha_c$ (deg/sec)	Maximum Lag Angle (deg)		
	Analytical	Analog	3-Axis Simulator
1.4	16.3	17	13
3.6	11.2	12	10.5

Table 6. Again it is seen that the  $20^\circ$  maneuver has not approached steady state ramp conditions at completion of the command. Also, for lag angles of the order indicated,  $17^\circ$  maximum, the position signal is not so significantly affected by the nonlinearities. Figure 50 shows that for  $\alpha_c = 1.4 \text{ deg/sec}^2$ , a continuous thrust pulse exists from initiation of command through the time at which maximum lag angle occurs. That is, the switching line is not encountered prior to  $\psi_{E_{\max}}$ . Figure 51, where  $\alpha_c = 3.6 \text{ deg/sec}^2$ , shows a single pulse dropout with recurrence in the same direction to the completion of the  $20^\circ$  command and the point of  $\psi_{E_{\max}}$  occurrence. It appears that for a  $20^\circ$  command,  $\psi_{E_{\max}}$  is then primarily dependent on the magnitude of command,  $\psi_{C_{\max}}$ , the command rate,  $\dot{\psi}_C$ , and the acceleration level,  $\alpha_c$ , as follows:

$$\psi_{E_{\max}} = \psi_{C_{\max}} - \frac{1}{2} \alpha_c \left( \frac{\psi_{C_{\max}}}{\dot{\psi}_C} \right)^2$$

Table 13 compares the  $\psi_{E_{\max}}$  obtained in the simulations with that obtained from the above equation solved for nominal values. The major difference is that the 3-axis simulator shows a somewhat lower  $\psi_{E_{\max}}$  at  $\alpha_c = 1.4 \text{ deg/sec}^2$ . This difference is most likely the result of differences in parameters which appear in the right hand member of the above equation or is attributable to external disturbing torques in the three-axis simulation. The  $\dot{\psi}_{\max}$  obtained for  $20^\circ$  maneuvers are roughly the same in both simulations.

#### 4.5.7.2 ACQUISITION EVALUATION

Acquisition time,  $T_{AC}$ , is the most important characteristic associated with acquisition in that a  $T_{AC}$  increase or decrease is in direct trade-off with an on-target viewing time decrease or increase, respectively. Acquisition results from the analog simulation are shown in Tables 14 and 15. These may be compared with the three-axis simulator results of Tables 8 and 7, respectively.

Table 14

EFFECT OF ACCELERATION ON ACQUISITION,  
CONFIGURATION I

Mixing Ratio = 2

SACS - Enable Detector at 0.4 Degree

Variation - High Thrust Acceleration  
(Low Thrust Jet Switching at  $\pm 22.5$  Arc Seconds)

Control Acceleration (deg/sec <sup>2</sup> )		Acquisition Time (Seconds)			Number of Changeovers			Analog Run
High Thrust	Low Thrust	$\psi_{EO} = +3^{\circ}$	Yaw $= 0^{\circ}$	$= -3^{\circ}$	$\psi_{EO} = +3^{\circ}$	Yaw $= 0^{\circ}$	$= -3^{\circ}$	
1.4	0.12	8.5	2.5	11.0	2	1	2	21A
1.9	0.12	11.6	5.9	11.9	2	1	2	22A
3.0	0.12	9.0	4.9	7.9	2	1	2	23A
3.6	0.12	10.9	3.4	7.5	2	1	2	24A

Variation - Low Thrust Acceleration  
(Low Thrust Jet Switching at  $\pm 10$  Arc Seconds)

Control Acceleration (deg/sec <sup>2</sup> )		Acquisition Time (Seconds)			Number of Changeovers			Analog Run
High Thrust	Low Thrust	$\psi_{EO} = +3^{\circ}$	Yaw $= 0^{\circ}$	$= -3^{\circ}$	$\psi_{EO} = +3^{\circ}$	Yaw $= 0^{\circ}$	$= -3^{\circ}$	
3.6	0.12	11.6	3.4	8.0	2	1	2	25A
3.6	0.06	9.8	9.8	9.8	2	1	2	26A



Table 15

ANALOG SIMULATION EFFECT OF  
MIXING RATIO ON ACQUISITION

$$(\alpha_c = 3.6 \text{ deg/sec}^2, \alpha_f = .06 \text{ deg/sec}^2, e_{m1} = 0.4 \text{ deg}, \psi_{EO} = 0 \text{ deg})$$

<u>Configuration</u>	<u>K<sub>M</sub></u>	<u>Acquisition</u> <u>Time</u> <u>(sec)</u>	<u>Number of</u> <u>Changeovers</u>	<u>Analog</u> <u>Run</u>
		<u>Yaw</u>	<u>Yaw</u>	
I	2	10.0	1	1A
	3	6.2	2	3A
	4	4.4	1	2A
IV	2	10.5	1	11A
	3	8.0	2	13A
	4	6.9	2	12A

Acquisition characteristics are predominantly affected by  $\psi_{EO}$ , the difference between the fine sensor and gyro references at completion of maneuver.  $\psi_{EO}$  is readily controlled in the analog simulation but is neither easily controlled nor measured in the three-axis simulation. This and other differences in terminal maneuver conditions, rates for example, disallow a direct quantitative comparison of acquisition results from the two simulations.

In Table 14, the analog results show that for Configuration I and  $K_M = 2.0$ , a coarse thrust jet re-activation, identified as the "number of changeovers," occurs for the magnitude of  $\psi_{EO} = 3.0^\circ$  and does not occur for  $\psi_{EO} = 0$ . The three-axis simulator results in Table 8 show that, in general, coarse thrust jet re-activation did not occur. This indicates that  $\psi_{EO}$  was nearer to zero than  $3^\circ$  for the three-axis simulator runs. It is also noted that the acquisition times observed on the three-axis simulator were generally about the same as shown on the analog for  $\psi_{EO} = 0$ .

The analog simulation results in Table 15 show a trend of decreasing  $T_{AC}$  with increasing mixing ratio,  $K_M$ , in the range of  $K_M$  evaluated for both Configurations I and IV. This trend is apparent in the three-axis simulation results of Table 7 for Configuration IV only.

Typical acquisition and limit cycle oscillograph records from the analog simulation are shown in the following figures:

<u>Figure</u>	$\alpha_c$	$\alpha_f$	$\psi_{EO}$
	(deg/sec <sup>2</sup> )	(deg/sec <sup>2</sup> )	
54	1.4	0.12	0
55	1.4	0.12	+3
56	1.4	0.12	-3
57	3.6	0.12	0
58	3.6	0.06	0

#### 4.5.7.3 SACS LIMIT CYCLE EVALUATION

The analog simulation SACS limit cycle characteristics of Table 16 may be compared with those from the 3-axis simulation in Table 9. Limit cycle position amplitudes are in reasonably good agreement except for the 10 arc second threshold,  $\alpha_f = 0.12$  deg/sec<sup>2</sup> acceleration condition. Three-axis simulator runs at the 10 arc second threshold showed an increase in amplitude as  $\alpha_f$  was increased from 0.06 to 0.12 deg/sec<sup>2</sup>. Analog runs show the opposite effect as do the 3-axis simulator runs for a 22.5 arc second threshold. The limit cycle during 3-axis simulator tests exhibited a low thrust value duty cycle approaching 100% (see Figure 46) for the 10 arc second threshold with  $\alpha_f = 0.12$  deg/sec<sup>2</sup>. The corresponding analog record (see Figure 59) exhibits a much less severe duty cycle.

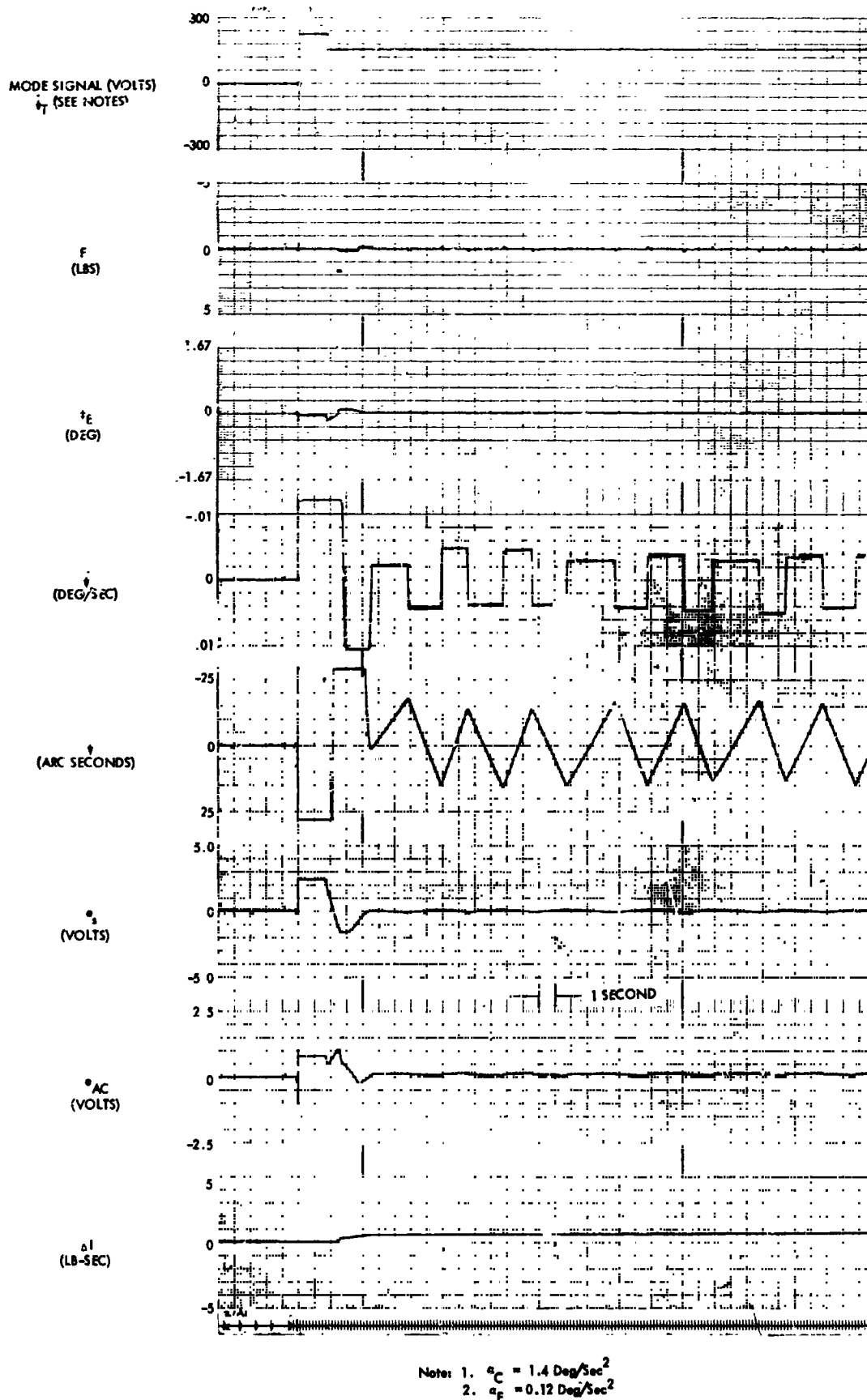
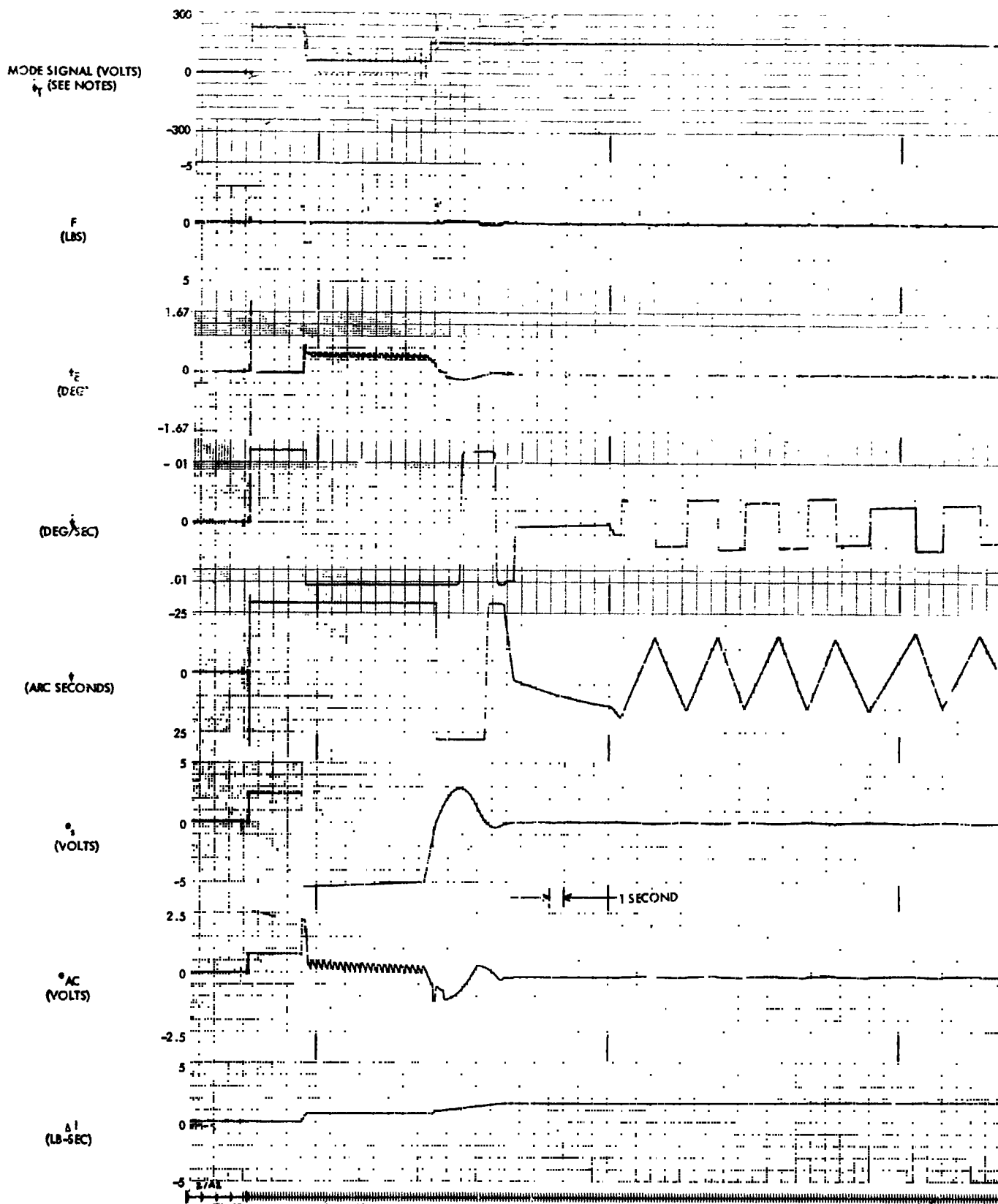


Figure 54. Acquisition and Limit Cycle for  $\psi_{EO} = 0$   
 (Analog Run 21A-1)



Note: 1.  $a_c = 1.4 \text{ Deg/Sec}^2$   
 2.  $a_f = 0.12 \text{ Deg/Sec}^2$

Figure 55. Acquisition and Limit Cycle for  $\psi_{EO} = +3^\circ$   
 (Analog Run 21A-2)

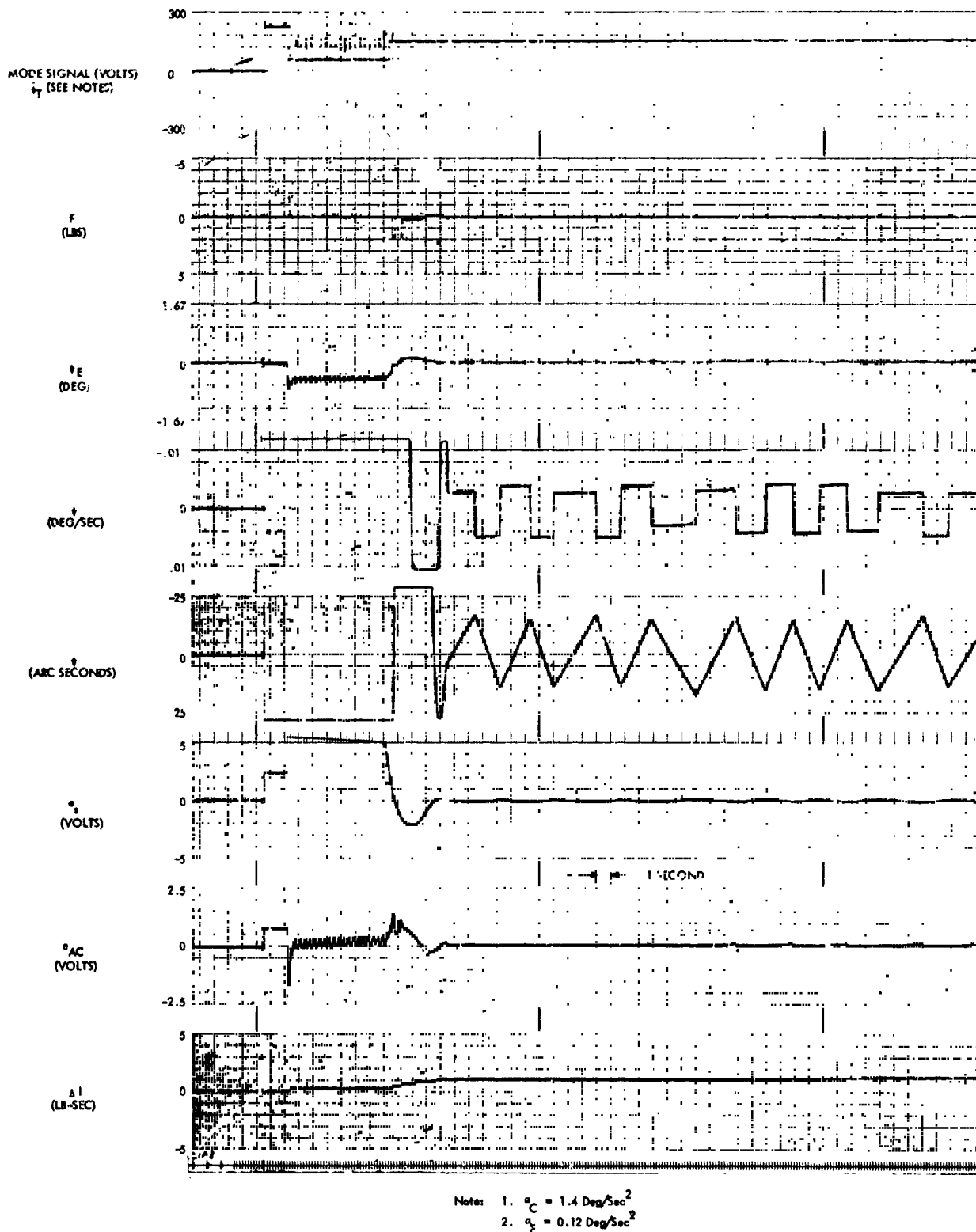
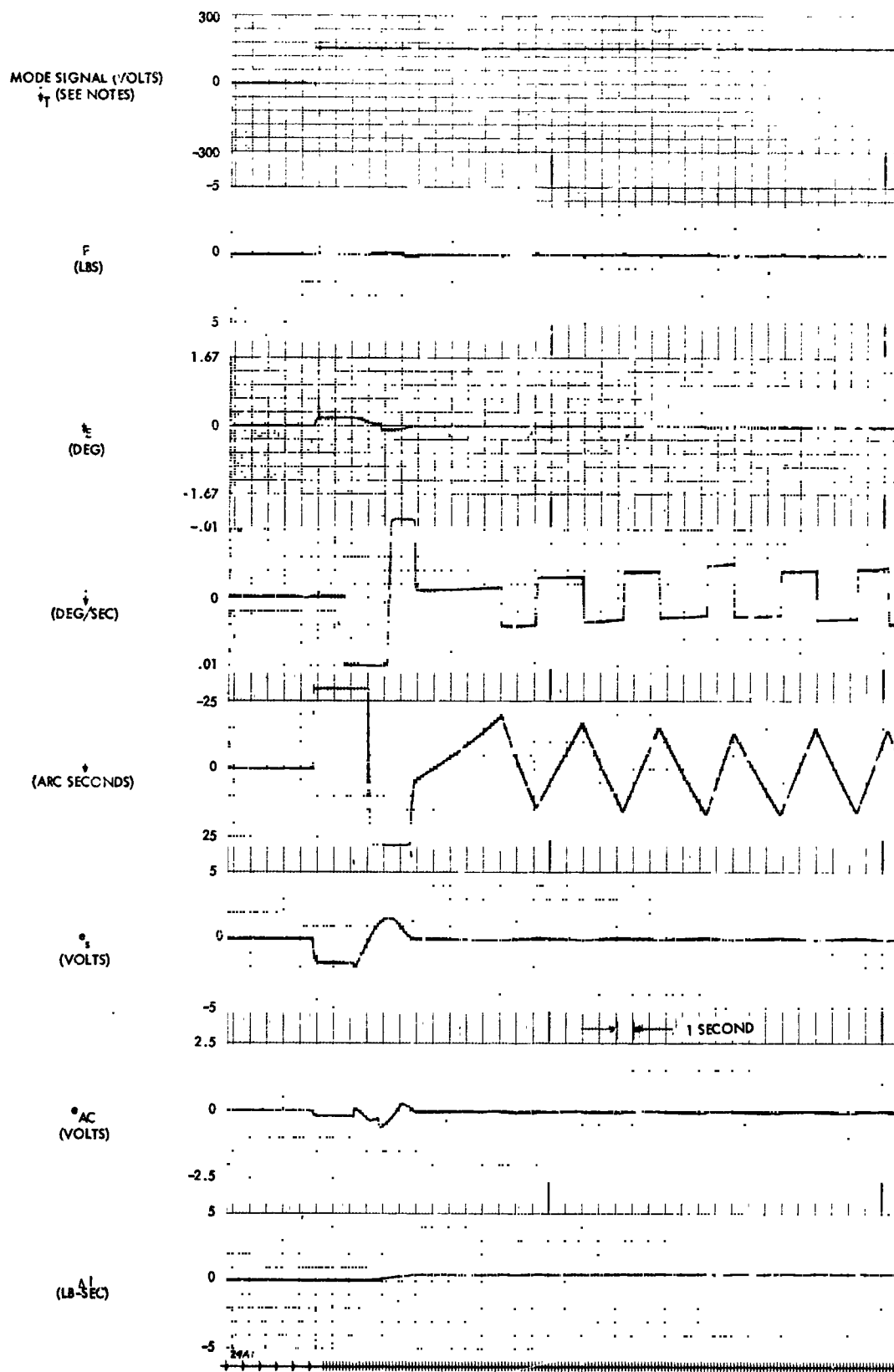


Figure 56. Acquisition and Limit Cycle for  $\psi_{EO} = -3^\circ$   
(Analog Run 21A-3)



Note: 1.  $a_C = 3.6 \text{ Deg/Sec}^2$   
 2.  $a_F = 0.12 \text{ Deg/Sec}^2$

Figure 57. Acquisition and Limit Cycle for  $\psi_{EO} = 0$   
 (Analog Run 24A-1)

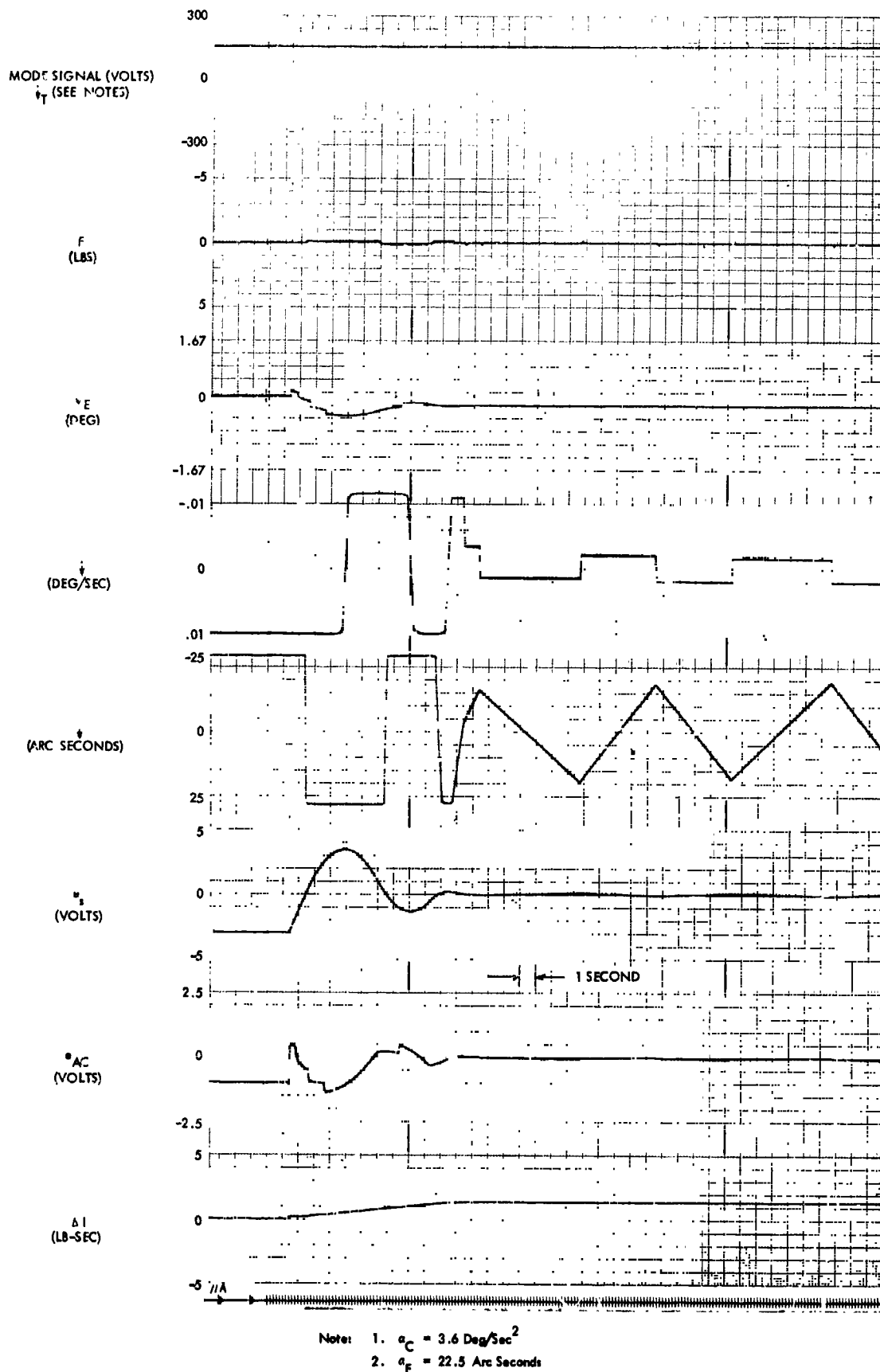


Figure 58. Acquisition and Limit Cycle for  $\alpha_F = 0.06 \text{ deg/sec}^2$  (Analog Run 11A-1)

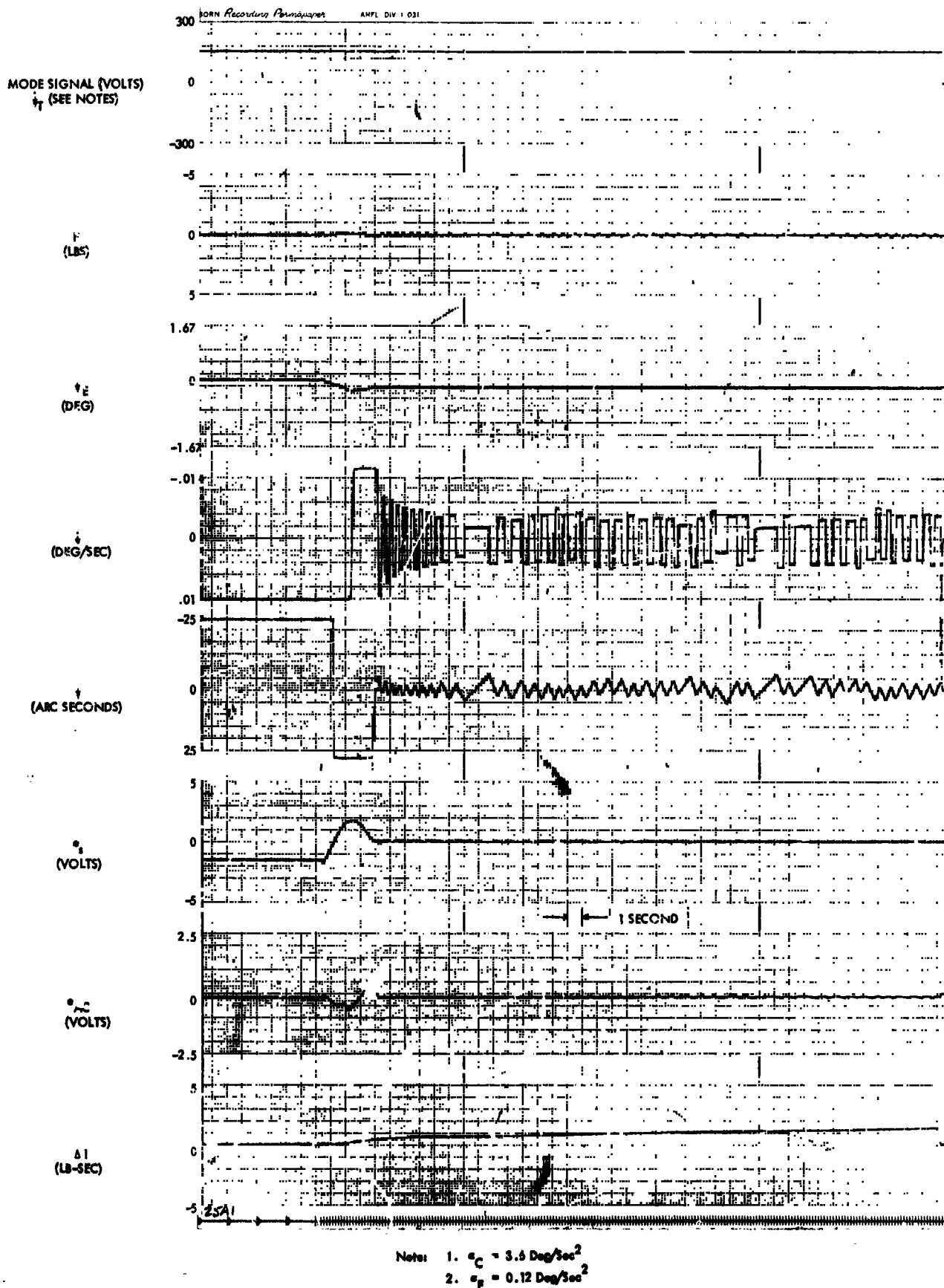


Figure 59. Acquisition and Limit Cycle for  $\epsilon_{TF} = 10 \text{ arc sec}$   
(Analog Run 25A-1)



Table 16

ANALOG SIMULATION SACS LIMIT  
CYCLE CHARACTERISTICS

(Without Delayed Feedback)

Switching Threshold Level (arc sec)	Low Thrust Acceleration (deg/sec <sup>2</sup> )	Max Peak-to-Peak Amplitude (arc sec)	Average Period (sec)	Max Vehicle Rate (arc sec/sec)	Analog Run Number
±22.5	0.12	30.0	4.35	18.0	21A2
	0.06	37.0	10.1	9.0	13A
±10.0	0.12	9.66	.93	18.4	25A1
	0.06	12.3	3.03	9.7	26A1

The three-axis simulator limit cycle rates are consistently higher and limit cycle periods consistently lower than those obtained in the analog simulation. Based on nominal parameter values, the rate amplitude is not highly sensitive to small variations in threshold in the SACS. Rate amplitude is sensitive to acceleration, but it is unlikely that accelerations would differ consistently in the same direction from one simulation to the other. It is relatively insensitive to small variations in derived rate gain about the nominal (cf. Reference 1, Section 7). Sensitivity to valve trigger hysteresis is relatively small. However, the limit cycle rate amplitude is highly sensitive to the effective cumulative lag in the system. The effective cumulative lag varies directly with valve dropout time, fine sensor exponential lag(s), and derived rate circuit exponential lags. The effective cumulative lag in the analog simulation is of the order of 70 ms and was so established to duplicate lag characteristics of the FACS system. Substantially greater lags would have to be introduced into the analog simulation to duplicate the limit cycle rates and periods seen on the three-axis simulator.

A series of 3-axis simulator tests was conducted to evaluate the effect of delayed feedback on SACS operation. An adjustment of parameters was achieved which produced a significant improvement in SACS operation. However, further improvement is considered possible and work is underway to realize the full potential of this technique. The findings shown herein are then considered preliminary.

The objective of this modification was to improve the SACS limit cycle characteristics by reducing body rate. The delayed feedback provides a relatively simple form of jet pulse-width control. Figure 60 shows the implementation. It may be seen that a voltage occurring at either valve trigger will be fed back through a delay circuit and summed with the solar sensor error voltage. The sign of the feedback voltage is selected so that it opposes the voltage which initially produced trigger action. The effect desired is to produce more rapid valve turn-off. By proper adjustment of the feedback circuit parameters, the minimum jet-on time may be substantially shortened and the body rates thereby reduced.

Figure 60 also shows the parameter values used during tests on the three-axis simulator. It may be noted that the transfer function for feedback from the clockwise valve trigger is more complex than its counterpart counter-clockwise circuit. This difference was not specifically desired but rather resulted from the manner in which the circuit was set up. Further investigations now underway utilize a simple first-order lag term on each side.

Nevertheless, using the implementation and parameter values shown, an encouraging improvement in SACS limit cycle was achieved. Simulator tests were run to demonstrate this improvement and to establish that no detrimental effect on acquisition performance resulted. With the low-thrust valve threshold set at  $\pm 10$  arc seconds, low-level acceleration at  $0.12 \text{ deg/sec}^2$ , and high-level acceleration at  $3.6 \text{ deg/sec}^2$ , it was observed that:

- ♦ Maximum limit cycle peak-to-peak amplitude was 19 arc sec.
- ♦ Maximum body rate was 35 arc sec/sec.
- ♦ Average acquisition time (8 acquisitions) was 2.6 seconds.

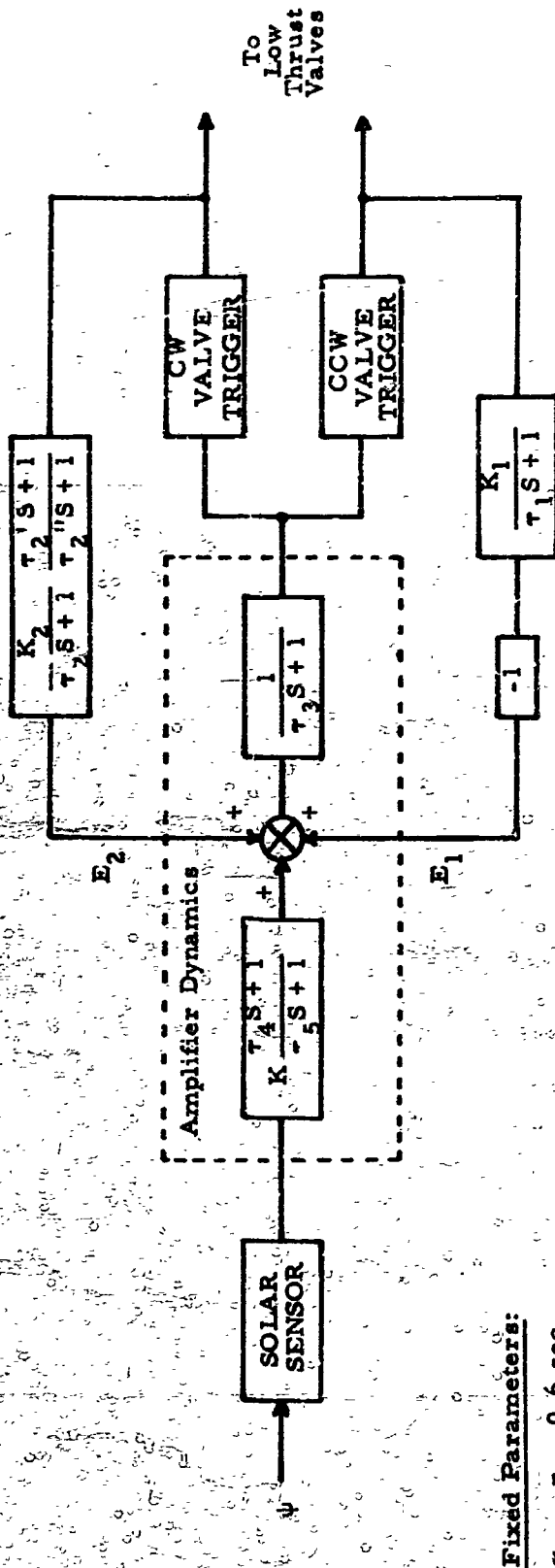


Figure 60. Delayed Feedback in SACS, Block Diagram

The extent of improvement is perhaps best seen by noting that the system without delayed feedback produced maximum limit cycle body rates of 145 arc sec/sec under these conditions. It is also observed that acquisition times were actually shorter with feedback installed although testing was limited and this may be coincidental.

It becomes difficult now to define the "period" of limit cycle. The delayed feedback causes the character of limit cycle to become much less periodic. This may be seen in Figure 61 which reproduces a portion of three-axis simulator run 56 showing acquisition and limit cycle behavior. The traces labeled "low-thrust valve" actually monitor the valve drivers. Thus a very short pulse may not result in valve opening. It appears, by correlating the valve trace and the sensor output trace, that much of the activity at the driver did not produce valve opening. In such cases the feedback removes the turn-on signal before valve action can occur. It can also be seen that the occurrence of body rates as high as the quoted 35 arc sec/sec maximum is restricted to short time intervals and is associated with CCW jet action. Generally, body rates are substantially lower.

These results have led to continued examination of the delayed feedback technique. Since improvement so substantial can be gained by use of simple circuits, delayed feedback will also be incorporated in the IACS control channels.

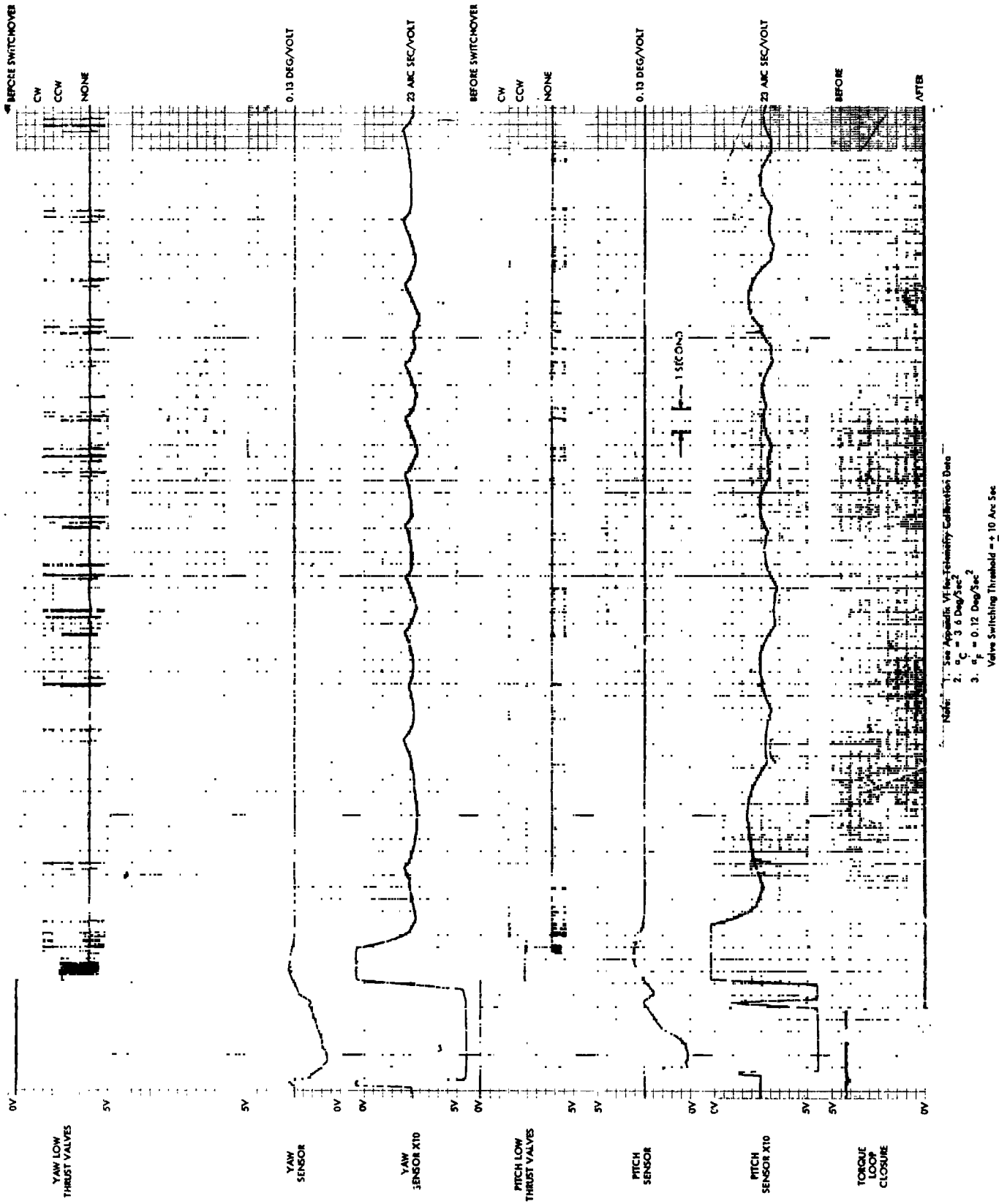


Figure 61. Acquisition and Limit Cycle with Delayed Feedback  
(Three-Axis Simulator Run 56)

## Section 5

### SYSTEM CHANGES (PHASE II)

At the conclusion of three-axis simulator tests, a review of findings was made and agreement reached on the essential features of the prototype FACS.

#### 5.1 OPTIONAL FEATURES - SELECTION OF ALTERNATE

The breadboard FACS was designed to permit evaluation of several optional features. A determination of the preferred features was made and the prototype FACS will reflect this determination as follows:

- ♦ Bi-level rate gain will be used in the IACS pitch and yaw channels.
- ♦ Dual detectors, one for IACS capture indication and one for SACS enabling, will be used in the pitch and yaw channels.
- ♦ Roll rate gain change will occur at the completion of roll capture and the lower rate gain will be retained thereafter.
- ♦ The rate-only control mode in pitch and yaw will be effective until roll capture is complete. Position plus rate control will be retained thereafter.

#### 5.2 DESIGN CHANGES

Design changes to FACS subassemblies will be carried out during Phase II. These changes are listed below:

- ♦ Roll Stabilized Platform
  - (1) The servo amplifier will be replaced to provide a better match of amplifier to motor.
  - (2) The platform will be modified to provide an improved static balance.
  - (3) The housing will be modified to incorporate seals.

- ♦ Static Inverter

- (1) The integral short circuit protection will be removed and provision made for replacement with external short circuit protection.
- (2) Design changes will be made to increase efficiency.

- ♦ IACS Control Unit

- (1) Gyro position signal limiters used in the breadboard FACS pitch and yaw channels will be retained and similar provision will be examined for the roll channel.
- (2) Delayed feedback circuits will be incorporated in the roll, pitch and yaw channels.
- (3) Series diodes at the despin and CW roll valve will be eliminated.
- (4) The amplifier provided for the single-level-detector option will be eliminated.
- (5) Capture level detector triggers will be redesigned to substitute fixed resistors for the potentiometers ZR4, ZR5, and ZR6.
- (6) Slave roll triggers will be redesigned to substitute fixed resistors for the potentiometers ZR14 and ZR15.

- ♦ SACS Control Unit

- (1) An improved version of the delayed-feedback circuits will be incorporated.

- ♦ Programmer

- (1) Based on optimization studies to be conducted during Phase II, the VTT circuits will be modified to the "current-only" mode.
- (2) The VTT compensation for inner gimbal lag angles will be extended in range.

- ♦ Telemetry Signal Conditioner

- (1) Isolation circuits shall be incorporated as necessary to permit FACS calibration without the conditioner installed.

- ♦ Junction Box

- (1) Series diodes will be removed from the valve circuits.
- (2) Umbilical and test cable requirements will be re-examined.

- ♦ Ground Support Equipment

- (1) The provision for 3-wire-synchro offset caging will be retained and the provision for 2-wire offset caging will be eliminated. Offset requirements become  $\pm 20^\circ$  in pitch and yaw,  $\pm 90^\circ$  in roll.
- (2) All cases of false indications will be eliminated from the console display.
- (3) Voltmeters will be incorporated in the console display.



## Section 6

### CONCLUSIONS AND RECOMMENDATIONS

Test of the Fine Attitude Control System has demonstrated performance meeting or exceeding all requirements:

- (1) Pointing accuracy better than  $\pm 10$  arc seconds was achieved.
- (2) Target acquisition times better than 10 seconds were demonstrated.
- (3) IACS-only operation was accomplished without degradation of performance.
- (4) Programming capability suited to multiple stellar target use is provided.
- (5) Low rate limit cycle capability was achieved by use of delayed-feedback techniques.
- (6) Gyro offset caging provisions met range and accuracy requirements.
- (7) The FACS and all subassemblies successfully underwent specified environmental tests.
- (8) Ground support equipment compatibility was established by bench test and three-axis simulator test.

Based on this successful demonstration of acceptability, follow-on development of FACS prototype and flight units is recommended.

## References

1. Report SGC 742R-5, "Fine Attitude Control System - Phase I, Analog Simulation Report," December 1964.
2. NASA-GSFC Stabilization and Controls Branch Report 108, "A Single-Axis Analog Simulation of the Aerobee FACS: Review of Space-General Corporation Work and Description of GSFC Work," February 18, 1965.
3. Report SGC 742-TR1, "Optimization of Variable-Time Torquing System for Aerobee FACS," 16 March 1965.
4. Report SGC 254R-8, "Fine-Attitude Control System - Design Study Program Final Report," July 1963.
5. NASA-GSFC Stabilization and Control Branch Report No. 66; "A Study of the Aerobee 150 IACS/SACS Control System"; April 2, 1963.
6. NASA-GSFC Stabilization and Control Branch Report No. 96; "Design, Testing, and Evaluation of the Aerobee FACS Breadboard Sun Sensor"; July 29, 1964.